

MASTER THESIS

Thesis submitted in partial fulfillment of the requirements for the degree of Master of Science in Engineering at the University of Applied Sciences Technikum Wien - Degree Program Renewable Urban Energy Systems

Technology comparison and profitability analysis of PV and CSP for large-scale electricity production in South Africa

By: Florian Haag, BEng

Student Number: 1310578031

Supervisors: FH-Prof. Dipl.-Ing. Hubert Fechner, MSc,

MAS

Prof. Dr.-Ing. Frank Dinter

Stellenbosch, South Africa, N



Declaration

"As author and creator of this work to hand, I confirm with my signature knowledge of the relevant copyright regulations governed by higher education acts (for example see §§21, 46 and 57 UrhG (Austrian copyright law) as amended as well as §11 of the Statute on Studies Act Provisions / Examination Regulations of the UAS Technikum Wien).

In particular I declare that I have made use of third-party content correctly, regardless what form it may have, and I am aware of any consequences I may face on the part of the degree program director if there should be evidence of missing autonomy and independence or evidence of any intent to fraudulently achieve a pass mark for this work (see §11 para. 1 Statute on Studies Act Provisions / Examination Regulations of the UAS Technikum Wien).

I further declare that up to this date I have not published the work to hand nor have I presented it to another examination board in the same or similar form. I affirm that the version submitted matches the version in the upload tool.“

Place, Date

Signature

Kurzfassung

Hier ist die Kurzfassung

Schlagworte: Schlagwort1, Schlagwort2, Schlagwort3, Schlagwort4

Abstract

This is the Abstract BLABLA

Keywords: Keyword1, Keyword2, Keyword3, Keyword4

Contents

1. Introduction	1
1.1. Description of the objective of the thesis	3
1.2. Relevance of results	3
1.3. Methodology	3
1.3.1. Information procurement	3
1.3.2. Quality assurance	3
1.3.3. Implementation of present resources	3
2. The South African energy sector	4
2.1. Electricity supply and demand	6
2.1.1. Rising energy consumption and security of supply	7
2.1.2. Structure of power distribution	7
2.2. Renewable energy potential in South Africa	9
2.2.1. Energy outlook for South Africa	9
2.2.2. Government Incentives	9
2.3. Chapter summary	9
3. Solar power in South Africa	10
3.1. Solar radiation	10
3.2. Solar power plants in SA	12
4. Large scale solar power plants	15
4.1. Large-scale CSP plants	16
4.1.1. Parabolic-trough concentrating solar power	21
4.1.2. Central tower concentrating solar power	31
4.1.3. Heat transfer fluid	39
4.1.4. Storage systems for CSP	40
4.1.5. Power cycles for CSP systems	47
4.2. Large scale PV power plants	49
4.2.1. Large-scale PV power plants	49
4.2.2. Large-scale electrical energy storage systems	49
4.3. Environmental impacts of CSP and PV	49
4.4. Chapter summary	49

5. Simulation-based comparison between CSP- and PV-power plants	51
5.1. General assumptions	52
5.1.1. Simulation scenario	52
5.1.2. Location and weather data	54
5.2. CR power plant design and simulation	57
5.3. PTC power plant design and simulation	64
5.4. PV power plant with electrical energy storage design and simulation	74
5.5. Simulation results	87
5.6. Interpretation and comparison of results	89
6. Current economical situation and digression potential of main technologies to a long therm marked potential	91
6.1. CSP	91
6.2. PV plant	91
6.2.1. Electrical storage	91
7. Conclusion and outlook	93
A. Appendix I	94
A.1. Part A	94
B. Appendix B: Methodology for calculating the LCOE	98
B.1. CR power plant	99
B.2. PTC power plant	100
B.3. PV power plant	102
Bibliography	104
List of Figures	117
List of Tables	119
List of Code	120
List of Abbreviations	121

We are like tenant farmers chopping down the fence around our house for fuel when we should be using Nature's inexhaustible sources of energy —sun, wind and tide. . . I'd put my money on the sun and solar energy. What a source of power! I hope we don't have to wait until oil and coal run out before we tackle that.

Thomas Edison

1. Introduction

It is generally known that the worldwide energy demand is nearly entirely covered by fossil energy sources such as coal, oil, natural gas and uranium. Also, the consequences of fossil fuels to the environmental, social and economic development are globally well known and discussed. Especially the greenhouse gas emissions need to be reduced for the purpose to dilute their effects on climate change. Furthermore, the world population and the energy demand is rising. By 2035 the world population is projected to reach 8.7 billion, this means an additional 1.6 billion people who will need energy. This leads to a rise in primary energy consumption by 37 % between 2013 and 2035 (BP, 2015).

Especially newly industrialized countries with a rapid population growth like China and India showed a strong rising primary energy consumption. Also the prognosticated primary energy demand in the newly industrialized country South Africa (SA), officially the Republic of South Africa, is growing from 1 639.83 TWh in 2012 to 2 163.18 TWh (including solid biomass and waste) in 2040. Coal is the mainstay of the South African energy system, meeting around 70 % of primary energy demand and accounting for more than 90 % of domestic electricity output. The prognosticated electricity demand is also rising by more than 70 % from 212 TWh in 2012 to 364 TWh in 2040 (International Energy Agency, 2014a).

Depending on the growing electricity demand and missing investments in the power supply system in the last decades, the reserve margin in electricity capacity declined from almost 40 % in 1990 to 8 % at these days (Trollip et al., 2014; Eskom, 2015). The region of Western Cape experienced serious blackouts in late 2005 dependence on combination of inadequate reserve margin, insufficient reliability, a stressed system and system element failures. Those were the causes which forced Eskom (Eskom Holdings SOC Ltd.), the South African public utility, to start scheduled load shedding during peak hours, from 2007 on (Trollip et al., 2014). The economic and social impacts are clearly noticeable already. Load shedding was also the main trigger for Bureau for Economic Research (BER) senior economist Hugo Pienaar to revise down the 2015 GDP growth forecast from 2.9 % to 1.9 % for SA. (Bisseker, 2015).

The high dependency and the scarcity of fossil resources, the intention to reduce greenhouse gas emissions and other environmental pollutants, the rising fuel price, the predicted increase of energy demand, are also forcing SA to promote the investments in renewable energy sources. In 2009, the South African government began to implement feed-in tariffs (FITs)

for renewable energies. These were later rejected in favor of competitive tenders. The resulting program, the Renewable Energy Independent Power Producer Procurement Program (REIPPPP) is an extensive initiative to install 17.8 GW of electricity generation capacity from renewable energy sources, such as wind, solar, biomass, biogas and hydropower, over the period 2012-2030. (Department of Environmental Affairs, 2015; Department of Energy, 2013; Eberhard et al., 2014)

SA has a high level of renewable energy potential, especially the solar irradiation is one of the highest in the world (Hermann et al., 2014). In some parts of the country the direct normal irradiance (DNI), the direct beam radiation, rises above 3 000 kWh/m² per year. In comparison to that, Austria has ca. one third of DNI per year (?; SolarGIS, 2013). Also the global horizontal irradiance (GHI), so the direct and diffuse solar radiation, is with about 2 300 kWh/m² per year comparatively high (?). The high solar irradiation allows SA a very effective electricity generation from an infinite source of energy.

Solar energy cannot be used as such, it has to be captured and converted into higher forms of energy, primarily heat and electricity. The conversion from solar energy into electrical energy is carried out by two mechanisms: the photovoltaic conversion and the thermal conversion. For the generation of solar thermal electricity (STE) it is common to concentrate the solar radiation with reflectors onto a receiver where a heat-transfer fluid (HTF) circulates. The fluid is heated up to high temperatures to be used in a thermodynamic cycle to generate electrical power. This technology is called concentrating solar power (CSP). The direct conversion from solar radiation into electricity is based on the photovoltaic effect using photovoltaic (PV) panels. The main difference between those two solar conversion technologies is the type of radiation that can be converted. The CSP technology can only capture and convert the component of the solar radiation that is directly hitting the collector i.e. the DNI. The PV technology, instead, can furthermore convert the scattered component by clouds, water vapor and particles in the atmosphere and the reflected component due to the albedo effect. Although the CSP systems can exploit only the direct fraction of the overall solar irradiation, CSP plants allow to store the thermal energy with lower costs and lower environmental impacts than storing electric energy generated by PV systems. (International Energy Agency, 2014b; EASAC, 2011) The levelized cost of electricity (LCOE) of STE and PV varies widely with the location, technology, design and intended use of plants. According to the U.S. Energy Information Administration the estimated total system LCOE for new generation resources in 2019 for PV is at about 130.0 US\$/MWh and for STE at about 243.1 US\$/MWh (U.S. Energy Information Adminisstration, 2014).

At first it can be summarized that STE technology is more expensive than PV technology, but it allows the use of the cheaper thermal storage technology. The stressed electricity grid in SA needs a constant and controllable energy supply. For a fluctuating energy source a balance mechanism is necessary to guarantee a support and not a pressure for the electricity supply.

1.1. Description of the objective of the thesis

The objective of this thesis was an technical and economical comparison between an concentrating solar and an photovoltaic power plant. This comparison is limited to the region South Africa and including as well the most reasonable storage systems for both technologies.

Also the medium- and long-term cost digression potential technologies are considered. This is an necessary indicator for common power plants investments in South Africa.

The research question is as follows:

Which technology, concentrating solar or photovoltaic power plants in combination with suitable storage systems, will prevail in South Africa in a technical and economical comparison? What are the medium- and long-term cost degression potentials of these technologies?

1.2. Relevance of results

Was sagt mein Ergebniss aus und was kann man damit anfangen

1.3. Methodology

1.3.1. Information procurement

used SI-Units = always

1.3.2. Quality assurance

1.3.3. Implementation of present resources

2. The South African energy sector

The Republic of South Africa is one of the most developed country in Africa. SA accounting for about 30 % of the primary energy consumption and 36.5 % of the electricity generation of the entire continent Africa in 2013. The primary energy consumption was about 1 425 TWh in total. Therefore the South African society is strongly depend on fossil fuels as primary energy source. As shown in Figure 1, coal is with about 72 % the main primary energy source. Also crude oil (22.2 %) is a very important energy source for SA. Therefor the primary energy consumption from renewable energies in SA is just about 0.3 %. Comparing to this, the global share of renewable primary energy consumption was about 8.9 % in 2013. The consumption in natural gas is about 2.9 % which is mainly coming from industrial consumers. 2.6 % of the primary energy consumption was from nuclear energy in 2013. (BP, 2014; International Energy Agency, 2015)

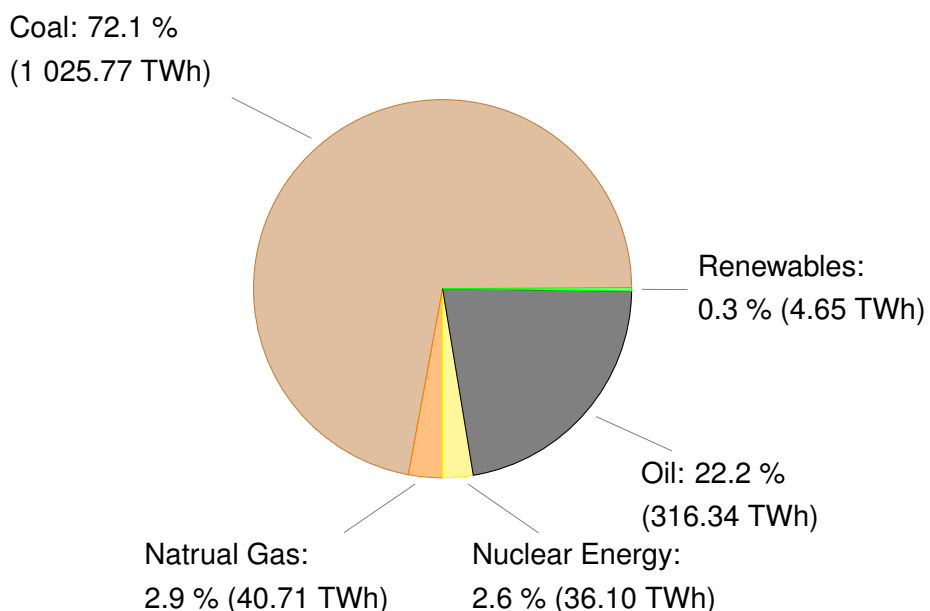


Figure 1.: Primary energy consumption by fuel excluding solid biomass and waist in South Africa 2013 (BP, 2014).

Between 1991 and 2011 the annual primary energy consumption in SA has risen from 996.79 TWh by over 43 % up to 1 431.01 TWh (excluding solid biomass and waist). Also the annual primary energy consumption per capita rises in the same time period by over 23 % up to 33.82 MWh per person. Figure 2 shows the growing South African primary energy consumption

in comparison to primary energy consumption per capita. The Figure shows that not only the population growing but also the rising demand per capita is the reason for the increasing total primary energy consumption in SA. (BP, 2014)

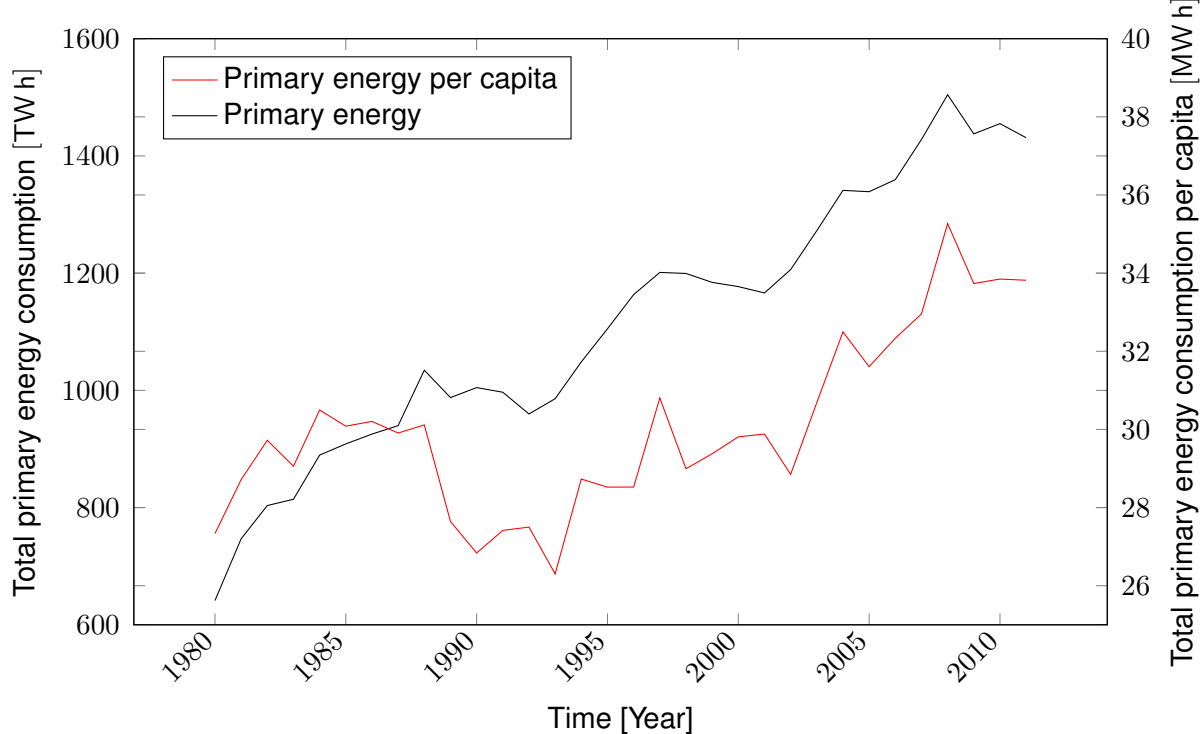


Figure 2.: Total primary energy consumption and total primary energy consumption per capita 1980 to 2011 in South Africa (BP, 2014; US Energy Information Administration, 2015).

The three major consumption groups are the industry sector with about 34.9 %, the transport sector which consumes about 28.6 % and other sectors with about 36.5 %, which includes agriculture, commerce and public services, residential and non-specified consumers. According to the South African Department of Energy (DoE) was the total final consumption about 738.18 TWh in 2012. (Department of Energy, 2012)

2.1. Electricity supply and demand

Coal-fired power stations restrained the electricity generation in SA. 92.8 % was generated thought coal (239 344 GWh) in 2012, while 5.1 % of the annual supply was generated by nuclear power (13 075 GWh) and 1.3 % was generated from hydropower applications (4 860 GWh). Less significant electricity sources for SA are 0.08 % Oil (194 GWh), 0.11 % bio-fuels (293 GWh), 0.02 % PV (50 GWh) and 0.04 % wind (103 GWh). (International Energy Agency, 2015)

The final electricity consumption in SA was about 197 092 GWh in 2012. The final consumption consist also three main consumers. The largest consumer group with about 59.5 % are industrial consumers, followed by residential consumers (19.7 %) and commercial and public services (14.3 %). The complete electricity flow is shown in Annexure I, Part A, Table 24, on page 95. (International Energy Agency, 2015)

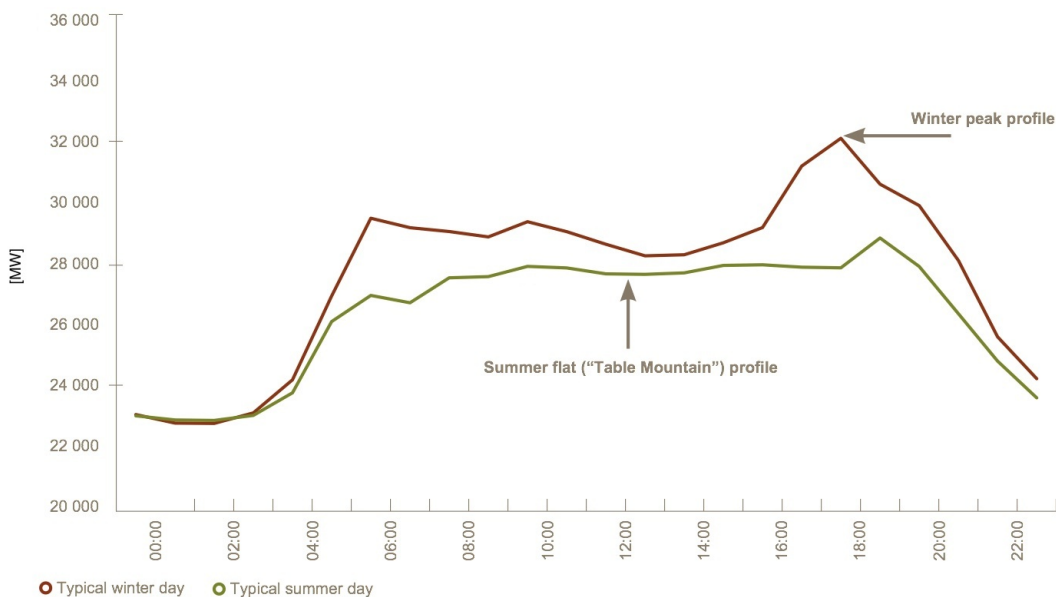


Figure 3.: Summer and winter load profiles (Eskom, 2014a).

The demand in South Africa has different load profiles during winter and summer as shown in Figure 3. The peak demand is usually in the evening hours and particularly high during winter time. According to Eskom is the peak demand at about 32 GW, while the usually demand during daytime is between 26 GW and 29 GW. (Eskom, 2014a)

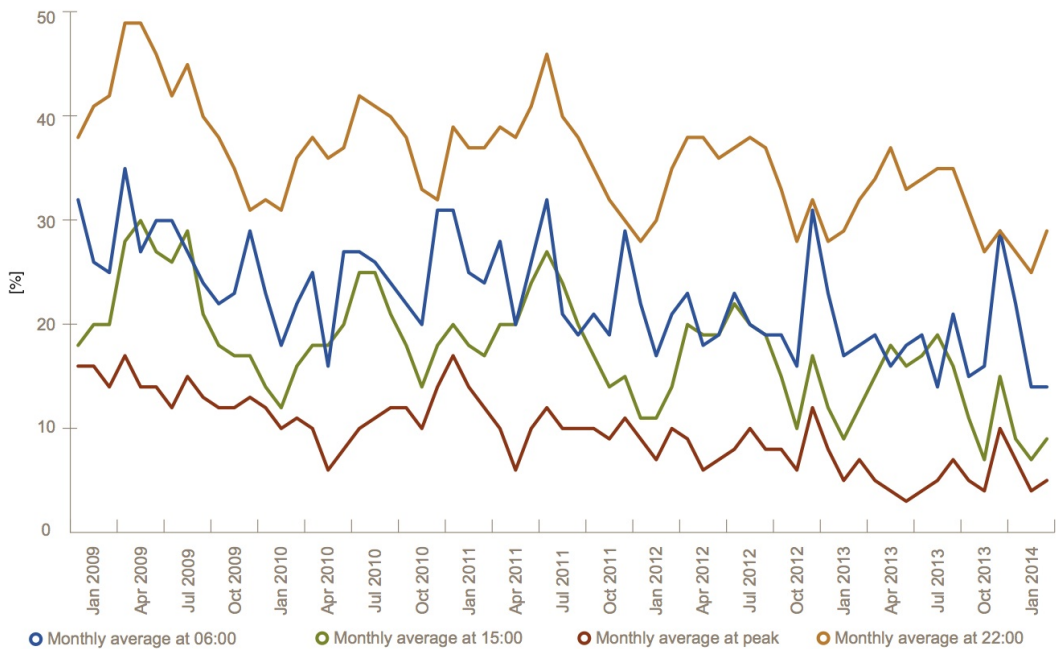


Figure 4.: Average monthly % operating reserves(Eskom, 2014a).

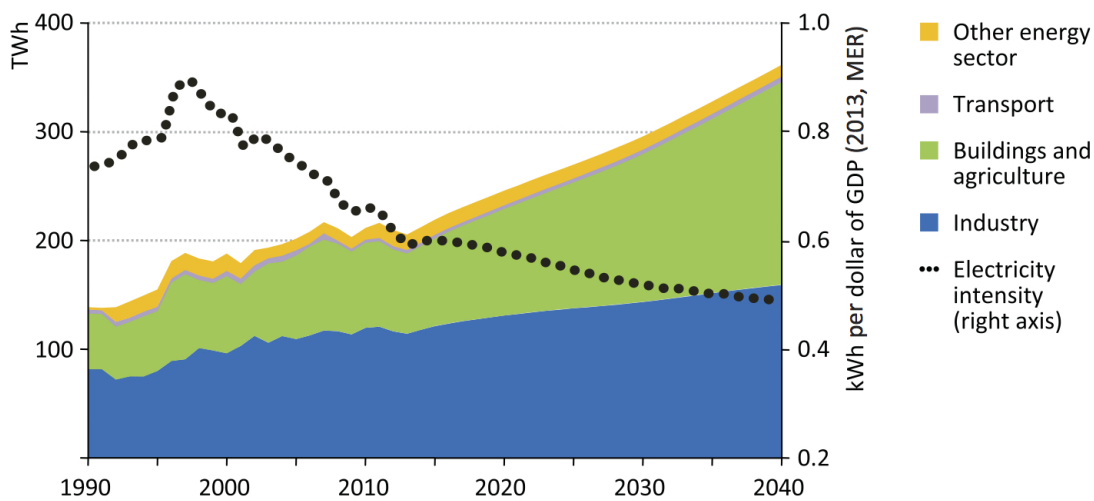


Figure 5.: Electricity demand growth by sector in South Africa in the New Policies Scenario (International Energy Agency, 2014a).

2.1.1. Rising energy consumption and security of supply

2.1.2. Structure of power distribution

Kilometerlängen, Verluste im Netz (Eskom, 2014b)

On mainland sub-Saharan Africa, SA has with around 85 % the highest electrification rate.

About 11 % of households don't have access to electricity and a further 4 % rely on illegal access (non-paying) or obtain access informally (from one household to another but paying). (International Energy Agency, 2014a)

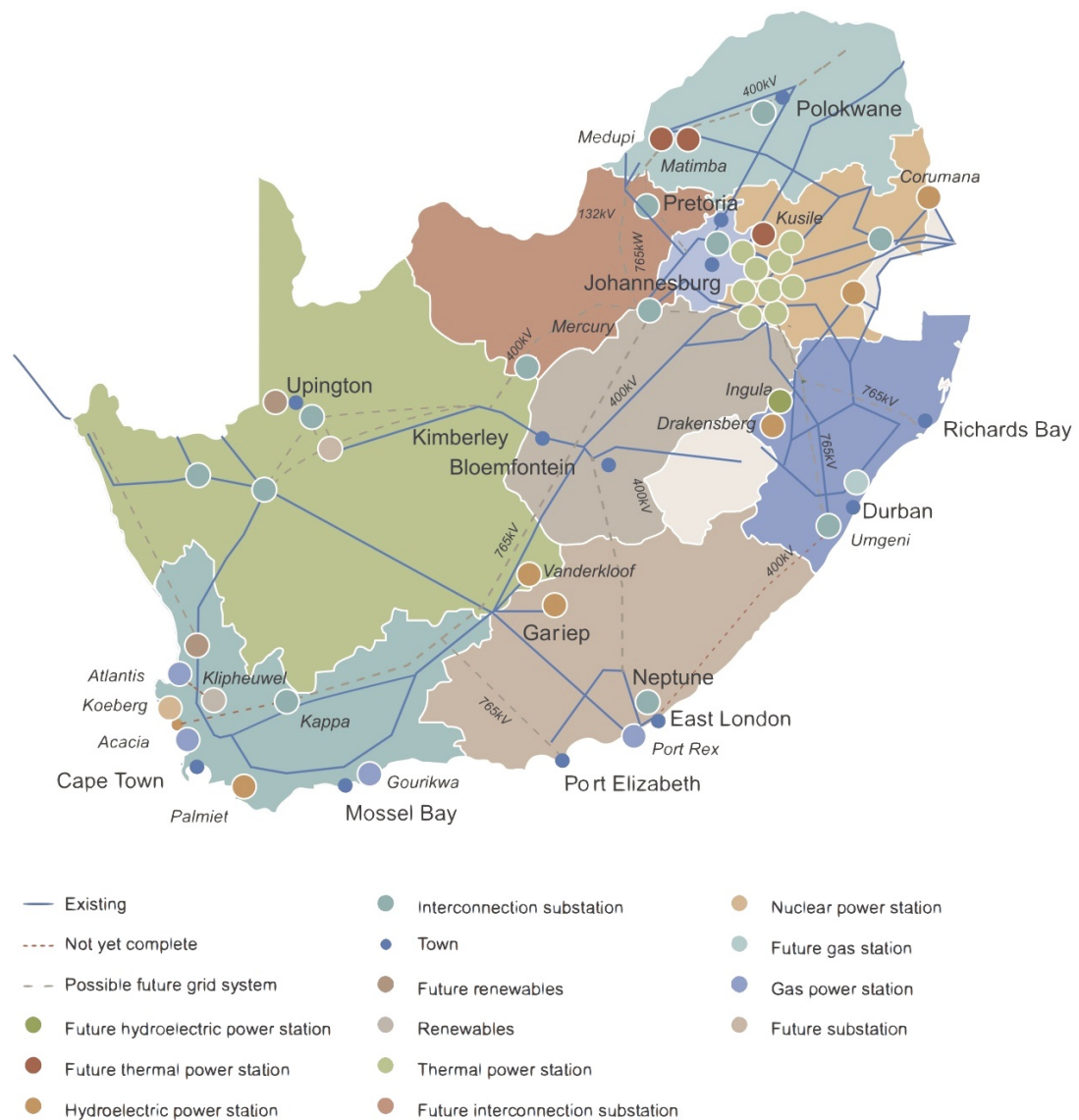


Figure 6.: Eskoms transmission projects as at 31 March 2014 (Eskom, 2014a).

<http://integratedreport.eskom.co.za/supplementary/app-transmission.php>

2.2. Renewable energy potential in South Africa

2.2.1. Energy outlook for South Africa

Development of a Renewable Energy Power Supply Outlook 2015 for the Republic of South Africa Achieved by Sebastian Giglmayr, BSc (Giglmayr, 2013)

2.2.2. Government Incentives

2.3. Chapter summary

3. Solar power in South Africa

South Africa is one of the countries with the highest potential for generating solar thermal electricity in the world. Figure 7 shows the daily sum of global irradiation in Aberdeen, United Kingdom and Upington, South Africa. The yearly share of diffuse irradiation in Aberdeen overlaps 60 %. In winter month the share reaches 90 %. The share in Upington is approximately 25 % and is in total significantly higher than Aberdeen. The direct comparison shows also the difference of the solar irradiation between northern and southern hemisphere during the year. It is obviously, that the seasons are the other way around between both hemispheres.

This chapter shows energy impact from the sun and how it is distributed in SA. Furthermore the chapter comprised the current situation of solar power plants in SA.

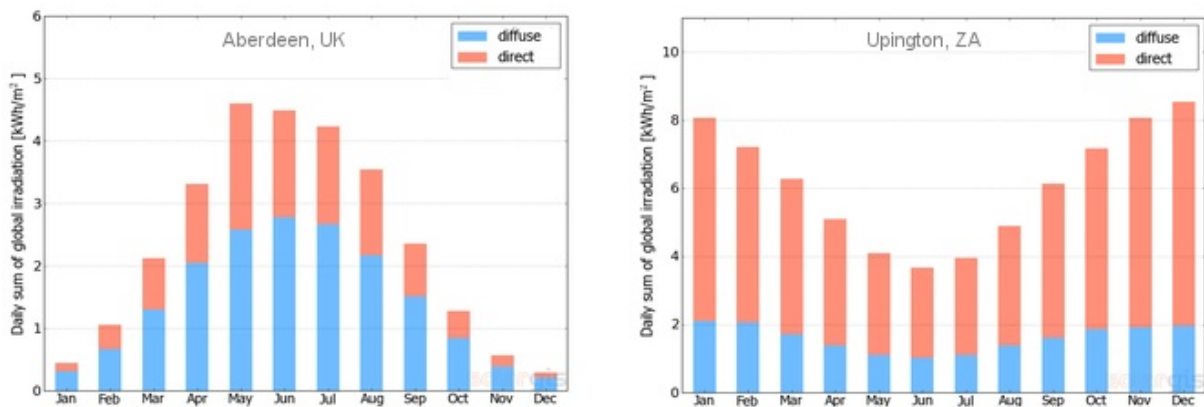


Figure 7.: Long-term monthly variability of direct (DNI) and diffuse (DHI) irradiation throughout the year for Aberdeen in the United Kingdom and Upington in South Africa (SolarGIS, 2015a).

3.1. Solar radiation

The most important solar radiation parameters for designing a solar power plant are here defined:

- **GHI** ($\text{kWh}/\text{m}^2/\text{a}$ or W/m^2): Global Horizontal Irradiance is the total amount of shortwave radiation received from above by a horizontal surface. It includes direct (beam) and a

diffuse (scattered) irradiation. This value is of particular interest to PV or solar water heater with a fixed inclined angle.

- **DNI** (kWh/m²/a or W/m²): Direct Normal Irradiance is the amount of solar radiation received per unit area by a surface that is always held perpendicular (or normal) to the rays that come in a straight line from the direction of the sun at its current position in the sky. Diffuse irradiation is totally excluded from the DNI. This quantity is of particular interest to installations that track the position of the sun.
- **DHI** (kWh/m²/a or W/m²): Diffuse Horizontal Irradiance is the amount of radiation received per unit area by a surface that does not arrive on a direct path from the sun, but has been scattered by molecules and particles in the atmosphere and comes equally from all directions.

Furthermore is irradiance understood as instantaneous density of solar radiation incident on a given surface, typically expressed in W/m² and irradiation is the sum of irradiance over a time period expressed in J/m² or more commonly used in Wh/m². The connection between the solar radiation parameters is shown in Equation 1. The angle θ_z is the angle between the direction of the sun and the zenith (directly overhead).

$$GHI = DNI * \cos(\theta_z) + DHI \quad (1)$$

Figure 8 shows the solar GHI and the DNI data for the country. It is shown, that the ceiling value for GHI can be more than 2 300 kWh/m²/a, whereas in some parts of the country the DNI value attains about 2 900 kWh/m²/a. This is significantly high than in the most regions worldwide, therefor SA is predestined for using solar technologies. The figure shows, that the southeastern coastline has predominantly the lowest irradiance values. The solar irradiation rise significant in the inland. The highest GHI can be find close to the Namibian boarder in the northeast of the country. The direct beam is also at highest in the western part of SA. The area around Springbok in the province Northern Cape has the highest DNI value of the country.

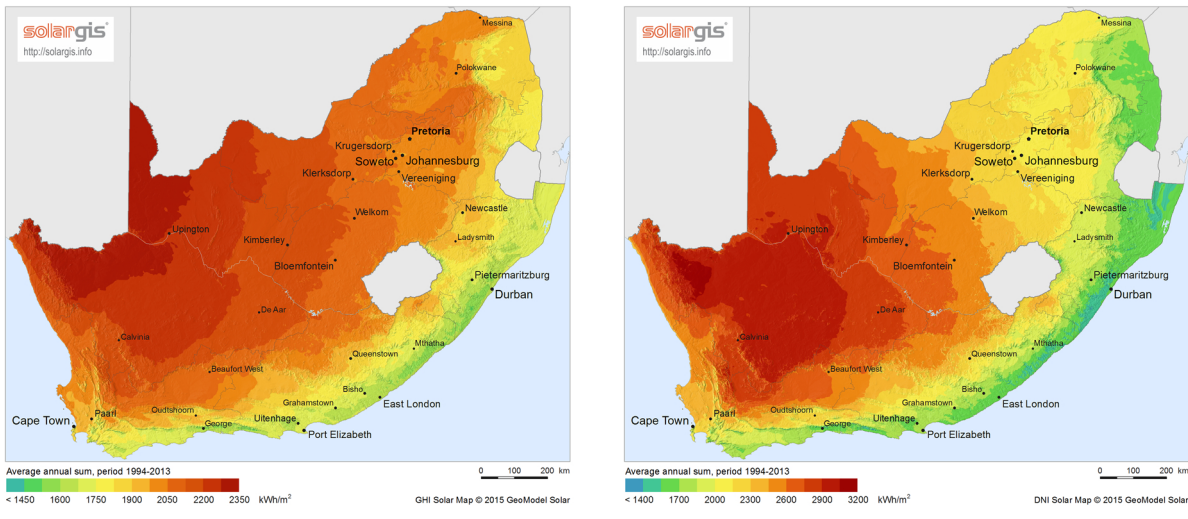


Figure 8.: Solar radiation maps of South Africa.

3.2. Solar power plants in SA

South Africa started their expansion in the field of solar power plants in the first round of the Renewable Energy Independent Power Producer Procurement Program (REIPPPP) in 2011. Now in 2015 starts the fourth round of the REIPPPP. Figure 9 shows the allocation of all solar power plants of the REIPPPP. PV-power plants are marked in yellow and CSP-power plants are marked in orange. The numbers in the single marks expose in which REIPPPP-Round it belongs.

Currently SA has 26 fully operational PV-power plants with a total capacity of 1 048.7 MW, further seven PV-power plants with 135.35 MW are under construction, four more with 307.5 MW awaiting construction (approved & financed) and there are six more PV-power plants in approvals, planning and financing with a total capacity of 415 MW.

Mainly PV-power plants are allocated in the Northern Cape. So 26 of 39 of the operational and planned plants are located there. Five more in the Western Cape, three each in the provinces Free State and Limpopo and each one in Eastern Cape and the North-West Province. (Forder, 2015)

"KaXu Solar One" is the first fully operational CSP-plant in SA and is shown in Figure 10. It is using parabolic trough technology and a 2.5 h thermal energy storage for generating of 100 MW capacity electricity. The CSP-plants "Khi Solar One" and "Bokpoort CSP Project" with a capacity of each 50 MW are under construction. Further three CSP-plants are awaiting construction, they have all a capacity of each 100 MW.

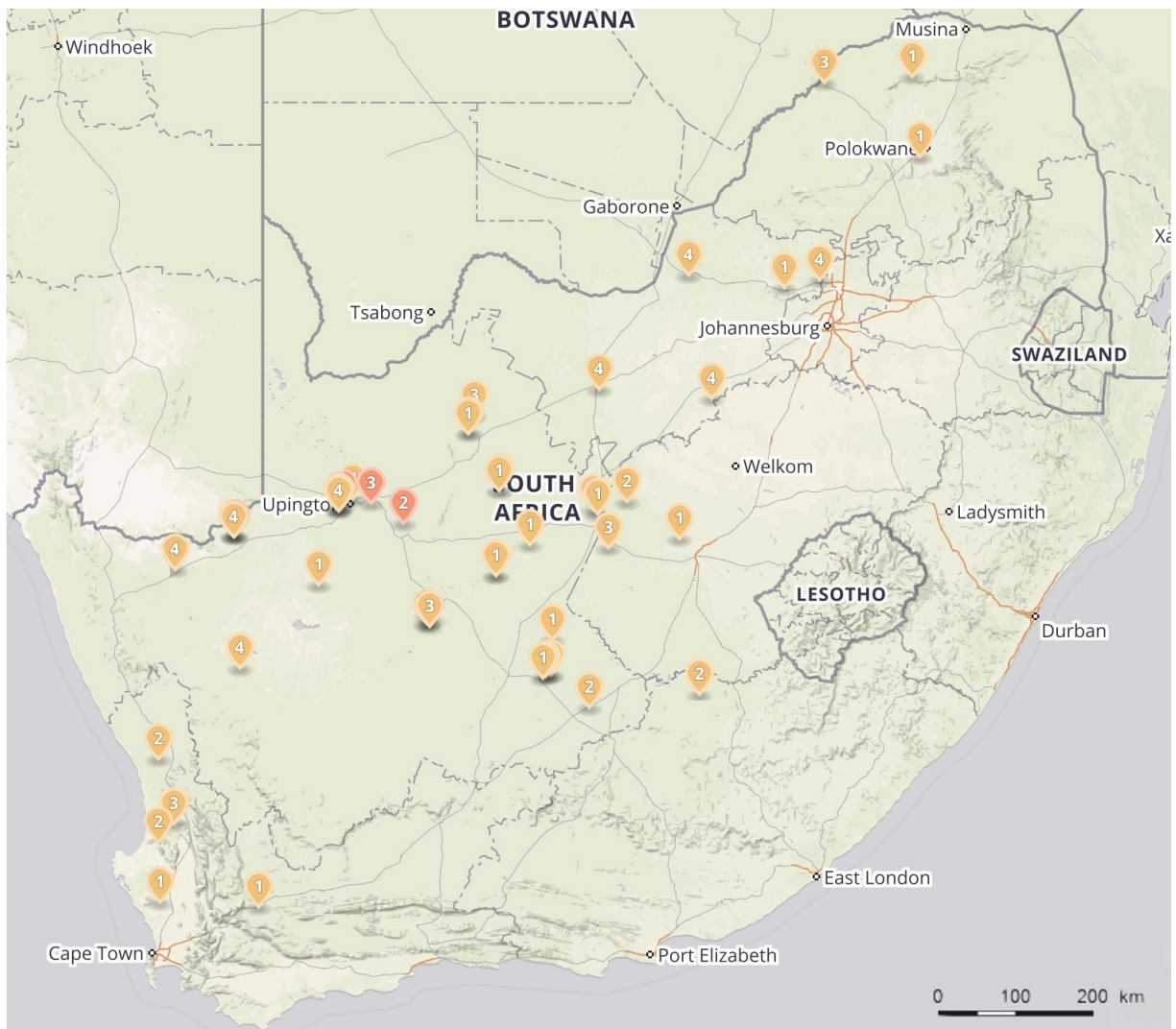


Figure 9.: Allocation of all REIPPPP solar power plants in SA (Forder, 2015).

All six CSP-plants are located in the region around the cities of Upington or Pofadder in the Northern Cape. This region is predestined for CSP-plants, because it has high DNI (around 2 900 kWh/m²/a) and a water connection through the Orange River. (Forder, 2015)



Figure 10.: KaXu Solar One, a 100 MW parabolic trough plant with 2.5 hours of thermal storage in molten salts (Abengoa Solar, 2015a).

4. Large scale solar power plants

Almost all power that we use on our planet comes from the sun. Direct in form of radiation or indirect during wind, water and vegetation. Also the fossil power resources and reserves are stored energy from the sun in form of organic carbon compounds. There are two main technologies for generating electricity out of direct sun radiation. One is the direct conversion of solar irradiance to electrical energy while using photovoltaic. The other is to generate heat and convert it to electrical power. Figure 11 gives an abstract of the common technologies using direct solar power to generating electric power. This chapter has the focus on large-scale solar power plants and describes parts from both technologies.

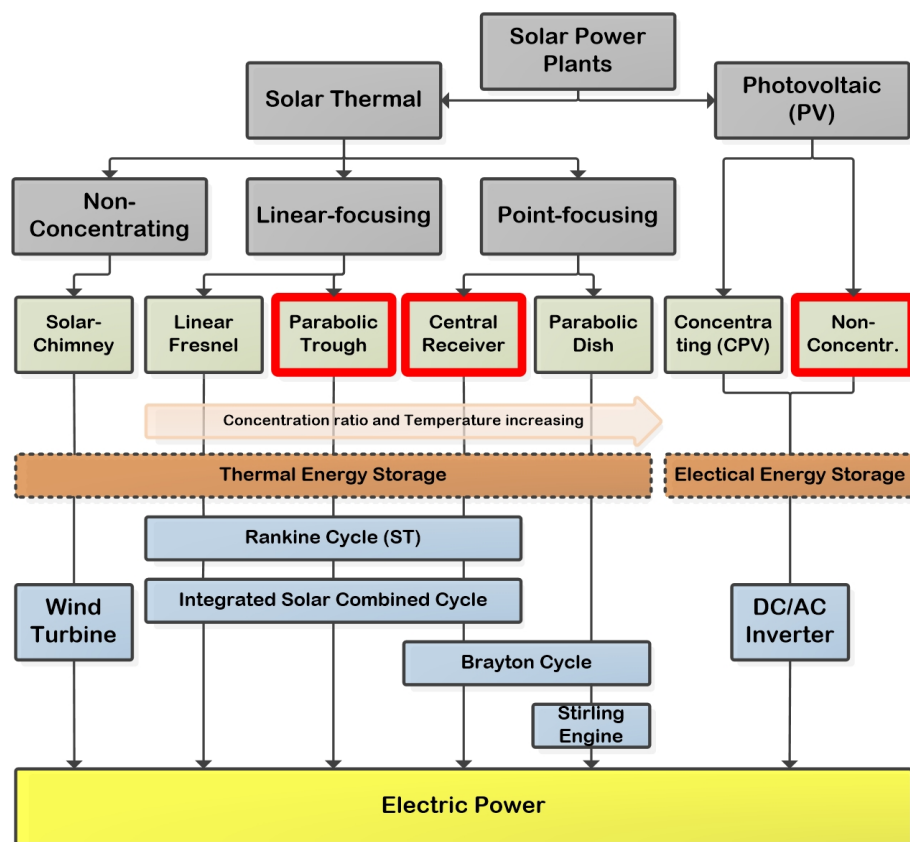


Figure 11.: Overview of Solar Power Technologies.

Therefore it is split in the technology fields of large scale concentrated solar power plants (4.1) and large scale photo voltaic power plants (4.2). In detail the technologies with a large-scale

power plant potential – parabolic trough, central receiver and non-concentrating photovoltaic – are described. Also the storage systems for both systems.

4.1. Large-scale CSP plants

Concentrating solar power (CSP) systems use combinations of mirrors or lenses to concentrate direct beam solar radiation to produce forms of useful energy such as heat, electricity and others. This happens by use of various downstream technologies. Generally the CSP technology includes not only the concentrating solar thermal (CST) technology, but also concentrating photovoltaic (CPV) energy conversion. However, there is no focus on CPV in this thesis. That is why the term CST is put on a level with CSP.

A CSP plant comprises four main sub-systems: concentrating system, solar receiver, storage and power block. Also supplementary firing is used in some cases, but is basically not necessary nowadays. A graphic scheme of such a sub-system is shown in Figure 12. The separate components are linked together by energy flow in mostly radiation transfer or fluid transport. This chapter describes the function and gives an application overview of the individually components.

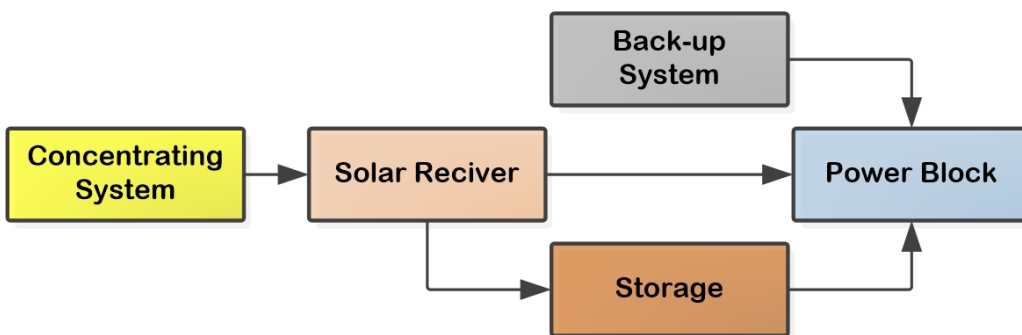


Figure 12.: Main components of a CSP plant.

The main advantage of CSP in opposite to other renewable energy producers is the thermal storage to provide power for cloudy days or during night time. Therefore the concentrating system and solar receiver have to produce more thermal energy than the power block can use directly. The ratio of the power capacity of the collector field to the capacity of the power block is defined as Solar multiple (SM). For CSP systems with storage, the number of hours of storage is based on the capacity of the power block. Chapter 4.1.4 describes technical possibilities and application of thermal storage system for CSP.

The solar receiver or concentrating system is eponymously for the main CST technologies. The two most common CSP plant technologies are parabolic trough collector (PTC) and central receiver (CR) systems (also known as solar power towers). Further types of CSP plant are

linear Fresnel reflectors (LFR) and parabolic dish. The main difference of the technologies is the concentrating system. Thereof results the differences in optical design, shape of receiver, nature of the transfer fluid and capability to store heat before it is turned into electricity. In systems with a line focus (PTC trough and LFR) the mirrors track the sun along one axis. In those with a point focus (CR and parabolic dish), the mirrors track the sun along two axes. The receiver may be fixed, as in LFR and CR, or mobile as in PTC and parabolic dish systems. An overview of the technologies and their differences in relation to the focus and the receiver is shown in Table 1.

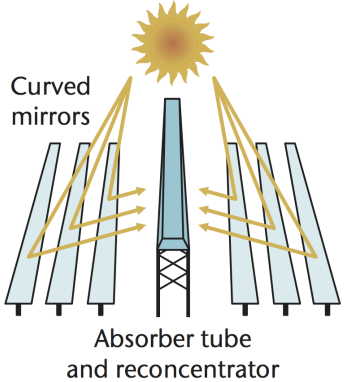
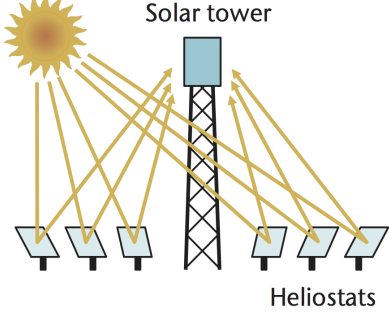
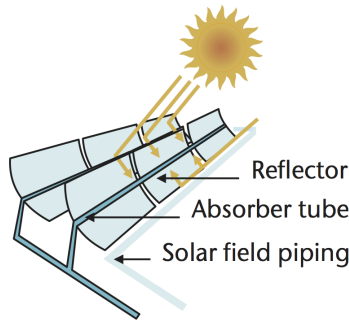
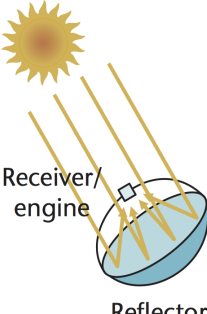
	Line focus	Point focus
	Collectors track the sun along a single axis and focus irradiance on a linear receiver. This makes tracking the sun simpler.	Collectors track the sun along two axes and focus irradiance at a single point receiver. This allows for good receiver efficiency at higher temperatures.
Fixed receiver		
Fixed receivers are stationary devices that remain independent of the plants focusing device. This eases the transport of collected heat to the power block.		
	Linear Fresnel reflector (IFR)  Curved mirrors Absorber tube and reconcentrator	Central receiver  Solar tower Heliostats
Mobile receiver		
Mobile receivers move together with the focusing device. In both line focus and point focus designs, mobile receivers collect more energy.		
	Parabolic trough  Reflector Absorber tube Solar field piping	Parabolic dish  Receiver/engine Reflector

Table 1.: The main CSP technologies families (International Energy Agency, 2014d).

As mentioned above is main difference between the CSP technology families how they concentrate the solar radiation. This strongly affects their overall efficiency. The parabolic dish has the best annual optical efficiency (about 90%) because the concentrator axis is always parallel to the sun rays. The worst (about 50%) is observed for linear Fresnel systems because of poor performance in the morning and in the evening. Intermediate values (65-75%) are obtained for parabolic trough and tower systems. For each family the actual efficiency varies with the location, the time of day and the season of the year. (EASAC, 2011)

The capacity range of an CSP-plant is also strongly affected by the concentration ratio. The most common definition of concentration ratio is the ratio of the area of reflector aperture (A_a) to the area of receiver (A_r). The area concentration is:

$$C = \frac{A_a}{A_r} \quad (2)$$

The concentration ratio from Equation 2 has an upper limit that depends on whether the concentration is a three dimensional (point focus) concentrator such as a parabolic dish and central receiver solar tower or a two-dimensional (linear focus) concentrator such as parabolic trough and linear Fresnel reflector. The maximum concentration ratio is based on the second law of thermodynamics applied to radiative heat exchange between the sun and the receiver. The maximum possible concentration ratio for circular concentrators is 45 000, and for linear concentrators is the maximum 212. (Duffie & Beckman, 2013)

Technology	Capacity range (MW)	Concentration	Peak system efficiency (%)	Annual system efficiency (%)	Thermal cycle efficiency (%)
Parabolic trough	10-280 ¹	70-100	21	10-16	35-42 ST
Fresnel reflector	10-200	25-100	20	9-13	30-42 ST
Solar tower	10-200	300-1 000	23	8-23	0-45 ST
Dish-Stirling	0.01-0.4	1 000-3 000	29	16-28	30-40

ST = Steam Turbine

Table 2.: Performance Characteristics of main CSP technologies families (Pitz-Paal. et al., 2013) (Abengoa Solar, 2013b)¹.

But actually the technical implementation of concentration ratio is the main parameter for the capacity range of a CSP plant. Table 2 gives an overview of some of the performance characteristics of the concentrating solar power concepts. More details are listed in Annexure I, Part A, Figure 53 on Page 96 and Figure 54 on Page 97. PTC, LFR, and CR can be coupled to steam cycles of 10-280 MW electric capacity (and more), with thermal cycle efficiencies of

30-45 %. Also the applies for stirling engines which are coupled to dish systems have similar efficiency ranges. The conversion efficiency of the power block remains essentially the same as in conventional-fired power plants. The annual system efficiency are the net power generation over incident beam radiation. They are lower than the conversion efficiencies of conventional steam or combined cycles, because they include the conversion of solar radiative energy to heat within the collector and the conversion of the heat to electricity in the power block. (Pitz-Paal. et al., 2013)

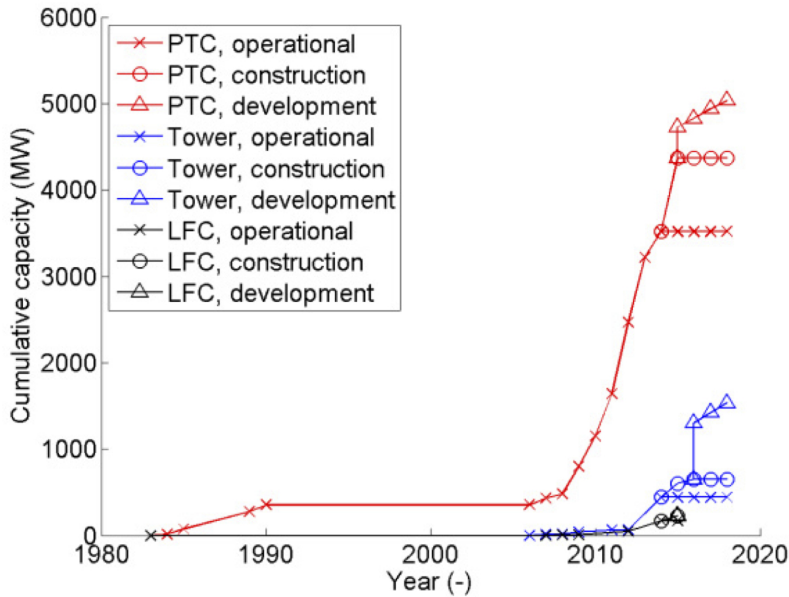


Figure 13.: Historical development of CSP technologies (Abbas et al., 2015).

The development of the actual CSP plant technology goes back in the 1970's and 1980's, which is a consequent from the first two Oil crises. Figure 13 shows the historical development of PTC, LFR in the Figure called linear Fresnel collector (LFC) and the CR (tower). The parabolic dishes have not succeeded at all and aren't shown here. The reason for that is mainly due to the high structural costs of moving an large diameter dish with two-axes tracking. One might observe that the predominant technology is the PTC, with an installed capacity well above 3 GW. CR have started the exponential development some years later compared to PTC, which explains why the operational installed capacity is much lower. Similarly the development for LFR have started even later, which drives to the lowest installed capacity of the three technologies. The difference in the timing of the three successful technologies is very influenced by the CSP development in its first golden period, the 1980's. In such period important central tower prototypes were built in USA (Solar One, Solar Two, CESA-1) and a 365 MW PTC solar plant was installed in the Mojave Desert. When the oil prices dropped at the end of the second oil crises interest on renewable energies was lost until the last decade.

With regard to the past development in the different CSP technology dealt the following chapters with the PTC (4.1.1) as well as with the solar tower technology (4.1.2). The necessary concepts

of the storage systems (4.1.4) and an overview of common heat transfer fluids (4.1.3) are also included. The systems for the converting thermal to electrical power will be also summarized (4.1.5). Parabolic dishes and LFC are not further considered depending to the development stage.

4.1.1. Parabolic-trough concentrating solar power

Parabolic trough power plants consist of many parabolic-trough-shaped concentrator that reflects direct solar radiation onto a receiver or absorber tube (also called receiver tube) located in the focal line of the parabola. The heated fluid is used in a steam generation system, to drive a steam turbine/generator cycle. Optional thermal storage and/or fossil-fired backup systems are possible. A schematic concept of a parabolic trough power plant is shown in Figure 14. The collector field is made up of a large number of single-axis-tracking parabolic trough solar collectors and receivers. The solar field is modular in nature and comprises many parallel rows of solar collectors, normally aligned on a north-south horizontal axis. The collectors track the sun from east to west during the day to ensure that the sun is continuously focused on the linear absorber tube.

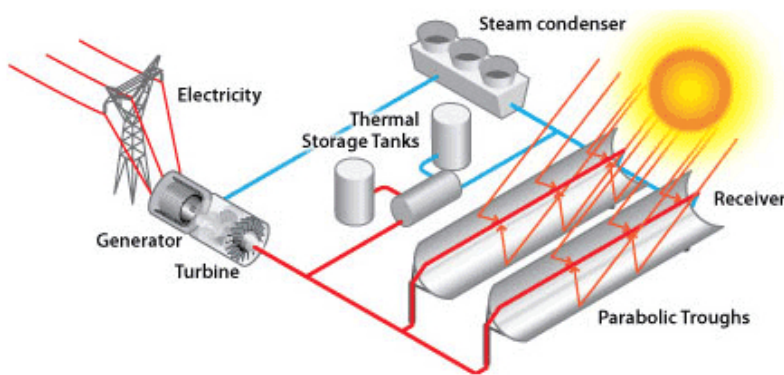


Figure 14.: Schematic parabolic trough power plant concept (U.S. Department of Energy, 2013).

The first graphically documented parabolic-trough solar collector was designed and built in 1870 by Swedish engineer John Ericsson. This collector produced 373 W by a steam engine had and had a solar radiation collecting surface of 3.25 m². (Fernández-García et al., 2010)

Current PTC are based on developments in the united states which began after the first oil crisis. In the 1980s the first commercial used PTC plants was build. Most outstanding the implementation of the nine SEGS (Solar Electricity Generating System) plants. Build from 1984 (SEGS-I) to 1990 (SEGS-IX) in the Mohave Desert (California, USA) by LUZ International Limited and still operating. In total they have an electrical output of 354 MW and more than two million square meters of parabolic-trough collectors. They using oil to produce steam in heat exchangers before being circulated back to the solar field. Like in a electricity generating plant the steam is used in a conventional steam turbine. After the cutting down of government incentives for renewable systems and the oil price fell again in the 1980s the installation of more SEGS plants went unfeasible. (Kalogirou, 2014)

But the technology is still applied in most of the present build commercial parabolic trough power plants. Today they are using as HTF synthetic oil, typically out of biphenyl/diphenyl

oxide fluid. The maximum cycle temperature is limited to values below 400 °C in order to avoid decomposition of the HTF. The thermal energy from the solar field is transported by the HTF to the heat-exchanger steam generator systems providing the superheated steam for the turbine of typically 370-380 °C. The limitation of the upper process temperature to about 400 °C can be overcome by changing the HTF. A higher process temperature leads to a significant increase in the thermodynamic conversion cycle efficiency. A summary of current applied HTFs can be found in Chapter 4.1.3.

An alternative HTF is water/steam, which is used in the steam cycle any way. The direct steam generation (DSG) in parabolic trough collectors demonstration loops steam reaches temperature of 550 °C. Aside from the process temperature, the benefits of DSG compared with oil are based on savings in the heat exchanger, in reduced pumping effort, and the uncritical handing of the medium. But there are still barriers for commercial scale application. Some of the most important technological challenges of the DSG parabolic trough plant are the control stability, receiver tube viability, and collector interconnection feasibility. (Alguacil et al., 2014)

Another alternative HTF for PTC is molten salt. Salts already proved their competence in solar tower power plants and also application of liquid salts in parabolic trough systems have been investigated. Salts has suitable thermophysical properties, namely high boiling and decomposition point, low vapor pressure, high specific heat capacity, high thermal conductivity, and high density at low pressures (Cordaro et al., 2011). Molten salt has also the advantage to be the art of science in thermal storage for large- scale CSP plants (see Chapter 4.1.4). Furthermore, typical salt mixtures are significantly cheaper than synthetic oils (Gil et al., 2010). The 5 MW Archimede commercial PTC plant is using a mixture of sodium nitrate (60%) and potassium (40%) nitrate since 2010 (NREL, 2012). The upper solar-field outlet temperature is 550 °C but starts crystallization of the non-eutectic melt occurs at 238 °C (Cordaro et al., 2011). That is one concern with molten salt-based parabolic trough plants. The solar plant needs to be fully equipped with impedance and trace heating systems in order to ensure non-freezing of the salt. Therefore also the process setup needs to be modified. But according to the researcher of the "Archimede Solar Energy molten salt parabolic trough demo plant" the molten salt parabolic trough (MSPT) technology is mature for large scale commercial applications without any critical points to be addressed (Maccari et al., 2015). Also the higher investment costs in solar field and piping, as well as maintenance and operation cost seems to be manageable and will be overcome to the increase in total plant efficiency and lower storage and HTF costs. Therefore the expected levelized cost of electricity (LCoE) of PTC power plants will decrease around 20% (Richert et al., 2015). Component manufacturers are starting to introduce products specifically aimed at this technology. Upcoming projects need to validate this expected decrease of LCoE in commercial scale and represent their profitability.

As mentioned above a PTC power plant consists out of the components collector and receiver, which held together by support structure. These components are connected in loops, which

building the solar field.

Parabolic Trough Collectors

The task of PTC module is to reflect the radiation of the sun accurately to the receiver tube. So the main components of a PTC module are actually the curved mirror and the absorber tube. But usually the PTC means the reflector and its support structure. The absorber tubes are separately regarded. The structure holds the components in place and connects the reflector modules between each other. To concentrate the radiation to the absorber tube the shape of the reflective surface is in parabolic form like in Figure 15. There shown is a section of a PTC with the dimensions of the commercial used LS-3, EuroTrough and Senertrough-1 and their focus point. This focus point is only at this position when the z-axis is in the direction of the Sun. Therefor the PTC is controlled by means of astronomical calculations, often supplemented by a Sun position sensor. The absorber tubes mounted in the focal line move with the collector and are connected to the stationary field piping via flexible hoses or rotating joint arrangements.

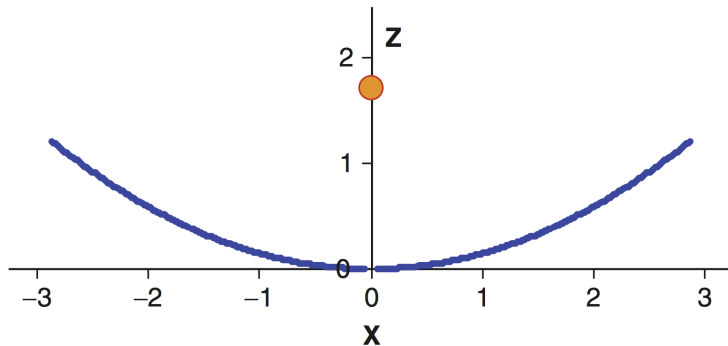


Figure 15.: PTC section dimensions of EuroTrough, LS-3, and other designs, in meters (Lüpfert, 2013).

The history of PTC goes far back to 1870, where they already used small engines with solar power (Fernández-García et al., 2010). With the time of the first oil crisis in the 1980s also new PTC were developed. In this decade also the collector family LS-1, LS-2 and LS-3 was developed by LUZ. These PCT were implemented in the first large-scale solar thermal power plants SEGS 1 (1984) to SEGS 9 (1990) in California. The used PTC features a modular design based on steel structures with parabolic preshaped, silvered glass mirrors and improved efficiency by implementation of evacuated tube receivers. A European consortium designed in the late 1990s the EuroTrough. Which was based on the LS-3 concentrator geometry with a focal length (the shortest distance from the mirror to the focal line) of 1.71 m and an aperture (the projection of the concentrator area in the direction of the optical axis) width of 5.77 m, but offered advantages in stiffness and costs (Osuna et al., 2001). Some years later, SENER developed a different structural approach, but still maintained the basics of LS-3 concentrator geometry (Fernández-García et al., 2010).



Figure 16.: Solar Collector Assembly (SCA) composed of 12 EuroTrough collector elements (SCE) (Von Reeken et al., 2014).

PTC are typically assembled from solar collector element (SCE), mounted on a series of aligned pylons. The center pylon is equipped with a hydraulic drive system to allow tracking of the total solar collector assembly (SCA). Figure 16 shows the SCA of the EuroTrough. From 12 SCE of the SCA results a total length of approximately 150 m and 816 m² (Von Reeken et al., 2014).

Table 3 illustrates that recent developments show a continuing trend towards larger aperture sizes such as for the Heliotrough, Senertrough-2 and Ultimate Trough. The development steps of the aperture size are exemplary shown in Figure 17 for EuroTrough, Heliotrough and Ultimate-Trough.

Property	LS-1	LS-2	LS-3	Euro-Trough		Helio-trough		Sener-trough-	Sener-trough-	Ultimate-Trough
				Trough	trough	trough	trough	trough	trough	
Start of development	1984	1985	1989	1998	2005	2005	2006	2005	2006	2009
Aperture width [m]	2.55	5.00	5.77	5.77	6.78	5.77	6.87	7.51		
Length per module/SCE [m]	6.3	8	12	12	19	12.27	13.23	24		
SCA length [m]	50.2	47.1	99	147.8	191	n.a.	158.8	242.2		
Focal length [m]	0.68	1.40	1.71	1.71	1.71	1.71	2	n.a.		

Table 3.: Characteristics of different parabolic trough collectors (Pitz-Paal. et al., 2013).

The use of larger collector units with more aperture area brings some advantages. The Ultimate Trough shows a cost reduction of about 20 to 25% compared to the EuroTrough. Coming from lower specific costs and increased optical performance. Also the amount of heat transfer fluid can be reduced by 25%. This promises a decreased LCoE by about 11% compared to EuroTrough. (Von Reeken et al., 2014)

Another approach to reduce costs is the utilization of other reflector materials. The Skytrough uses reflectors made from silvered polymer film laminated to aluminum sheets mounted on a space frame. Compared to the costs of components of the EuroTrough, the Skytrough contributes an additional 34% cost savings in combination with an aperture width of 6.0 m (Mason & Reitze, 2014). Thin glass on a glass-fiber/foam sandwich was used for the SL4600 construction (Solarlite CSP Technology GmbH, 2014). Both approaches take advantage of the mechanical strength of the mirrors to reduce the amount of additional steel structure required.

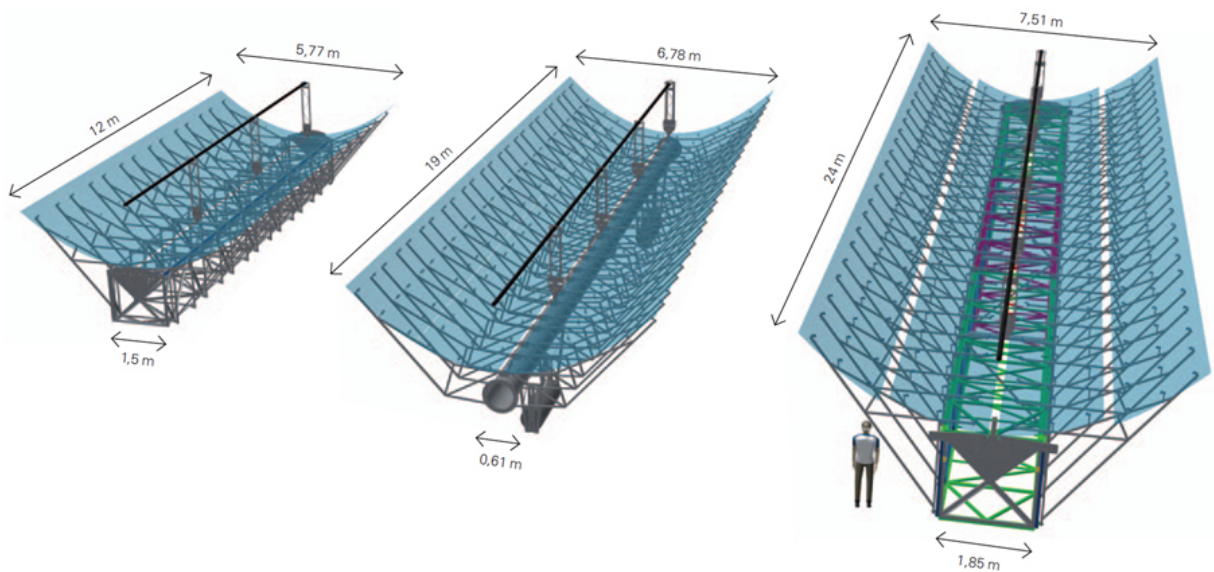


Figure 17.: Evolution of parabolic trough collector sizes over 3 development cycles (Eurotrough, Heliotrough, Ultimate Trough)(bergermann und partner, 2010).

Abengoa Solar is developing currently the "SpaceTube" concept, using 8 m aperture width and will use 80 mm diameter absorber tubes. (Abengoa Solar, 2013a)

Absorber tube (Receiver)

The absorber tube or also called receiver is the component where solar energy is converted to thermal energy in the form of sensible or latent heat of the fluid that circulates through it. This component produces the predominant share of thermal losses in an parabolic trough power plant, for that reason it is also one of the most critical and important performance components (Lüpfert, 2013). Currently, there are just two types of receiver for parabolic trough power plants, classified as either evacuated or non-evacuated. Evacuated receivers are commonly used for temperatures above 300 °C and its consist of three main parts. The metal absorber tube, an protection glass tube and the connection unit with expansion bellows. In order to reduce thermal losses and increasing the overall efficiency of the PTC the receiver unit uses a high vacuum (i.e., 10-5 mbar) between the metal absorber tube and the protection glass. Figure shows 18 the structure of an typical vacuum tube receiver.

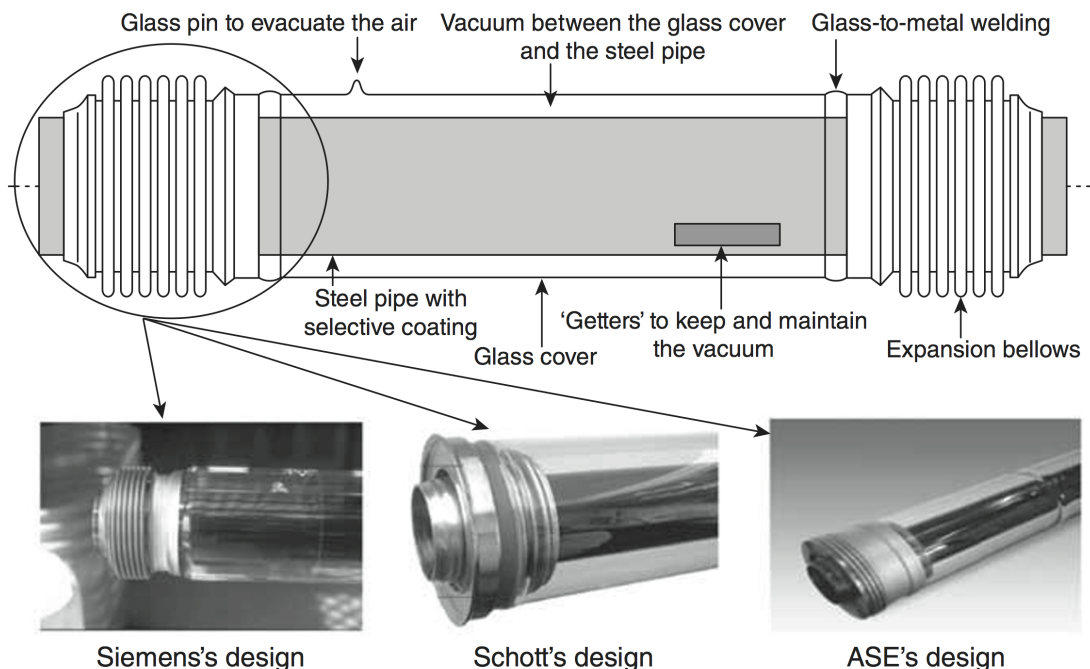


Figure 18.: A typical evacuated receiver for parabolic-trough collectors (Moya, 2012).

The metal absorber tube is a dark-coated to absorb the incoming solar radiation. It absorbs the concentrated radiation reflected from the mirror, and also the global radiation hitting from top. The outer surface of the metal absorber tube has an optically selective surface with a high solar absorptance and low emittance for thermally generated infrared radiation. This is achieved with sputtered Cermet coatings consisting of several layers of metallic and ceramic coatings. Also, galvanic black-nickel and black-chrome coatings are applied but have less temperature resistance and higher emissivity. (Platzer & Hildebrandt, 2012)

The protection glass is connected to the metal absorber tube by means of stainless steel expansion bellows. These bellows compensate the thermal expansion of glass and steel which results at nominal working temperature. Therefore one end of these expansion bellows is directly welded to the outer surface of the metal absorber tube, while the other end is connected to the end of the protection glass by means of a glass-to-metal welding. The glass-to-metal welding is a weak point in the absorber system and has to be avoided by high thermal and mechanical stress that could cause the welding to crack. The receiver provider has various solutions for the expansions bellows. Figure 18 shows also the solutions of three manufacturers (Schott, Siemens and ASE) joining the protection glass and the inner metal absorber tube. The expansion bellows also provide a tight annular gap between both tubes to make the vacuum. To support the shelf life of the vacuum chemical getters can be placed in the gap between the metal absorber tube and the protection glass to absorb gas molecules.

	Schott PTR-70	Siemens UVAC-2010	ASE HEMS08
Solar absorptance	≥ 0.95	≥ 0.96	≥ 0.95
Solar transmittance	≥ 0.96	≥ 0.96	n.a.
Thermal emittance	≤ 0.1 at 400°C	≤ 0.9 at 400°C	≤ 0.1 at 400°C ≤ 0.14 at 580°C
Steel pipe inner/ outer diameters	70/65 mm stainless steel	70/65 mm stainless steel	70/65 mm stainless steel
Thermal losses	250 W/m at 400°C	n.a.	230 W/m at 400°C
Glass cover	Borosilicate	Borosilicate	Borosilicate
Active length ratio at 350°C	>96%	96.4%	n.a.
Maximum fluid tem- perature	400°C	400°C	550°C

Table 4.: Technical parameters of the receivers commercialized by Schott, Siemens and ASE (Moya, 2012).

Most of the parabolic-trough solar thermal power plants implemented around the world until 2009 had receivers manufactured by either the Israeli company, Solel (purchased in 2009 by Siemens and 2013 from Abengoa (Alcauza, 2013)), or the German company, Schott. In 2009, the Italian company, Archimede Solar Energy (ASE), announced that they were launching a new receiver tube called HEMS08, suitable for fluids up to 550°C . The first plant using HEMS08 receivers was the Archimede Plant, located in Syracuse (Italy) and ready to operate in 2010

using molten salt as HTF. Most widespread geometry is the receiver, with 70 mm absorber tube diameter, but due to larger aperture width of the trough reflectors, also the absorber tube diameter is raising. The technical details of the receivers manufactured 2012 by Schott, Siemens and ASE are shown in Table 4. Schott's PTR-70 is now in the 4. generation, the actual UVAC 70-7G is now in production by Rioglass a subsidiary from Abengoa Solar and ASE's present molten salt receiver tube is the HCEMS-11, but in generally the technical parameters are still up-to-date (Schott, 2015; Archimede Solar Energy, 2015; Rioglass Solar International, 2014).

Most widespread geometry is the receiver, with 70 mm absorber tube diameter, but due to larger aperture width of the trough reflectors, also the absorber tube diameter is raising. This is a further contribution to using molten salt as future HTF in large-scale PTC power plants.

Field

The heat-collecting portion of the PTC power plant is the solar field. It consists of one or more parallel loops of SCAs. A common header pipe provides each loop with an equal flow rate of HTF. A second header collects the hot HTF to return it either directly to the power cycle for power generation or to the thermal energy storage system for use at a later time. To minimize pumping pressure losses, the field is typically divided into multiple sections, each section with its own header set, and the power cycle is situated near the middle of the field. The size of the field depends on required thermal power for the power block and the storage system. The orientation of the field depends obviously on the orientation of the parabolic collectors, which are installed with their north-south oriented rotation axis. Figure 19 shows one example plant

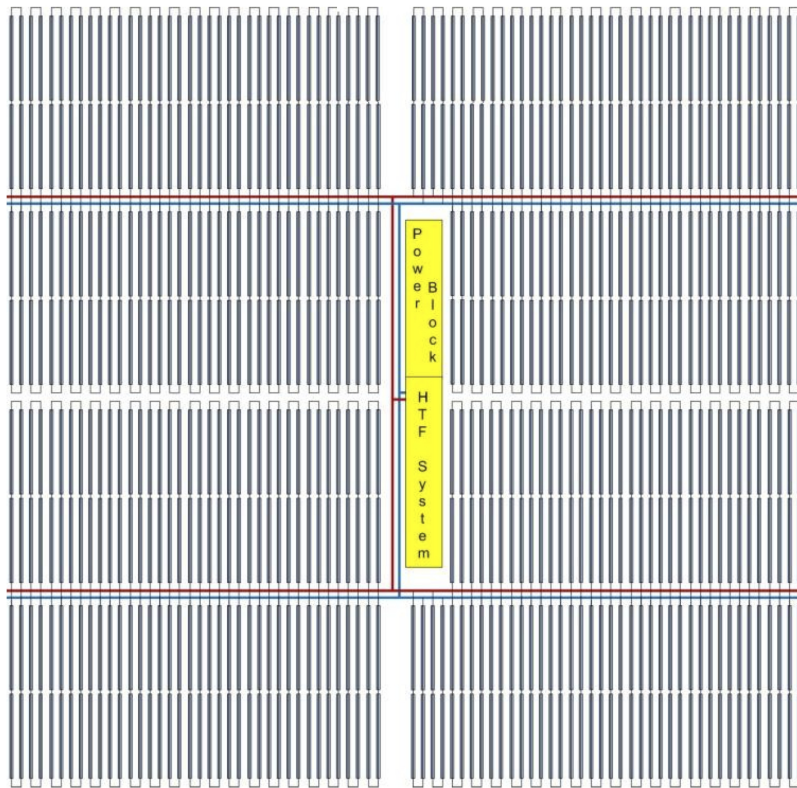


Figure 19.: Example of EuroTrough collector field layout with 152 loops (Von Reeken et al., 2014).

layout for where 152 total loops are used, each loop with four SCA. The loop length depends on heat transfer fluid properties and rise in temperatures between inlet and outlet temperature (ΔT). The flow rates through the receivers must be high enough to ensure appropriate heat removal from the absorber walls and low enough to keep pumping power for the fluid reasonably low.

Current stage of commercial scale PTC power plants

On the commercial scale the "Solana Generating Station" is currently one of the world largest PTC power plants. It was built from December 2010 to October 2013 southwest of Phoenix, Arizona. The solar-field aperture area of $2\ 200\ 000\ m^2$ concentrates in 808 loops with 4 SCA per loop drives two 140 MW_{el} turbines. This plant uses synthetic oil as HTF and has a storage capacity of 6 h in molten salt (described in Chapter 4.1.4). The fed-in tariff of approx. 944 GWh/a is fixed for 30 years. The costs of the plant were approx. 2 USD billion. This power plant constitutes the current state of art in commercial scale PTC systems. (NREL, 2015a)



Figure 20.: 280-MW Solana PTC power plant near Phoenix, Arizona (Abengoa Solar, 2013b).

4.1.2. Central tower concentrating solar power

Central receiver systems (CRS) use a large number of reflectors (heliostats) to concentrate direct solar radiation to a focal point, in most cases on top of a tower. In order to reflect the incident sunlight to the focal point, the heliostats are tracked in two dimensions. The receiver is located at the focal point. The receiver absorbs the concentrated solar radiation and heats a HTF, such as a liquid or a gas. The generated heat drives a turbine to produce electricity by a generator. The basic principle of a solar CR power plant is shown schematically in Figure 21. Average concentration levels on the receiver are typically in the range 500-1 000 kW/m² (Pitz-Paal. et al., 2013). This concentration level is significantly higher than those achievable in linear focus systems such as PTC systems. The higher concentration level enables higher operational temperatures in the receiver, while maintaining good thermal efficiencies.

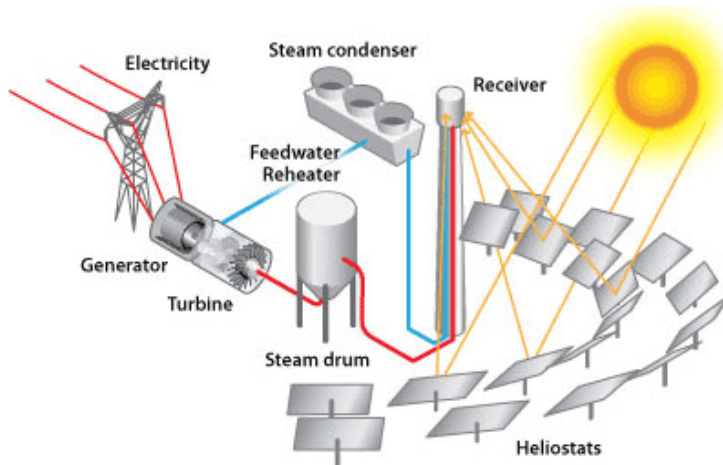


Figure 21.: Schematic CR power plant concept (U.S. Department of Energy, 2013).

A variety of solar tower concepts exist or are under development. These concepts differ mainly in the type of heat transfer medium, which dominates the layout and selection of all other components except for the heliostat field. Liquid or gaseous HTFs are state-of-the-art in solar tower technology. Water/steam, molten salt, and air are typical fluids (Pitz-Paal. et al., 2013). A HTF in a central receiver absorbs the highly concentrated radiation reflected by the heliostats and converts it into thermal energy to be used for the subsequent generation of superheated steam for turbine operation. The different HTF mediums are described in chapter 4.1.3. Not like the more or less uniform design of PTC systems is the optical design and optimization of CRS more complicated. A multitude of variables one must be consider such as the continuous variation in configuration and performance of each of the heliostats as they track the sun and interact with one another.

The first documented concept of using ground-based segments (heliostats) to reflect direct-beam sunlight on a receiver comes from the Russian Victor Baum (Baum et al., 1957). But at this point no experimental device was built.

After several central receiver concepts and first 'commercial' used heliostats (Trombe, 1957), Alvin Hildebrandt published in 1972 the basic concept of nowadays CR systems as a hemispherical or cylindrical receiver atop a tall tower surrounded by a field of carefully positioned heliostats. The described power plant should have a tower height of 450 m with an heliostat field of 1.8 km diameter and produce 565 MW_{th} . There were no technical impediments expected with the tower or heliostat field. (Hildebrandt et al., 1972)

Outgoing from more basic concepts and further research the Solar One, a 10 MW_{el} CR pilot plant was operated successfully from 1982 to 1988, in the desert near Barstow, California. This facility used a cylindrical receiver with water-steam as HTF at the focal point in 76 m height. The tower was surrounded by 1 818 heliostats, each with almost 40 m^2 area. After several problems in terms of storage and continuous turbine operation, the Solar One was upgraded to the Solar Two using molten salt as HTF and as direct storage concept. The Solar Two operated from 1996 to 1999 pumping molten nitrate salt at 290°C from a cold storage tank through the receiver, where it was heated up to approximately 565°C and afterwards to a storage tank, which had a storage capacity of 3 h. A simplified scheme of the Solar Two system is shown in Figure 32 on Page 46. (Reilly & Kolb, 2001)

The Planta Solar 10 (PS10) is the first solar central-receiver system producing grid-connected electricity under a purely commercial approach and started generating 11 MW_{el} in 2007 near Seville, Spain. 624 heliostats with surface area of 120 m^2 each, concentrates direct irradiance to a cavity receiver using saturated steam as HTF on top of a 115 m high tower. The function of the PS10 is schematically shown in Figure 22.

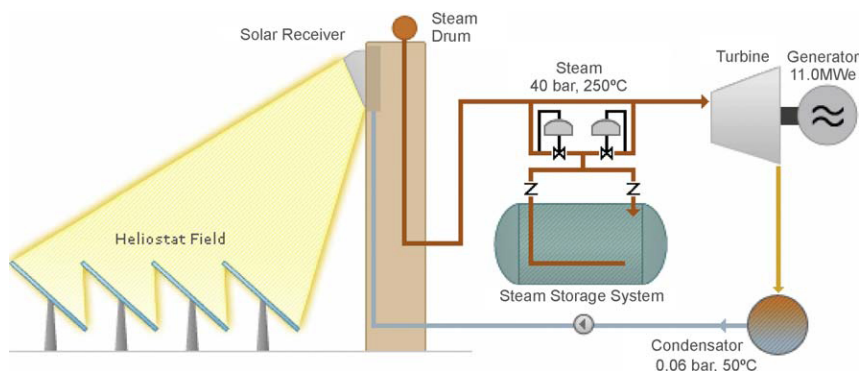


Figure 22.: Schematic diagram of the PS10 solar tower using water/steam as HTF (Medrano et al., 2010).

The first commercial solar thermal power plant to supply uninterrupted power for a full 24 h is the 19.9 MW_{el} Gemasolar power plant, which started operation also near Seville in 2011. 2 650 heliostats focusing on the tube receiver on top of a 140 m height tower. The molten salt, which is used as HTF and for storage, reaching temperatures of 565°C .

Current commercial planned large-scale CR power plants are based on the PS10 and the

Gemasolar power plant. Their main components are the heliostats and their field design, the receiver, and the tower itself. These are described below. Chapter 4.1.4 examined the storage possibilities.

Heliostats

Current heliostat technology differs mainly in the area of the reflecting surface. Studies of the heliostats area reaches from 1.1 m^2 up to 320 m^2 (Tyner & Wasyluk, 2014; Blackmon, 2012). One of the largest heliostats in commercial application will have a total area of 140 m^2 (Abengoa, 2014) and are built of several smaller facets, mounted on a back structure. Classical heliostat design is dominated by mirrors brought into position by steel structures and drives that guarantee high accuracies under wind loads and thermal stress situations. To the structures that hold the mirrors include struts, beams, the pylon, and the foundation. The linear actuators enable moving of the heliostat in two dimensions. There exists a zenith and an azimuth actuator together with their step motors. The orientation of the rotation axes may also differ between heliostat types. Several different types of heliostat mirrors exist. They can be differentiated according to size, shape, basic design concept, or even according to their tracking system. Each heliostat type has its own characteristics in terms of wind-performance and tracking during windy conditions, costs, and complexity of control. A field made up of more small heliostats will require a more complex control system than a field of fewer heliostats. Therby, large heliostats are mostly more cost-efficient than small ones (see Figure 23). Improvements in controllability may cause this to change, however, and several companies are attempting the strategy of many small heliostats as opposed to fewer large heliostats.

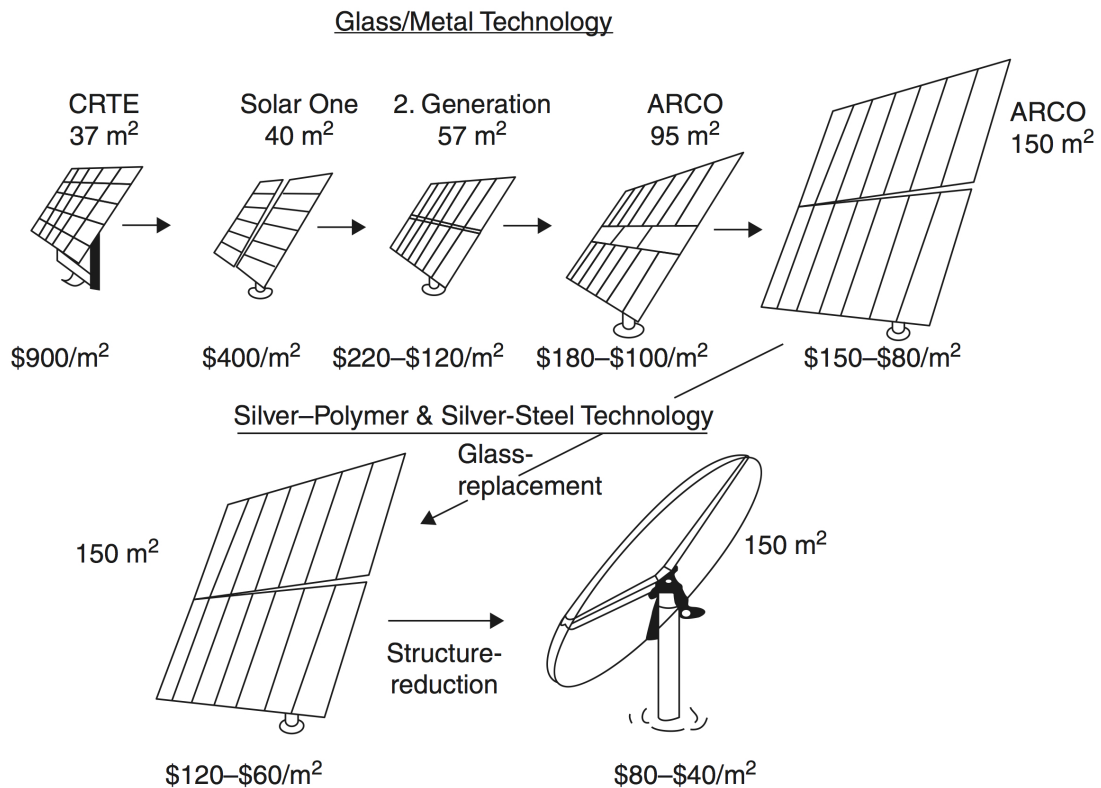


Figure 23.: Heliostats used in solar power plants and their costs (Kolb et al., 2007).

Heliostat field design

The heliostat field layout is a complex topic. Decisions regarding the best position for locating heliostats relative to the receiver and how high to place the receiver above the field constitute a multifaceted problem, in which costs and heliostat loss mechanisms are among the variables, and which is solved by an iterative process. Therefore the location and the receiver type is decisive. In the northern hemisphere, the position of the sun is to the south of the plant and the field must be placed to the north of the tower. In the southern hemisphere the opposite is true. The general terminology for this position would be the "polar side" of the tower, which can be applied to towers in both the northern and southern hemispheres. The opposite side of the tower is the "equatorial side" (Alexopoulos & Hoffschildt, 2013). The basically distinguishable field design types are shown in Figure 24 and can either surround the tower (Surround-field) for larger systems or be spread out on the shadow side of the tower (Polar-field) in the case of smaller systems. With a field on only one side of the tower, a cavity receiver is usually used.



(a) Polar-field layout.

(b) Surround-field layout.

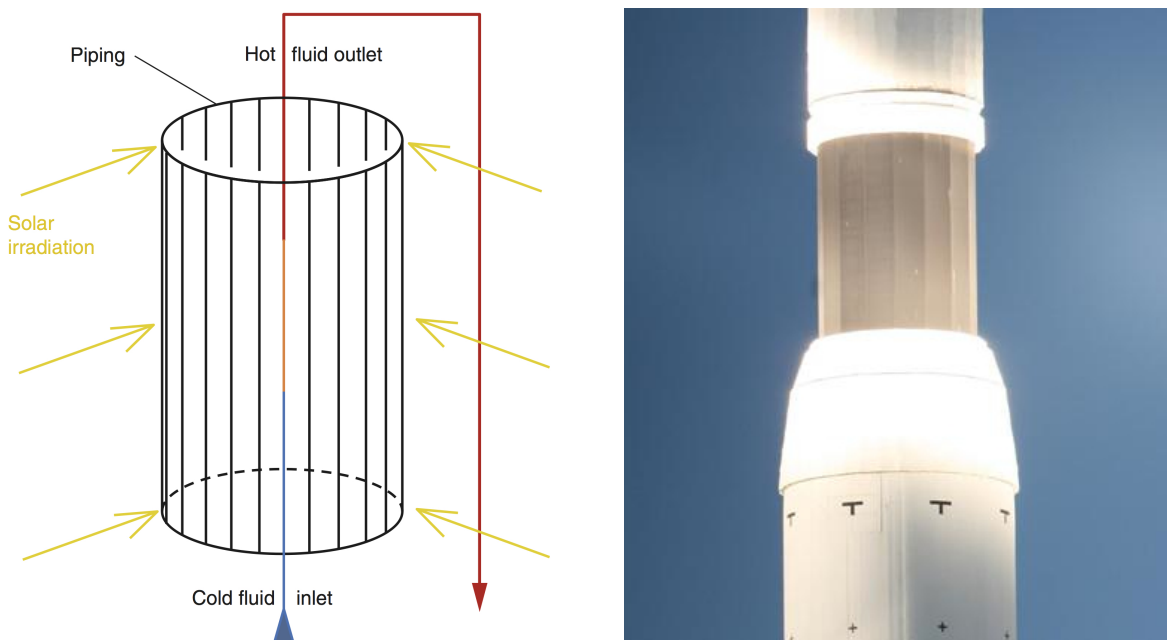
Figure 24.: Basically distinguishable field design types (Kulichenko & Wirth, 2012).

Close to the equator, where the sun passes directly overhead, a surrounding-field can be used in combination with an open receiver (Tube receiver, see below). Another possibility is the use of two or three fields one on either side of the tower, in combination with a cavity receiver for each side (see Figure 26b). With higher power levels, surround field layouts are usually more economical. The higher the site latitude of a plant (i.e., the further away from the equator), the more the heliostat field tends to be shifted polewards. When laying out a heliostat field there are several types of losses that must be considered. These are not only the optical losses, so called, the cosine losses and losses due to shadowing, blocking, spillage (reflected radiation miss the receiver surface), and atmospheric attenuation, but also technical considerations, that is, the mirror reflectivity, mirror surface defects, tracking accuracy, wind load, and tower oscillations (due to wind load) as well as the heliostat fault rate. The aim in the designing of a heliostat field is to reliably produce the power required by the power block whilst keeping land usage and total costs to a minimum. (Vant-Hull, 2012)

Tower and receiver

The function of the tower is to positioning the receiver in the required height above the heliostat field. So the choice of tower constructions depends primarily on the required height of the tower. But the height of the tower is limited by its cost. Towers are mainly constructed of steel or reinforced concrete.

The function of a receiver is to absorb the concentrated solar irradiation energy impinging from the heliostat field and transfer it to the working fluid. Requirements to a solar receiver include high thermal conductivity, dark color of the body for high absorptivity, and temperature resistance. According to Prof. Dr. Hoffschmidt (Hoffschmidt, 2014) from the German aerospace center (DLR) there are actually two main receiver types state of art for CR power plants, which uses molten salt and water for direct steam generation: external (tube) receiver and cavity receiver.



(a) External tube receiver concept (Alexopoulos & Hoffschmidt, 2013). (b) External tube receiver implemented in Gemasolar power plant (Microthermő, 2012).

Figure 25.: External tube receiver concept and example of application.

An external receiver consists a large number of vertically arranged pipes or flat plates through which the HTF is pumped in upward direction. There are variations of shapes for the external receiver, mostly cylindrical or square-shaped. The tubes in the receiver can be crosswise arranged with different zones for pre-heating, evaporation and superheating (in case of super heated steam). Typical solar heat fluxes in this type of receiver are up to 1 MW/m^2 (Pitz-Paal. et al., 2013). An basic concept for an external receiver is shown in Figure 25a with a cylindrical shape. An example for such a external tube receiver is the receiver of the Gemasolar power

plant, that used molten salt as HTF. The receiver consists of a great number of HTF pipes. The external receiver pipes are fixed vertically whereby the salt smelt is pumped in upward direction. The receiver outlet temperature of the molten salt is approximately 565 °C. The tube receiver of the Gemasolar power plant is shown in Figure 25b. An other example is the Ivanpah Solar Electric Generating System (ISEGS) in California's Mojave Desert where they produce direct steam at 550 °C using an external tube receiver which is square-shaped. A disadvantage for using the pipe receiver is the high reflection loss which is higher than for other receiver types. One way to reach reduction of thermal losses is an cavity arrangement and a face down arrangement. (Hoffschmidt, 2014)

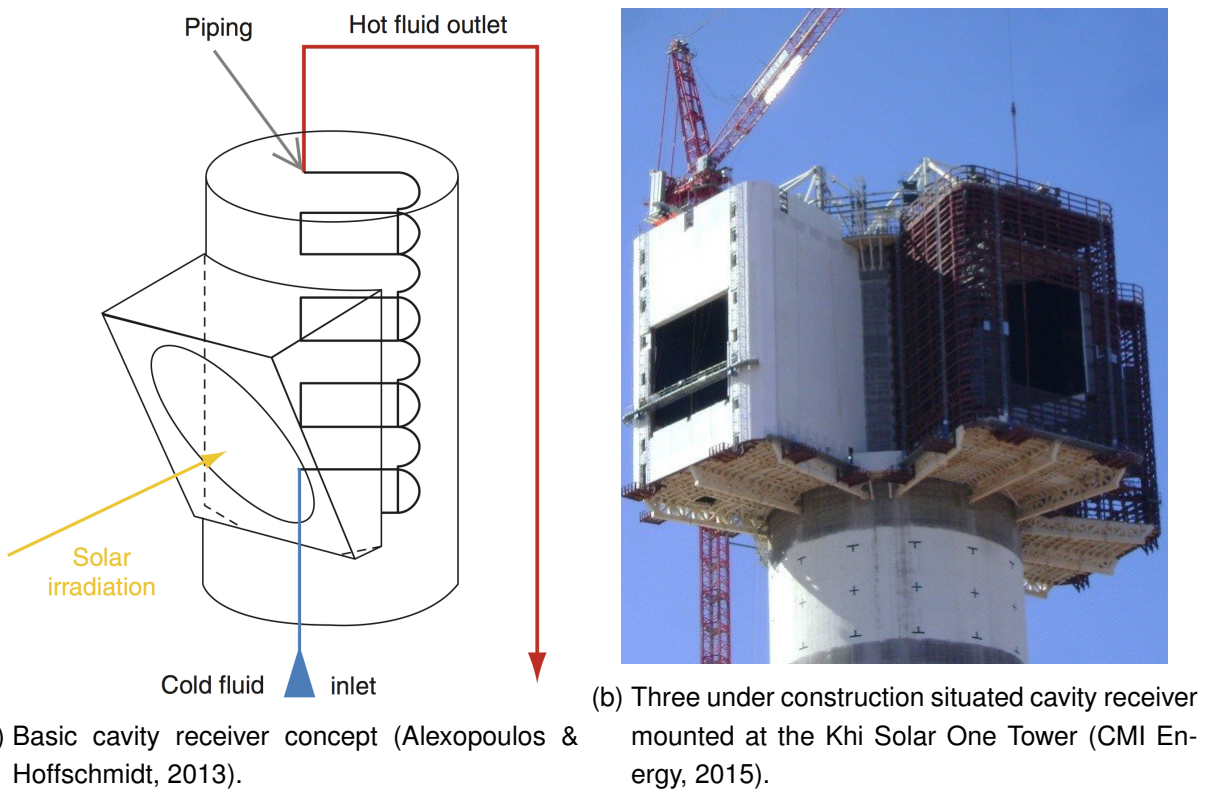


Figure 26.: Cavity receiver concept and example of application.

A cavity receiver consists of a cavity with a small opening where the receiver is located. The concentrated solar irradiation is directed into the small opening where it impinges on tubes carrying the working fluid. The idea of the cavity receiver is the reduction of thermal and optical losses. From the radiation entering the inlet aperture, only small amounts are reflected back into the atmosphere through the inlet aperture. Figure 26a shows the basic concept of a cavity receiver. The cavity receiver concept is implemented in the PS10 solar tower plant in Spain. The direct irradiated absorber tubes is basically a forced circulation radiant boiler with low ratio of steam at the panels output, which produce saturated steam at 250 °C and 40 bar. A schematic diagram of the PS10 is shown in Figure 22. A first solar power tower will also use a cavity receiver technology. Figure 26b shows the three under construction situated cavity

receiver of the Khi Solar One. Two steam generator (east and west orientated) and one super heater (south orientated) using the cavity receiver concept are external mounted on the tower (Prof. Dinter, 2015).

Current stage of commercial scale CR power plants

As shown above there is a variety of CR concepts also for commercial scale. But there are three outstanding CR projects worth mentioning for large-scale commercial application. The Khi Solar One, the Ivanpah Solar Electric Generating System (ISEGS) and the Atacama-1.

Fore SA obviously the Khi Solar One, which will be the first commercial scale CR power plant in the country. This 50.0 MW_{el} power tower is under construction and will be operated by Abengoa Solar. The Polar-field consists out of 4 120 heliostats with a reflection surface of 140.0 m^2 each concentrate direct solar irradiance on three cavity receiver. (NREL, 2014b; Prof. Dinter, 2015)

The Ivanpah Solar Electric Generating System (ISEGS) is currently the largest CSP plant operating by BrightSource. The three-unit power system with in total 377.0 MW was started operation 2014 in Ivanpah Dry Lake, California. The three external square-shaped receiver on each tower are focused by 173 500 heliostats with a aperture area of 15.0 m^2 each. The costs for the power plant which consists out of three CRS are approx. 2 200 USD million. But instead of an storage system BrightSource using a natural gas fired backup for the ISEGS. (BrightSource Energy, 2014; NREL, 2014a)

One of the highly promising CR projects for large-scale commercial application is Abengoa Solars Atacama-1. The eponymous Atacama desert in Chile, where the plant is under construction, has the highest levels of solar radiation worldwide. The scheduled operation start of the plant is in 2018. 10 600 heliostats each 140 m^2 in aperture area will concentrate on a external cylindrical shaped receiver with 32 m in height and 19 m in diameter. The receiver will be positioned in a 243 m-tower to heat molten salt to drive a 110 MW_{el} steam turbine and 17.5 h direct thermal storage. This will generate electricity 24 h per day, similar to the Gemasolar power plant, but more than five times that powerful. This project constitutes the current state of art in commercial scale CRS. (NREL, 2015a; Abengoa Solar, 2015b; Abengoa Solar, 2015a)

4.1.3. Heat transfer fluid

In each CSP family, various options exist for the heat transfer fluid, the storage technology, and the thermodynamic cycle. The heat transfer fluid (HTF) removes heat from the receiver and transfer it either to the storage system or to the final use. The correct choice of the fluid is determinant in order to reduce costs and increase the efficiency of the plant. The most important HTFs are:

- **Synthetic oils** They are used predominant in PTCs thanks to their low pumping losses, their adequate conductivity and the fact that they do not need very high pressures, around 16 bar. However, they face a temperature limit of 393 °C, which limits the efficiency of the plant. In addition, they are toxic and flammable.
- **Direct steam generation** If saturated or superheated steam is generated directly at the receiver two main advantages are found: first, no heat exchanger is required in order to generate steam from the HTF and second, the exergy loss that takes place at such heat exchanger is avoided. However, some issues are also found: high pressures are required, which makes it not suitable for PTC's due to leakages at the movable elements, different thermal regimes are found in the steam generation, which complicates transients and superheating, and no efficient method has been found for energy storage. This last point is a main issue, especially when the importance of dispatchability is considered.
- **Molten salts** Molten salts are playing a great role in CSP for energy storage. The most commercial molten salts have a working temperature range from 290 °C to 565 °C, and thus higher efficiencies are obtained at the power block (cf. Table 5). However, they have the issue of solidifying at relative high temperatures. As a result, if the receiver cannot be evacuated when there is no impinging sun, which is the working mechanisms in central towers with molten salts, the fluid must be recirculated from the hot tank to the cold tank, increasing thermal energy losses. Evacuation of linear receivers seems more difficult than in central towers due to the fact that tubes are horizontal.
- **Pressurized gasses** Gasses do not have any limit in temperature, neither by the upper nor by the bottom part. In addition, they are cheap, especially if the air is used as it is found in the atmosphere. However, pumping losses are much higher than in liquid HTFs due to the density difference. In order to overcome this issue, pressure must be increased, pumping power losses being inversely proportional to the squared power of the pressure. At current time no commercial power station uses pressurized gases, although they have been used in central tower (Solgate) and CCP research prototypes. Leakages of the gas found in the movable elements of PTCs due to the high pressures suggest the need of fixed receivers in order to use pressurized gasses.

4.1.4. Storage systems for CSP

The storage systems plays the decisive role that makes solar thermal power stand out from other renewable energy technologies. By the integration of heat storage capacity, STP plants are actually the only operational renewable energy option on the market offering dispatchable electricity power generation in multi-MW range. With the thermal energy storage (TES) system a CSP power plant offers the advantage of an integrated solution, which does not impose additional requirement on the electrical grid. Figure 27 shows the general scheme to store thermal energy into a CSP plant. The storage unit is connected both to the solar receiver and the power block. During charging the heat (high enthalpy mass flow) from the solar receiver is transferred to the thermal cycle, while the storage unit is charged by excess thermal heat. During the discharge process, the working fluid of the power block is heated by the energy from the storage systems. Alone or in combination with some fossil fuel backup, the storage system keeps the plant running under full-load conditions. The energy from the storage might be also used to preheat the collector system during the ramp up time of the power plant. From a technical point

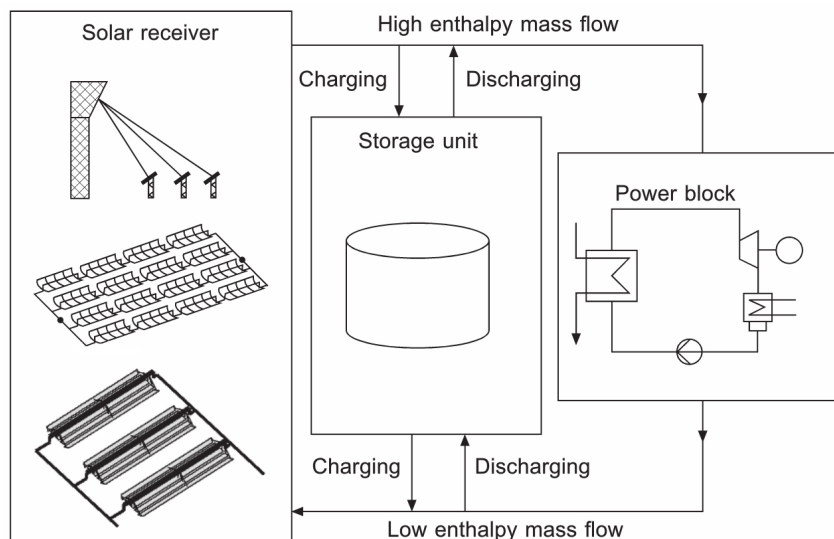


Figure 27.: Scheme for CSP plant with integrated storage unit (Steinmann, 2015).

of view, the storage must have high energy density, good heat transfer between the heat transfer fluid (HTF) and the storage medium, mechanically and chemically stable storage media, compatibility between the heat exchanger, heat transfer fluid and storage medium, complete reversibility, and minimum thermal losses. Actually, there are just four commercial used TES in CSP plants integrated (see below). But in generally a TES system, can store heat in the form of sensible, latent, or thermochemical energy. Latent and thermochemical based TES systems are still in the phase of research and development (Steinmann, 2015).

In Figure 28 is on one site the more basic concepts for a direct storage shown, which use the same working fluid for the storage system and the solar receiver and on the other site indirect

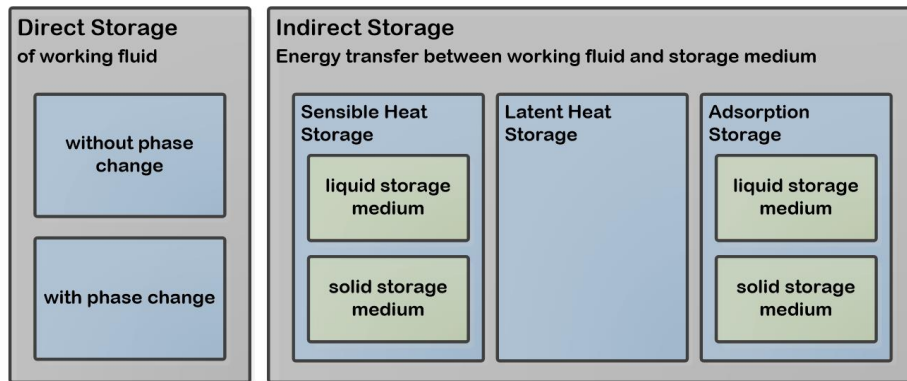


Figure 28.: Basic storage concepts for CSP systems.

systems transferring energy to a separate storage medium. The various storage concepts show different states of maturity. These commercial integrated storage systems and their application range will be described in the following (Steinmann, 2015):

- Direct storage of heat transfer oil (Direct Storage of Liquid Working Fluid)
- Indirect molten salt storage units (Indirect Storage in Liquid Media)
- Steam accumulators (Direct Storage with Phase Change)
- Direct molten salt storage units (Direct Storage of Liquid Working Fluid)

According to the "Technology Roadmap - Energy storage" of the International Energy Agency from 2014, alternative storage concept like heat storage with phase changing materials (PCM), thermochemical energy storage, and waste heat utilisation methods offer many potential opportunities. However, these technologies will need to overcome containment vessel design and material stability challenges at very high temperatures before they can achieve widespread deployment and will not be further described or discussed here. (International Energy Agency, 2014b)

Likewise alternative concepts in liquid storage media such as dual media concepts (thermo-cline) and floating barrier concepts are still in the phase of research and development and will not be further described.(Steinmann, 2015)

In the following sensible liquid media will be described. Therefore the physical principles of heat storage systems are necessary. The amount of heat, Q (in J), which can be stored in liquid sensible systems and the density, E (J/m³), related with this process can be calculated using the following equations:

$$Q = m * C_p * (T_{out} - T_{in}) = m * C_p * \Delta T \quad (3)$$

$$E = \rho * C_p * (T_{out} - T_{in}) = \rho * C_p * \Delta T \quad (4)$$

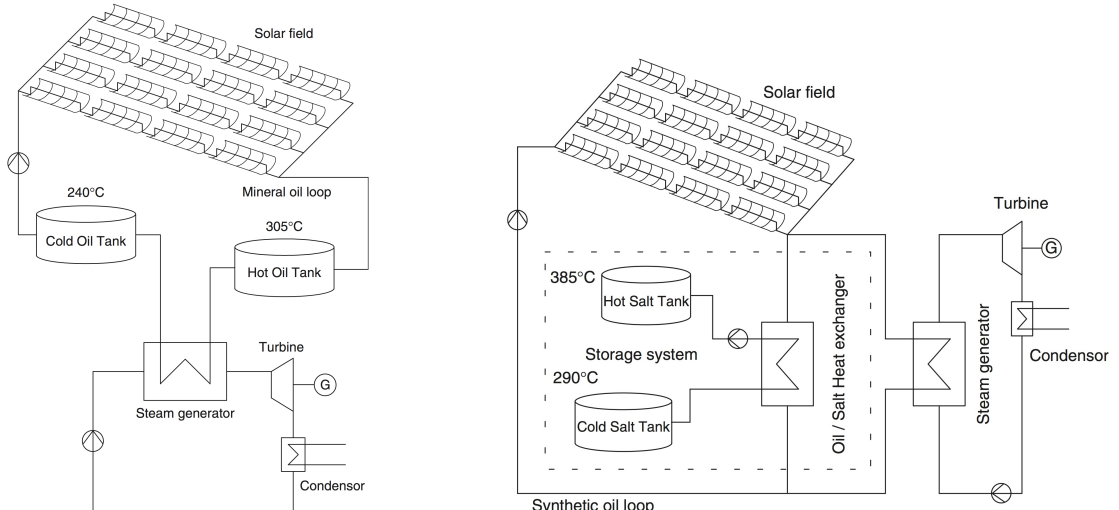
where T_{in} and T_{out} are inlet and outlet storage system temperatures, respectively [K], m is mass of storage liquid media [kg], ρ is density [kg/m^3], and C_p is specific heat capacity [$\text{J}/(\text{kg} \cdot \text{K})$]. Analyzing equation 3 and 4, it can be concluded that an optimum liquid sensible storage material must present high heat capacity, C_p , and a wide range of thermal stability, ΔT . Different fluids have been studied as HTF and liquid sensible storage media (Gil et al., 2010) and are shown in Table 5. (Ushak et al., 2015)

Storage medium	Temperature		Average density (kg/m^3)	Average thermal conductivity ($\text{W}/(\text{m K})$)	Average heat capacity ($\text{kJ}/(\text{kg K})$)	Volume specific heat capacity (kWh_t/m^3)	Media costs per kg (US\$/kg)	Media costs per kWh_t (US\$/ kWh_t)
	Cold ($^\circ\text{C}$)	Hot ($^\circ\text{C}$)						
HITEC solar salt	120	133	—	—	—	—	—	—
Mineral oil	200	300	770	0.12	2.6	55	0.30	4.2
Synthetic oil	250	350	900	0.11	2.3	57	3.00	43.0
Silicone oil	300	400	900	0.10	2.1	52	5.00	80.0
Nitrite salts	250	450	1825	0.57	1.5	152	1.00	12.0
Nitrate salts	265	565	1870	0.52	1.6	250	0.50	3.7
Carbonate salts	450	850	2100	2.0	1.8	430	2.40	11.0
Liquid sodium	270	530	850	71.0	1.3	80	2.00	21.0

Table 5.: Main characteristics of sensible heat storage liquid materials (Gil et al., 2010).

Direct storage of heat transfer oil

The simplest concept to implement a TES into a CSP plant is the direct storage of the working fluid which is circulated through the solar absorbers. The first commercial used parabolic trough power plant SEGS-1, built 1984 in California, uses a mineral oil as heat transfer medium in the absorbers, which heats up from 240°C to 305°C . The heat from the terminal oil was used to generate a power of 13.8 MW through the Steam-electric power block. Two 4 700 m^3 carbon steel tanks were used to separate the cold from the hot oil. This made a thermal storage capacity of 120 MWh_{th} possible and allowed the system generate electricity for three hours. The storage system of the SEGS-1 was destroyed by a fire in 1999 and was not replaced. Figure 29a shows a simplified scheme of the SEGS-1 parabolic trough plant and their direct storage of heat transfer fluid. Mineral oil is today not considered to be an attractive medium for TES in large-scale CSP applications. The capital costs for large oil volume are substantial and needs additional investments for possible environmental hazards like oil leaks. Also the maximum operational temperature fore mineral oil is below 340°C , which restricts the efficiency of the thermal process. Present solar through power plants are using a synthetic heat transfer fluid whose costs are significantly higher (cf. Table 5). Also increased the maximum temperature of the heat transfer fluid to 390°C and needs a vapor pressure up to 10 bar at these temperatures, which is not able to storage stable at these conditions. All this made the direct storage of heat transfer oil not longer to the state of the art. (Tamme et al., 2013)



(a) SEGS-1 PTC plant with direct storage of heat (b) PTC power plant with indirect storage system using molten salt.

Figure 29.: Simplified scheme of PTC power plants and storage concepts (Steinmann, 2012).

Indirect molten salt storage units

Since the direct storage of the synthetic HTF is not attractive, an indirect storage concept was proposed. This should use a low cost storage medium, which can be stored at ambient pressure between 290 °C and 390 °C. The use of molten nitrate salts was a nearby solution whose elements is considered and development since the early stage of CSP technology in the 1980's. Depending on the importance of material costs and there thermal stability, an sodium-nitrate-rich (NaNO_3) mixture containing 60% NaNO_3 and 40% KNO_3 (potassium nitrate) is preferred if an large quantities is required. The maximum temperature is in range of 550-580 °C and the melting temperature is in the range of 230 °C. (Tamme et al., 2013)

Figure 29b shows a simplified scheme to implement a indirect two tank molten salt storage concept into a parabolic trough plant. Two separate insulated cylindrical tanks made of steel and carbon are used. Each tank can contain the total molten salt volume. Due to the temperature-dependent density of molten salt, the volume of the hot fluid tank has to be 4% lager. To prevent freezing of molten salt an electrical immersion heaters are located at the bottom of the tanks.(Kelly & Kearney, 2006).

The Andasol-1 facility, completed 2008 in Andalusia, Spain was the first commercial CSP plant using indirect molten salt storage. This plant can be operated for 7.5 h at 50 MW_{el} by thermal energy provided by an indirect two-tank molten salt storage system. The molten salt storage fluid of 28 500 tons is cycled between 385 °C and 295 °C, resulting a storage capacity of 1 050 MWh_{th} (Reloso & Delgado, 2009). The storage tanks have a height of 14 m and a diameter of 36 m. The similar CSP plants Andasol-2 and Andasol-3 started operation in 2009 and 2011. (Solar Millennium AG, 2008; NREL, 2008; NREL, 2013a; NREL, 2013b)

Figure 30 shows the Solana facility located in Arizona, USA. This plant was completed in 2013 and is the largest parabolic trough plant so far. The indirect molten salt storage system uses 12 tanks to provide 280 MW_{el} for a duration of six hours. (Abengoa Solar, 2013b)

Since 2015 SA has also their first commercial CSP plant using indirect molten salt storage technology (Figure 10). KaXu Solar One is located next to Poffader in the Northern Cape and is a parabolic trough plant with 100 MW_{el} capacity and 2.5 h of thermal storage in molten salts. (NREL, 2015b)



Figure 30.: Overall view of Solana PTC facility with 12 storage tanks for molten salt (Abengoa Solar, 2013c).

Steam accumulators

In 2007 the first commercial CSP plant in Europe, the Planta Solar 10 (PS10) started near to Seville in Spain. The power tower uses saturated steam at 250°C and 40 bar to drive a 11 MW_{el} power circle. A schematic diagram of the PS10 is shown in Figure 22 on Page 32. The energy availability for storage is limited because the plant is designed for a small solar multiple value of 1.3. Therefore a stream accumulator was selected as storage concept. The cross-sectional view of an steam accumulator is shown in Figure 31, which is also denoted as Ruths' storage or saturated steam storage. During charging the surplus stream is fed into a pressurized liquid water volume. The liquid water acts as storage medium. So the condensing steam increases the pressure and temperature of the liquid water in the volume. The storage is designed in

horizontal cylindrical pressure vessel, whose volume is filled with 90% saturated liquid and the remaining volume is filled by saturated stream. Saturated stream will provided during discharge by the steam accumulator. While the saturated steam is taken out of the steam accumulator is the pressure in the liquid volume declining. The saturated liquid volume generates thereby additional saturated steam by a reaction of the pressure reduction. Meanwhile the mass reduction of the liquid volume is usually in the range of 10-20%. Pressure and temperature of the steam from the steam accumulator decline continuously during the discharge process. The PS-10 plant uses four separate tanks to store about 20 MWh_{th} which is sufficient to produce 50% load for 50 minutes. Attractive features of steam accumulators are their robustness and the simplicity of the concept. The fast reaction time makes the steam accumulator to an prefer storage concept of buffer storage solution intended for short fluctuation of solar radiation. But significant exergy losses occur due to the temperature difference between the steam and liquid volume during the charging. While steam accumulators are an attractive solution for small and medium sized solar process heat application, W.-D. Steinmann from the German Aerospace Center (DLR) (Steinmann, 2015) has the opinion they are not expected to play a major role in the future of CSP applications. (Tamme et al., 2013)

Nonetheless the first power tower in SA, Khi Solar One will use super-heated steam, dry cooling technology, and a 2 h steam storage system. Khi Solar One is a 50 MW solar power tower plant being built by Abengoa near the town of Upington in the Northern Cape Province. Operation was scheduled to begin in 2014 but is still under construction (Status Oct. 2015). (Abengoa, 2014; NREL, 2014b)

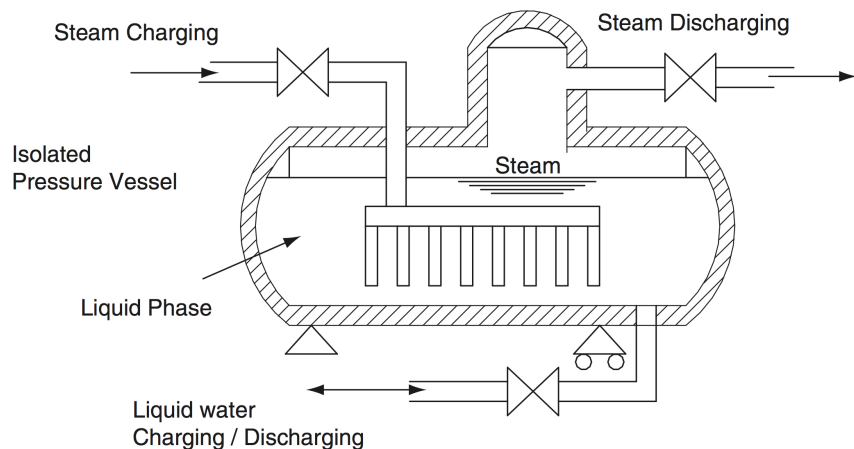


Figure 31.: Scheme of a steam accumulator (Steinmann & Eck, 2006).

Direct molten salt storage units

Increasing the maximum process temperature of the thermal cycle of an CSP plant seems to be an efficient way to improve the economics of solar thermal electricity generation. A higher

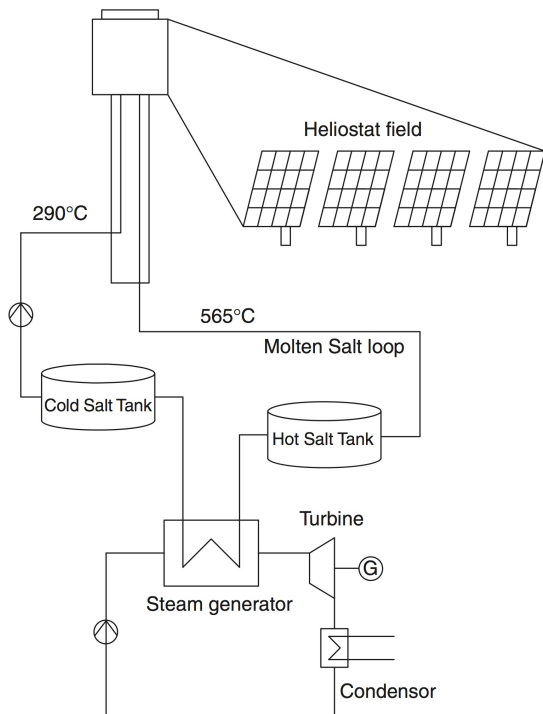


Figure 32.: Simplified scheme of Solar Two CRS power plant with direct storage of molten salt used as heat transfer fluid (Tamme et al., 2013).

maximum process temperature allows also to increase the thermal storage cycle temperature, which has a significant impact on the specific storage capacity for sensible heat. Thereby the required storage inventory and the volume of the storage tanks can be reduced. Also less electric power for pumping the storage medium is required. But on the other hand, increasing with the higher temperature as well corrosion problems and thermomechanical stress.

Using the solar central receiver concept is an opportunity to raise the temperature of the process up to more than 565°C . Figure 32 shows a simplified scheme of direct two-tank molten salt storage concept integrated into CRS. This concept was first tested in the Solar Two power plant. This pilot solar-thermal project was built in the Mojave Desert just east of Barstow, CA, USA in 1994 on basis of the Solar One facility and was operating until 1999. A 10 MW_{el} Rankine cycle was connected to the central receiver providing 35 MW_{th} . The two-tank storage system had an inventory of 1 400 t of a mixture of molten sodium nitrate (60% by weight) and potassium nitrate (40% by weight), with a total volume of about $1\ 700 \text{ m}^3$. The capacity of the storage system was 107 MWh_{th} and operated between 565°C and 290°C , which allowed the operation of the turbine for 3 h. The external isolated tanks had both a diameter of 11.6 m, the hot tank was made of stainless steel had a height of 8.4 m with thermal loss in the range of 100 kW, the cold tank made of carbon steel was 7.8 m tall and transferred about 50 kW to the environment. The Solar Two project also gained the operational experience for handling larger quantities of nitrate salt for storage applications. Although, there were some changes observed in the physical properties of molten salt during the duration of the project, there were no problems resulted. After

the 30 000 h project test and the analyses of the construction material, it was concluded that salt-induced no practical limitation on the useful life of tanks. Also the nitrate salt was recycled for use as fertilizer at the end of the project. (Steinmann, 2015)

The first commercial solar tower plant using molten salt with a direct storage system is Gemasolar, which was commissioned in 2011. It uses the first high-temperature solar receiver with molten salt, which provides 15 hours of thermal storage and an annual capacity factor of about 75%. The size of the storage allows the plant to operate 24 h per day. The facility generates 19.9 MW_{el} from 2 650 heliostats each 120 m² aperture area. The technology is based on the Solar Two and has the same temperature difference in the receiver from 275 K. (NREL, 2011)

The Atacama-1, which is currently under construction in the Atacama desert in Chile, will also use a direct storage in molten salt for 17.5 h of storage. (NREL, 2015a; Abengoa Solar, 2015b; Abengoa Solar, 2015a)

Also parabolic trough power plants using direct molten salt storage units. The commercial used Archimede solar power plant in Italy is the first parabolic trough plant using molten salt as HTF. It started 2010 the production with 5 MW turbine capacity. The storage capacity reaches for 8 hours and has a total mass of 1 580 t of molten salt. With a tank size of 6.5 m in height and 13.5 m in diameter, the capacity is 100 MWh_{th}. (NREL, 2012)

In a nutshell, the direct or indirect two-tank molten salt storage technologies are represent current state of art for commercial large-scale CSP applications. While this concepts shows a low technical and environmental risk, the potential for cost reduction is limited here.

4.1.5. Power cycles for CSP systems

As mentioned in the overview of solar power technologies in Figure 11 on Page 15, a range of different solar to electric energy conversion systems can be applied. Commonly used as conversion systems in current large-scale CR and PTC applications are steam turbines which are based on the Rankine cycle. Nearly all convectional fired power plants using the Rankine cycle to convert heat in electricity. If an conventional fired combined cycle power plant is supplemented with a CSP system it uses an integrated solar combined cycle (ISCC), which is also based on the Rankine cycle. An additional conversion systems for CRS and parabolic dishes is the Brayton cycle (also known as Joule cycle). However, for efficient cycle operation temperatures of 1 000 °C are needed. Therefore the Brayton cycle has just been operated in demonstration CSP systems. CSP systems also uses Organic Rankine cycles, Stirling engines and other opportunities to generate electricity. (Lovegrove & Pye, 2012)

A CSP plant with Rankine cycle is basically working in four steps using a steam turbine:

- Compressing pure feed water to high pressure.

- Pre-heating, boiling and superheating steam in a boiler which may be in the focal point, or may be heated using a heat exchanger with another HTF.
- Expanding the steam to low pressure via a series of turbines that drive a generator.
- At the end of the expansion process, condensing the low pressure steam, with the aid of a cooling tower and then re-using it in the cycle.

4.2. Large scale PV power plants

two axis tracking PV

4.2.1. Large-scale PV power plants

4.2.2. Large-scale electrical energy storage systems

electrical energy storage (EES) EESSchema

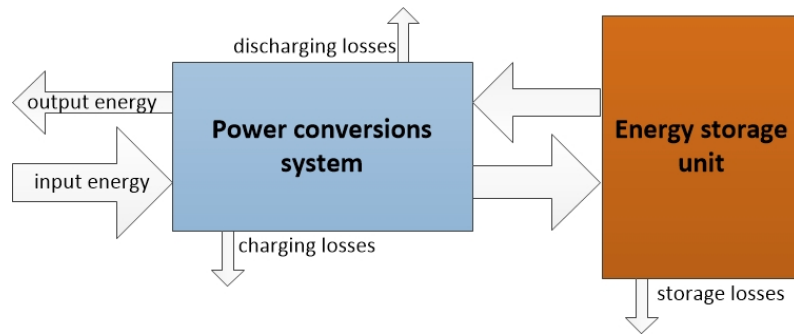


Figure 33.: Schema of an electrical energy storage (EES) system and there energy losses.

$$\text{Overall storage efficiency (AC-to-AC)} = \frac{E_{out} \text{ (kWh)}}{E_{in} \text{ (kWh)}} \quad (5)$$

4.3. Environmental impacts of CSP and PV

Co2

Water use in O & M

land use

energy use in operation and building (EASAC, 2011)

(Caldés & Lechón, 2012)

4.4. Chapter summary

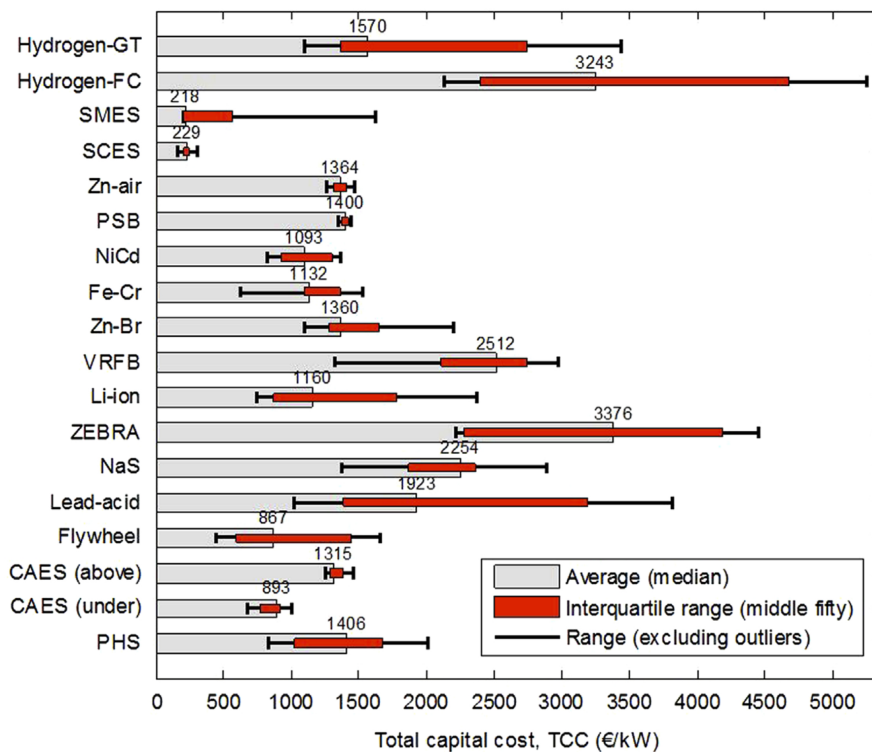


Figure 34.: Total capital cost in Euro () of large-scale EES systems per unit of nominal power rating including costs of power electronics, storage part, fixed obtain and maintainence and maybe incidental replacement costs (Zakeri & Syri, 2015).

5. Simulation-based comparison between CSP- and PV-power plants

To compare CSP and PV technologies, a simulated case study was performed on the basis of a CR system and PTC system. Specific attention was given to maximizing daytime operation and meeting the demand curve. The photovoltaic system was extended with battery storage. The storage capacity allocated for the simulation considerably exceeds the real capacity of electrical storage units currently available and is more than one-sixth the globally installed battery storage capacity of 690 GW.(IEA, 2015) Due to the scale and particularly with respect to the photovoltaic plant, the comparison is theoretical in nature.

5.1. General assumptions

With the aim of producing quantifiable and comparable results, the different solar supplied power plants will be simulated under different input parameters. After that, selected comparable output parameters will be analyzed, evaluated and rated.

The plant technologies selected for comparison are:

- CSP molten salt central receiver with thermal energy storage
- CSP synthetic oil parabolic trough with thermal energy storage
- PV fixed elevated flat plate collectors with adapted electrical energy storage

The PV plant has been extended with a lithium-ion battery storage for the simulation, while the thermal energy storage of the CSP plant uses molten salt technology. All plants were laid out for a maximum power output of 100 MW_{el} . The plants are driven to match a selected load scenario. In order to find an appropriate power plant design to match the load of the scenario, different layout parameters, using various storage and collecting field sizes, were tested. The scenario and requirements are defined and discussed in Section 5.1.1. The location and related weather data are described in Section 5.1.2. The solar power plants are implemented and simulated in NRELs System Advisor Model (SAM) version SAM 2015.6.30 r3 for OS X (NREL, 2015f). SAM is designed to simulate performance and financial models of different types of renewable energy. For this simulation, only the performance component was used. The financial analysis was done separately.

The financial parameters and the resulting levelized cost of electricity (LCOE) are calculated separately for all power plants in Microsoft Excel 2011 (vers. 14.5.7) for Mac, using a simplified method which is documented in Appendix B on page 98 using a lifetime of 25 years for each plant.

5.1.1. Simulation scenario

A hard requirement is that plants meet the full electrical demand in the system. Figure 35 shows the daily average system load/demand in South Africa for the winter and summer period. Both profiles feature a sharp rise at approx 7:00 and have their peak demand at 20:00 during the summer period. In winter, there is an initial peak at 9:00 and a second at 19:00. In order to match this system load, the simulated solar power plants must operate at full power output of 100 MW from 7:00 to 22:00. When the system demand drops during the night, the plants reduce their output from 22:00 to 7:00 to 50 MW . The scenario is called "night reduction". In this comparison, the system design must handle 90 % of the scheduled electricity production over the first year. Usually, in feed-in contracts, the deliverable energy is fixed. Any overproduction

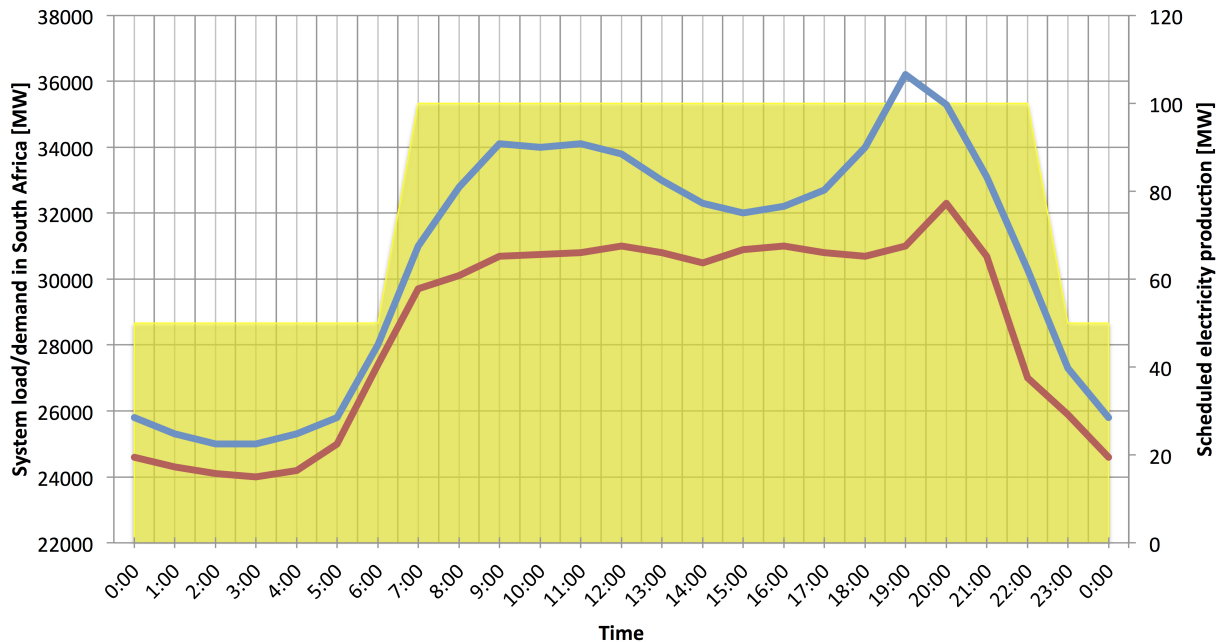


Figure 35.: South Africa daily average system load/demand for summer and winter days, with scheduled power production curve.

is not covered by such contracts and is not remunerated. In order to generate exploitable and comparable results and considering standard feed-in contracts, the hourly power production is cut to the planned values and thus overproduction is not considered in this analysis.

The results of the simulation and the financial analyses will be evaluated by the following quantitative measures:

- **Load curve covering factor [%]:** The load curve covering factor (LCCF) is an effectiveness measure describing how closely the plant follows the load curve.
- **Levelized cost of electricity [¢/kWh]:** The levelized cost of electricity (LCOE) represents the total project life-cycle costs. It is the present value of project costs expressed in cents per kilowatt-hour of electricity generated by the system over its life. (NREL, 2015e)

There is an important difference between the LCCF and the widely-used *capacity factor* (CF). The CF is the ratio of the system's electrical output in the first year of operation to the nameplate output, which is equivalent to the quantity of energy the system would generate if it operated at its nameplate capacity for every hour of the year (NREL, 2015e). The LCCF is calculated from the sum value of load coverage in each hour of the year.

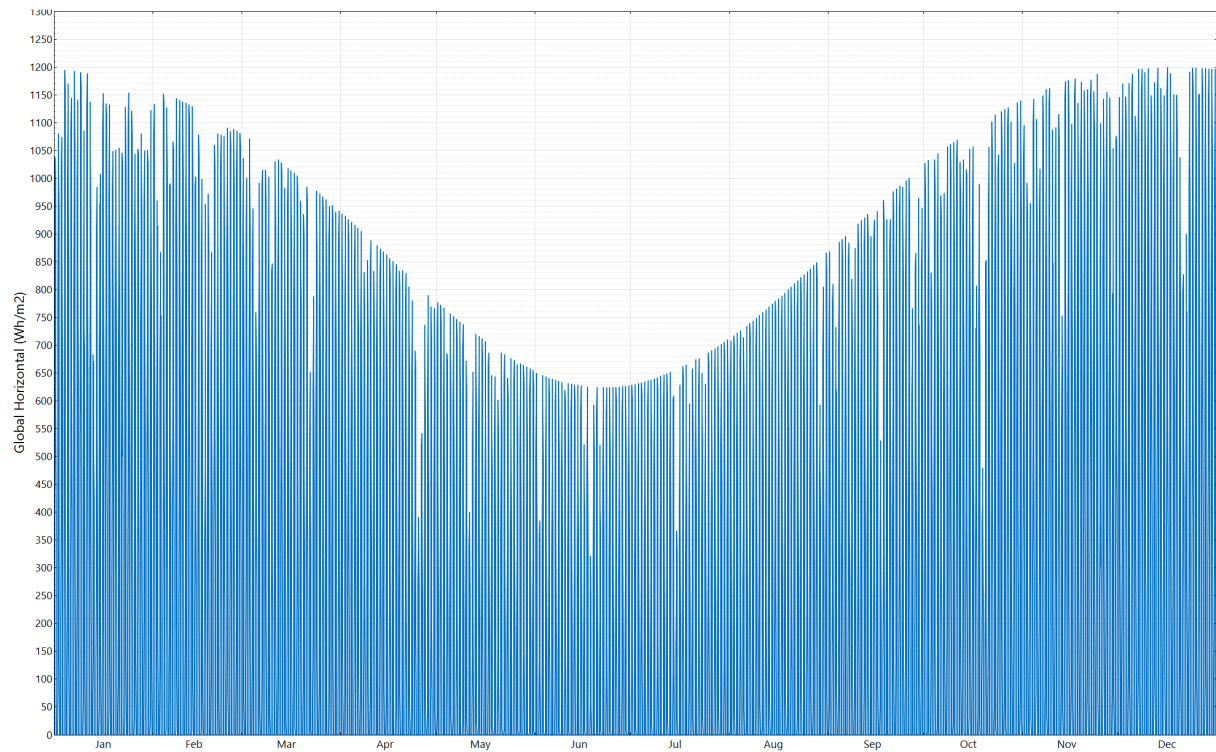
5.1.2. Location and weather data

In this simulation, locations and weather data for Upington, Northern Cape were used. This region has among the highest irradiation values in the country, but also has good water access due to the Orange River. This location was mentioned before in Chapter 3 and is marked in the GHI- and DNI-maps of SA in Figure 8 on Page 12.

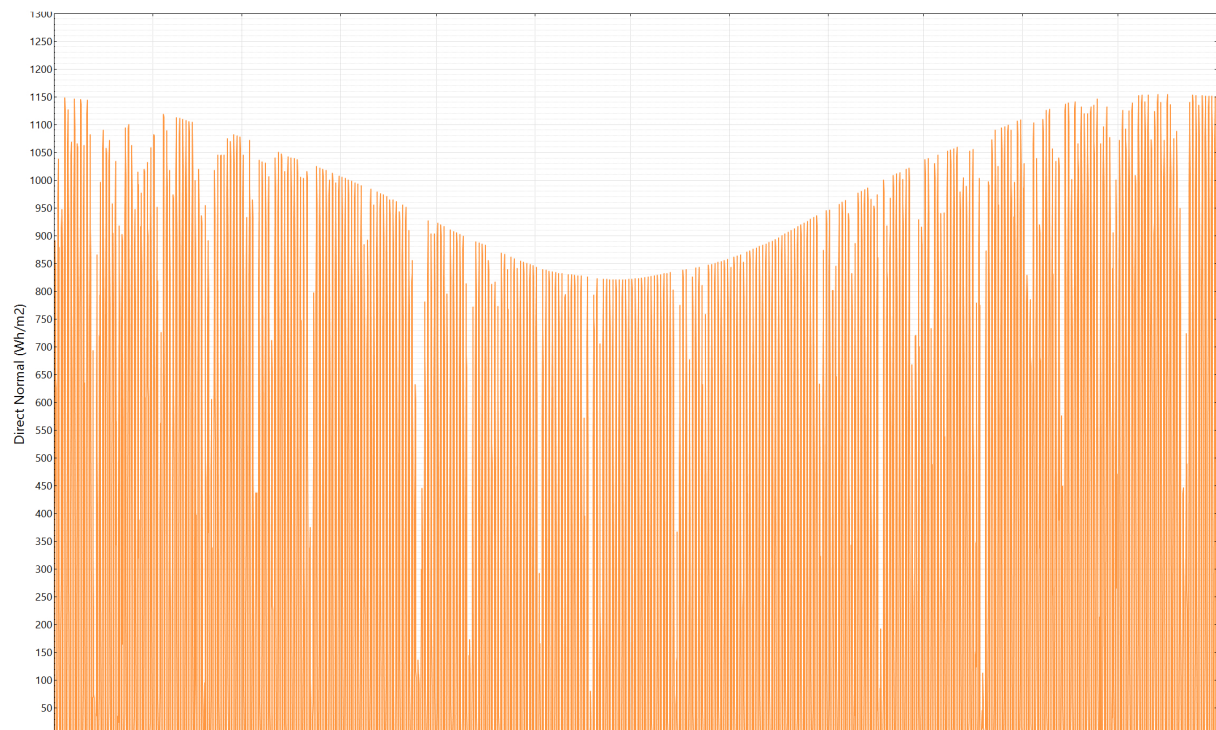
Item	Value	Unit
Location	Upington	-
Station ID	684240	-
Data source	White Box Technologies, Inc. (31.05.2015)	-
Latitude	-28.40	°N
Longitude	21.27	°E
Elevation	836	m
Total GHI per year	2 280	kWh/m ²
Total DNI per year	2 621	kWh/m ²
Total DHI per year	516	kWh/m ²
Mean temp.	21	°C
Mean wind speed	3.3	m/s

Table 6.: Location and characteristics for the simulation in SAM.

The weather data for the simulation in SAM are in EPW format (EnergyPlus Weather Data) and produced by White Box Technologies, Inc. (White Box Technologies, 2015). The EPW files are data sets of hourly values of solar radiation and meteorological elements for a typical one-year period. These include air temperature, dew point temperature, relative humidity, atmospheric pressure, global horizontal solar radiation, diffuse horizontal solar radiation, direct normal radiation, wind speed, wind direction and cloud cover. The most relevant parameters for this simulation are summarized in Table 6. The hourly values of global horizontal and direct normal irradiance from the EPW file are shown in Figure 36. The highest irradiance value during the summer is 1 199 Wh/m² for GHI and 1 154 Wh/m² for DNI. At the northern solstice, the highest irradiance is 625 Wh/m² for GHI and 820 Wh/m² for DNI.



(a) Global horizontal



(b) Direct normal

Figure 36.: Hourly values of irradiance over a full year from Upington used in the simulation.

SAM calculates the path of the sun by the position of longitude and latitude. Figure 37 shows the solar path diagram at Upington. It is apparent that the longest day in Upington has a duration of 13 h and 56 minutes with a maximum sun height of 85.05° while the shortest day has a duration of just 10 h and 19 minutes and a maximum sun height of 35.93° .

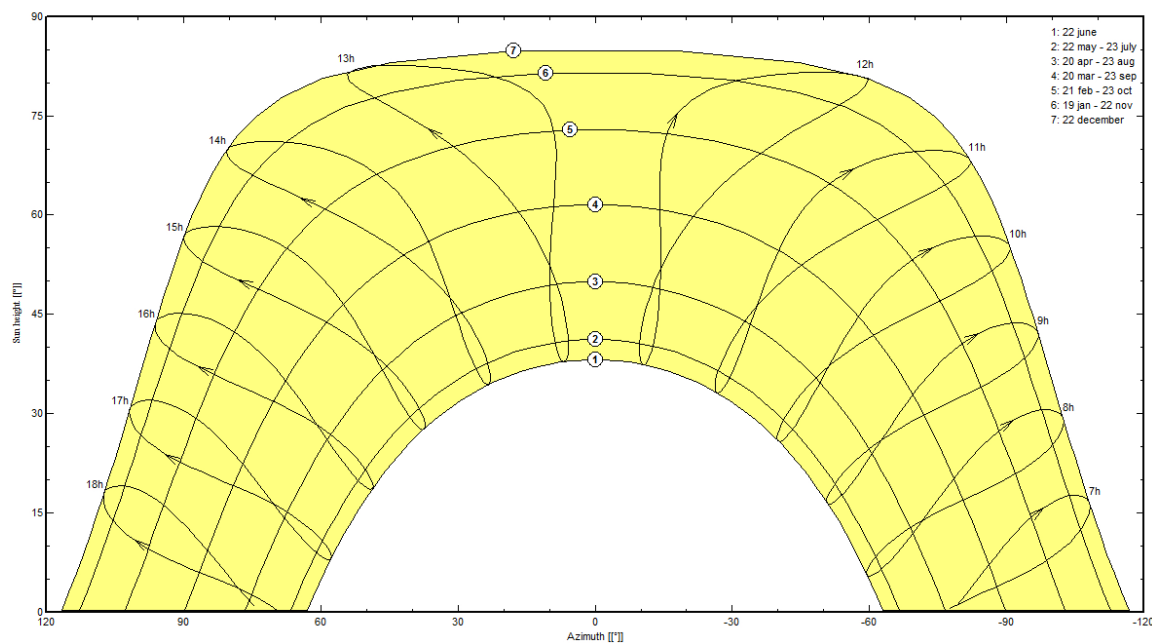


Figure 37.: Solar path diagram Upington (PVsyst SA, 2015).

5.2. CR power plant design and simulation

For the CR plant simulation in SAM, the “CSP power tower molten salt” model was used. The EPW weather file for Upington from Section 5.1.2 was used as an input file to specify the hourly atmospheric conditions. SAM uses the following input data for the simulation:

- Latitude (°)
- Longitude (°)
- Elevation above sea level (m)
- DNI (W/m²)
- Atmospheric pressure (mbar)
- Dry bulb temperature (°C)
- Wet bulb temperature (°C)
- Relative humidity (%)
- Wind velocity (m/s)

This Chapter describes in detail the crucial inputs of the CR power plant components, namely the power cycle, heliostat field, tower and receiver and thermal energy storage (TES).

As already mentioned, financial parameters and the LCOE are calculated separately in Microsoft Excel using a simplified method which is documented in Appendix B on Page 98.

Simulated configurations

The simulated configurations were to meet 90 % of the scheduled production curve by using variation of solar multiples and full load hours of TES. As mentioned in Section 4.1 the solar multiple (SM) is the ratio of the receiver’s thermal output to the power cycles thermal input at the design point. Thus, a CR system with a SM of 1 has a receiver and a heliostat field which provides the thermal power needed for the power block to run at full load at the system design point. A receiver and collector field with an SM of 1 do not produce enough thermal power to store energy in a TES while also feeding the turbine. A CR system with a SM of 1 is just sufficient for systems without TES. In order to cover the expected load, the solar multiple was varied from 2 to 3.5 in steps of 0.5, while storage full load hours were varied from 6 to 16 h in steps of 2 h. The target of 100 MW net capacity was reached with a gross capacity of 111 MW with an estimated gross-to-net conversion factor of 0.90. Table 7 summarizes the simulated configurations.

Item	Unit	Value											
Net turbine capacity	MW _{el}	100											
Gross turbine capacity	MW _{el}	111											
Solar multiple	-	2.0											
TES capacity	h	6	8	10	12	14	16	6	8	10	12	14	16
Solar multiple	-	3.0											
TES capacity	h	6	8	10	12	14	16	6	8	10	12	14	16

Table 7.: Simulated CR solar multiple and thermal energy storage configurations.

Power cycle

The power cycle of the simulated CR system features a Rankine-cycle steam engine, two open feed-water heaters, a pre-heater, boiler and super-heater (NREL, 2015e). As mentioned above has the turbine a gross capacity of 111 MW_{el} and a nameplate (net) capacity of 100 MW_{el}. The

Item	Value	Unit
Turbine design capacity, gross	111	MW _{el}
Turbine design capacity, net	100	MW _{el}
Boiler operating pressure	125	bar
Design inlet temperature	288	°C
Design outlet temperature	566	°C
Cycle conversion efficiency	41.2	%
Steam generator design thermal power	269.42	MW _{th}
Power block start-up time	0.5	h
Minimum required start-up temperature	500	°C
Plant availability	96	
Condenser type	air-cooled	-

Table 8.: CR power block and condenser input parameter in SAM.

steam generator has a HTF inlet temperature of 566 °C and outlet temperature of 288 °C at design point and operates at a pressure of 125 bar. In combination with a air-cooled condenser the CR power cycle system was simulated with a cycle gross efficiency of 41.2%. A wet-cooled condenser would reaches some higher efficiency, but because of the lack of water in the area

of Upington and the requirement by the South African government for CSP plants, a air-cooled condenser was selected. The HTF inlet temperature, pressure and efficiency values where adapted for the configuration from (Kolb, 2011). For starting up the system needs 30 minutes and a min. required temperature of 500 °C. A plant availability of 96 % was adapted from (Morin et al., 2012) in order to simulate system down-times for outages or scheduled maintenance.

Heliostat field

The heliostat field design was done in SAM using its heliostat field layout optimization tool. For the design, optimization and simulation process, heliostat data from the Sanlúcar 120 heliostat was used (Noone et al., 2012). The Sanlúcar 120 is used in the Planta Solar 10 (PS10) near Seville, Spain and is the origin of Abengoa's actual heliostat ASUP 140. For a simulation with the ASUP 140 no sufficient data was available. The Sanlúcar 120 heliostats have an effective

Item	Unit	Value			
racking	-	two-axis			
Height	m	9.45			
Width	m	12.84			
Reflective area	m ²	120.00			
Heliostat availability	%	99			
Design-point DNI	W/m ²	950			
Solar multiple	-	2.0	2.5	3.0	3.5
Number of heliostats	-	9 131	11 530	13 976	16 658
Max. distance from tower	m	1 528	1 708	1 883	2 010
Reflective area	ha	109.58	138.36	167.72	199.90
Field land area	ha	655.59	821.92	997.95	1 190.99

Table 9.: CR heliostat parameter.

reflective area of 120 m² and are tracked on 2 axes. The heliostat field layout optimization and there design depends on the turbine gross and the SM. The heliostat field was optimized therefore for all four considered configurations. SAM first generates a coarse layout and optimizes the number of heliostats and their position. The goal of the optimization is the maximum flux with minimum power constraints according to the specified design-point DNI which represents the DNI at which the power plant achieves its rated thermal capacity. Table 9 summarizes the heliostat datas and the values of the optimized field design for all considered solar multiples.

The optimized heliostat field layouts of the four considered SM are depicted in Figure 38. In order to avoid mutual shading from the heliostats the heliostat density decreases with distance from the tower. The maximum heliostat distance to the tower rises with the higher SM which can be seen in the field diameter.

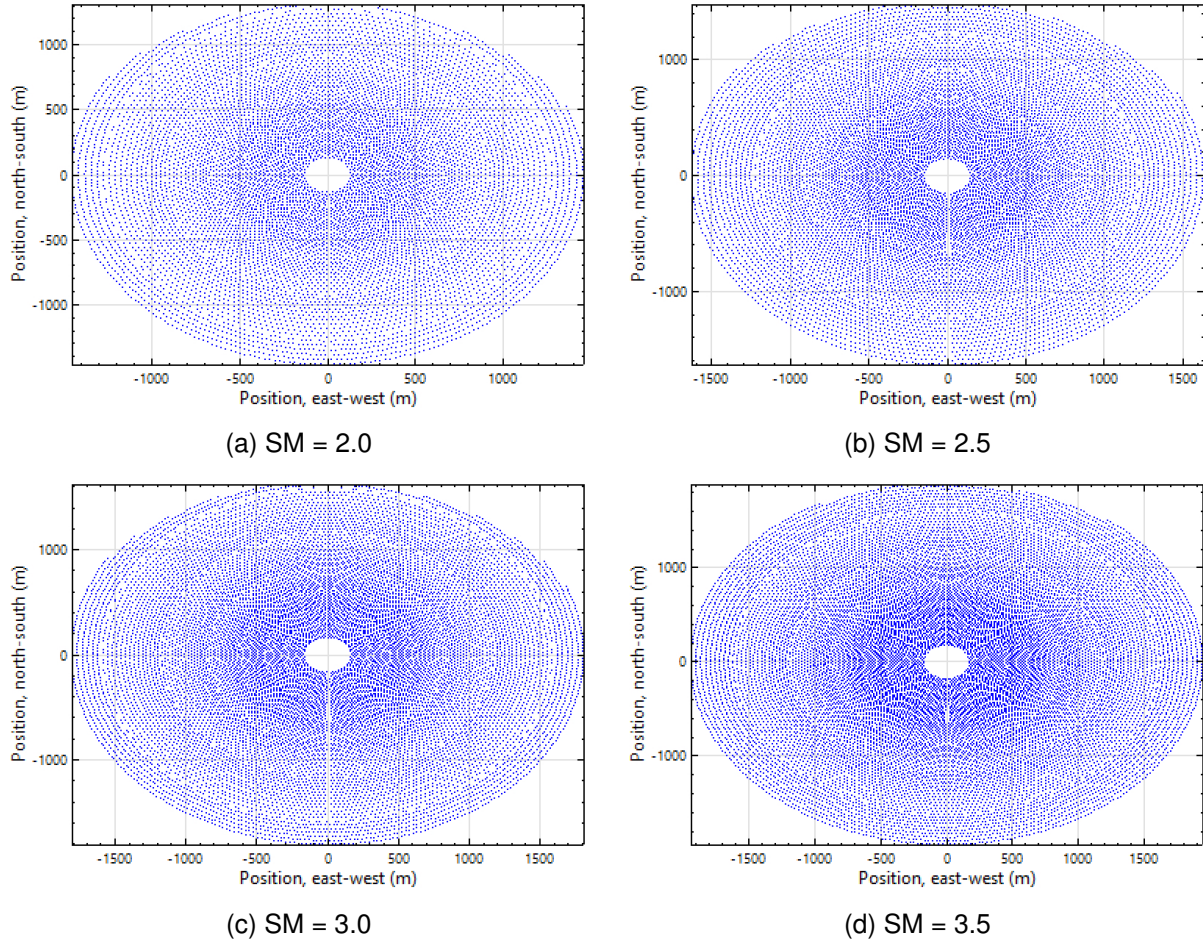


Figure 38.: Simulated heliostat field layout at different solar multiples (SM).

Tower and receiver

The receiver collects the concentrated irradiance from the surrounding heliostat field. The simulated receiver is built as an external cylindrical receiver and is configured with 24 panels of thin walled (1.25 mm) receiver tubes with an outer diameter of 60 mm arranged in a circle around the tower. The receiver tubes are made from 316H stainless steel and the external surfaces of the tubes are coated with a black Pyromark paint. The paint is resistant to high temperatures and thermal cycling, and absorbed 95% of the incident sunlight. This configuration is similar to the receiver of the Solar Two Project except of the outer diameter (Bradshaw

et al., 2002). The panels containing molten salt (60 % NaNO₃ and 40 % KNO₃) as heat transfer fluid (HTF). The receiver design inlet temperature of 288 °C and the outlet temperature of 566 °C was set before in the power block configuration. In order to achieve the desired receiver thermal power output, the height of the tower and receiver dimensions got also adjust with the optimization of the heliostat field design. The results of the optimization is shown in Table 10, as well as the fixed tower and receiver parameter. The heights of the tower range from 179.77 to 236.50 m. The receiver proportions rises with the SM and the field sizes and results in a receiver thermal power range from 538.8 to 943.0 MW_{th}.

Item	Unit	Value			
Receiver configuration	-	external cylindrical receiver			
Heat transfer fluid	-	60 % NaNO ₃ and 40 % KNO ₃			
Inlet temperatures	°C	288			
Outlet temperatures	°C	566			
Receiver tube material	-	AISI316 stainless steel			
Receiver tube outer diameter	mm	60			
Receiver tube wall thickness	mm	1.25			
Number of panels	-	24			
Absorption factor	-	0.95			
Solar multiple		2.0	2.5	3.0	3.5
Tower height	m	179.77	200.96	221.57	236.50
Receiver height	m	22.55	25.45	27.74	29.94
Receiver diameter	m	14.85	16.66	17.91	18.77
Receiver aperture area	m ²	1 052	1 332	1 561	1 765
Receiver thermal power	MW _{th}	538.8	673.5	808.3	943.0

Table 10.: CR heliostat field parameter.

Thermal energy storage (TES)

The CR system was simulated using a direct two-tank molten salt thermal energy storage (TES). The storage uses directly the HTF (60 % NaNO₃ and 40 % KNO₃) from the receiver as storage medium. Figure 32 on Page 46 shows a schema of the direct storage for CR system. The design temperature of the hot storage tank (566 °C) and the cold storage tank (288 °C)

depends also from the set value in the power block settings as before the design receiver temperatures. So the design temperature difference between the tanks is 278 °C.

As defined at the begining of this Chapter, the full load hours of TES are varied in steps of 2 h from 6 to 16 h. The TES full load hours represents the time in which the storage can supply enough energy to the steam turbine and the power block to run at full design capacity. So a higher value of TES full load hours extended the time that the power plant can run during nights or cloudy days. Table 11 shows that with higher TES full load hours the thermal capacity and tank volume increases as well. The simulated storage capacity is in a range of 1 617 MWh_{th} using 6 full load hours and 4 311 MWh_{th} using 16 full load hours.

Item	Unit	Value					
TES full load hours	h	6	8	10	12	14	16
Storage type	-						direct two-tank molten salt
Storage fluid	-						60 % NaNO ₃ and 40 % KNO ₃
Hot tank design temp.	°C						566
Cold tank design temp.	°C						288
Thermal capacity	MWh _{th}	1 617	2 155	2 694	3 233	3 772	4 311
Storage volume	m ³	7 757	10 229	12 787	15 345	17 902	20 460

Table 11.: CR system TES parameter.

SAM 2015.6.30 r3 don't have a power control to follow prescribed hourly net output values. The turbine output of each day needs to be scheduled in front for the simulation. Thereby the parasitic consumer needs highly attention. Figure 39 shows the for the simulation scheduled turbine output matrix. The individual values was fixed during experimental trial. It can be seen that the turbine output is reduced to 50% during the night as it is specified in the scenario. The power plant follows the schedule till there is no solar irradiance and no more thermal capacity in the storage left to generate power.



Figure 39.: TES dispatch control matrix for turbine output fraction of CR simulation in SAM.

Financial parameter

The financial parameter for the LCOE calculation of the CR power plant are separated in different specific cost parts and are summarized in Table 12. The method for calculating the LCOE is documented in Appendix B on Page 98 using a lifetime of 25 years and a real interest rate of 7.5 % (Fraunhofer ISE, 2013). The interest rate could be reduced with a rising market potential.

The specific costs of the heliostat field of 180\$/m² coming from J. B. Blackmon (Blackmon, 2012). He analyzed the costs of heliostat as a function of area for a representative solar central receiver power plant and calculated the total installed costs for a field of 5 000 heliostats with 148 m² reflective area of approximately 180 \$/m². The analyze results showed that the costs are increasing with the size of the heliostats from 40 m² on. So the adopted value of 180 \$/m² reflective area for 140 m² heliostats can be assumed as conservative.

The remaining investment costs are based on the "Power Tower Technology Roadmap and Cost Reduction Plan" (Kolb et al., 2011) from 2011.

On top of the investment costs came 15 % once-off surcharge for EPC and contingencies (Platzer, 2014).

Fichtner analyzed the annual O&M costs with 1.84-1.96 % of the total investment costs for CR power plants in SA (Fichtner, 2010). The value of 2 % can so also be assumed as conservative.

The costs for the land purchase comes from the "African Agriculture Review" report of the Nedbank Capital, which reported the prices for farmland in SA. For the LCOE calculation of the CSP and PV system was the land purchase costs of \$3,000/ha assumed which is based on these report (Cassell, 2012).

Item	Symbol	Value	Unit	Source
Heliostat field	c_{HF}	180	\$/m^2	(Blackmon, 2012)
Power block	$c_{PB,CR}$	1000	\$/kW_{el}	(Kolb et al., 2011)
Thermal energy storage	$c_{TES,CR}$	30	\$/kWh_{th}	(Kolb et al., 2011)
Tower and receiver	c_{T+R}	200	\$/kW_{th}	(Kolb et al., 2011)
Annual O&M	$f_{O\&M,CR}$	2	%	(Fichtner, 2010)
Land purchase	c_{LP}	3 000	\$/ha	(Cassell, 2012)
Lifetime	n	25	years	(Fraunhofer ISE, 2013)
Interest rate	i_{CR}	7.5	%	(Fraunhofer ISE, 2013)
Surcharge for EPC, project management and risk	$f_{EPC,CR}$	15	%	(Platzer, 2014)
Total plant availability	$f_{avail,plant,CR}$	96	%	(Morin et al., 2012)

Table 12.: Financial input parameter for CR-simulation in SAM.

5.3. PTC power plant design and simulation

The PTC power plant was simulated in the CSP parabolic trough (physical)" model in SAM using the option "no financial model". As before the input the EPW weather file to specify the hourly atmospheric conditions from Section 5.1.2 was used. For the PTC simulation SAM uses the following input data:

- Latitude (°)
- Longitude (°)
- Elevation above sea level (m)
- DNI (W/m²)
- Atmospheric pressure (mbar)
- Dry bulb temperature (°C)
- Wetbulbtemperature(°C)
- Relative humidity (%)
- Wind velocity (m/s)

This Chapter describes in detail the input data of the PTC power plant simulation by three components, namely the power cycle, solar collector, solar receiver, solar field and thermal energy storage (TES).

Also for the simulation of the PTC are the financial parameters and the LCOE calculated separately Microsoft Excel using a simplified method which is documented in Appendix B on Page 98.

Simulated configurations

In order to reaching the goal of covering 90 % of the scheduled production curve also the simulated PTC power plant used a variation of solar multiple and full load hours of TES. To covering the scheduled load the solar multiple was varied from 2 to 5.0 in steps of 5.0. This is significantly higher SM compared the simulated CR system was necessary to reach the 90 % covering factor. As before with the simulation of the CR, the storage full load hours were varied from 6 to 16 h in steps of 2 h. The target of 100 MW net capacity was reached with a gross capacity of 120 MW with an estimated gross-to-net conversion factor of 0.83. The comparatively high gross turbine output is necessary for the high parasitic burden of the system. Table 13 summarizes the simulated configurations.

Item	Unit	Value											
Net turbine capacity	MW _{el}	100											
Gross turbine capacity	MW _{el}	120											
Solar multiple	-	2.0	2.5										
TES capacity	h	6	8	10	12	14	16	6	8	10	12	14	16
Solar multiple	-	3.0	3.5										
TES capacity	h	6	8	10	12	14	16	6	8	10	12	14	16
Solar multiple	-	4.0	4.5										
TES capacity	h	6	8	10	12	14	16	6	8	10	12	14	16
Solar multiple	-	5.0											
TES capacity	h	6	8	10	12	14	16						

Table 13.: Simulated PTC solar multiple and thermal energy storage configurations.

Power cycle

The PTC system also uses the steam Rankine cycle technology. In the modeled cycle, feedwater is heated in open (mixed stream) feedwater heaters with two intermediate turbine extractions - once for high pressure and once for low pressure, and the steam generation equipment consists of a preheater, boiler, and superheater. The HTF temperature at the field outlet is bound primarily by HTF stability, so maximum HTF temperatures for oil troughs typically range between 370 °C and 410 °C. The turbine has a gross capacity of 120 MW_{el}. So the net turbine capacity output at design (nameplate) is 100 MW_{el}. The design inlet temperature of the HTF in the steam generator is 393 °C and outlet temperature of 293 °C at design point and operates at a pressure of 100 bar.

Table 14 shows the input parameter for the power block design in SAM. Besides the capacity of the turbine and the condenser type, the parameters are coming from (Wagner & Gilman, 2011). It is obviously, that the cycle conversion efficiency of the PTC power plant is lower than that one from the CR power plant. This is trace back to the lower cycle temperatures and the thereby resulting lower steam pressure in the turbine.

The air-cooled condenser was selected here as well, because water is an valuable resource in the region of Upington. The cooling system is designed to covers the stem generator thermal power.

Item	Value	Unit
Turbine design capacity, gross	110	MW _{el}
Turbine design capacity, net	100	MW _{el}
Boiler operating pressure	100	bar
Design inlet temperature	393	°C
Design outlet temperature	291	°C
Cycle conversion efficiency	37.74	%
Steam generator design thermal power	318.0	MW _{th}
Power block start-up time	0.5	h
Minimum required start-up temperature	300	°C
Maximum turbine over design operation	90	
Condenser type	air-cooled	-

Table 14.: PTC power block and condenser input parameter in SAM.

Solar collector (SCA)

For the simulation of the PTC system the Ultimate Trough was selected as solar collector assembly (SCA). This collector is currently not in commercial use, but comparable troughs with similar characteristics are under construction. So the Ultimate Trough can be adopted without technical modifications and no increase of risk. Figure 40 shows the information of the technical input parameter for SAM. These coming directly from a publication of the developer of the Ultimate Trough, Flabeg GmbH and sbp sonne GmbH (Riffelmann et al., 2014). The section

Collector name from library	Ultimate Trough (Flabeg)	Apply Values from Library	
Collector Geometry			
Reflective aperture area	1715.92 m ²	Number of modules per assembly	10
Aperture width, total structure	7.51 m	Average surface-to-focus path length	2.51 m
Length of collector assembly	245.3 m	Piping distance between assemblies	2 m
Optical Parameters			
Incidence angle modifier coefficients	Edit data...	Geometry effects	1
Tracking error	0.994	Mirror reflectance	0.94
General optical error	0.992	Dirt on mirror	0.97
Optical Calculations			
Length of single module	24.53 m	End loss at summer solstice	0.999063
IAM at summer solstice	0.857416	Optical efficiency at design	0.899079

Figure 40.: Screenshot of Ultimate Trough input parameter for SAM.

"Optical Calculation" shows, that the total optical efficiency at design of the Ultimate Trough is 89.9 %. The dimensions and main characteristics of the HCE is shown in the section "Receiver Geometry".

Solar receiver (HCE)

As heat collecting element (HCE) Schott's PTR80 was selected. This receiver tube has with 0.08 m an extended tube outer diameter. Thereby the tube can contain more HTF and reduce the mass flow in the tubes. Figure 41 shows the for the simulation inserted parameter. The values are the results of measurements of outdoor optical efficiency and indoor receiver heat loss of parabolic trough collector from researchers of National Renewable Energy Laboratory (Kutscher et al., 2012). The section "Parameter and Variations" shows the different conditions of the HCE. Variation 1 shows the optimal condition of the HCE with annulus pressure of 0.0001 torr (0.000133 hPa), so an vacuum. The estimated average heat lost is 190 W/m. This Variation counts for 98.5 % of all HCEs. In Variation 2 the vacuum is lost and which strongly affects the heat loss. It is 1 270 W/m and counts for 1 % of all HCEs. In Variation 3 also the protection glass is broken, so the heat loss increase to 1 500 W/m. The total weighted losses is 207.35 W/m heat loss at design and about 0.85 optical derate and is shown at the last section most below.

Receiver name from library Schott PTR80

Receiver Geometry

Absorber tube inner diameter	0.076 m	Absorber flow plug diameter	0 m
Absorber tube outer diameter	0.08 m	Internal surface roughness	4.5e-05
Glass envelope inner diameter	0.115 m	Absorber flow pattern	Tube flow
Glass envelope outer diameter	0.12 m	Absorber material type	304L

Parameters and Variations

	Variation 1	Variation 2	Variation 3	Variation 4*
Variant weighting fraction*	0.985	0.01	0.005	0
Absorber Parameters:				
Absorber absorptance	0.963	0.963	0.8	0
Absorber emittance	<input type="button" value="Value"/> <input type="button" value="Table..."/>	0.65	<input type="button" value="Value"/> <input type="button" value="Table..."/>	0.65
Envelope Parameters:				
Envelope absorptance	0.02	0.02	0	0
Envelope emittance	0.86	0.86	1	0
Envelope transmittance	0.964	0.964	1	0
	<input type="checkbox"/> Broken Glass	<input type="checkbox"/> Broken Glass	<input checked="" type="checkbox"/> Broken Glass	<input type="checkbox"/> Broken Glass
Gas Parameters:				
Annulus gas type	Hydrogen	Air	Air	Hydrogen
Annulus pressure (torr)	0.0001	750	750	0
Heat Loss at Design:				
Estimated avg. heat loss (W/m)	190	1270	1500	0
Optical Effects:				
Bellows shadowing	0.935	0.935	0.935	0.963
Dirt on receiver	0.98	0.98	1	0.98

* The variant weighting fractions and Variation 4 inputs are not part of the library.

Total Weighted Losses

Heat loss at design	207.35 W/m
Optical derate	0.850118

Figure 41.: Screenshot of Schott PTR80 input parameter for SAM.

Solar field

PTC solar fields are separated in sections. In the simulation of the PTC system the solar field is designed in two sections. Each section carries a feed pipe and a return pipe to transport the thermal energy to the power block. Attached to the header pipes are many loops, which contains the SCAs, the HCEs and the HTF. Figure 42 shows an typical layout for PTC system with two field subsections. As in the Figure is the simulated PTC system designed by four SCAs per loop (Riffelmann et al., 2014).

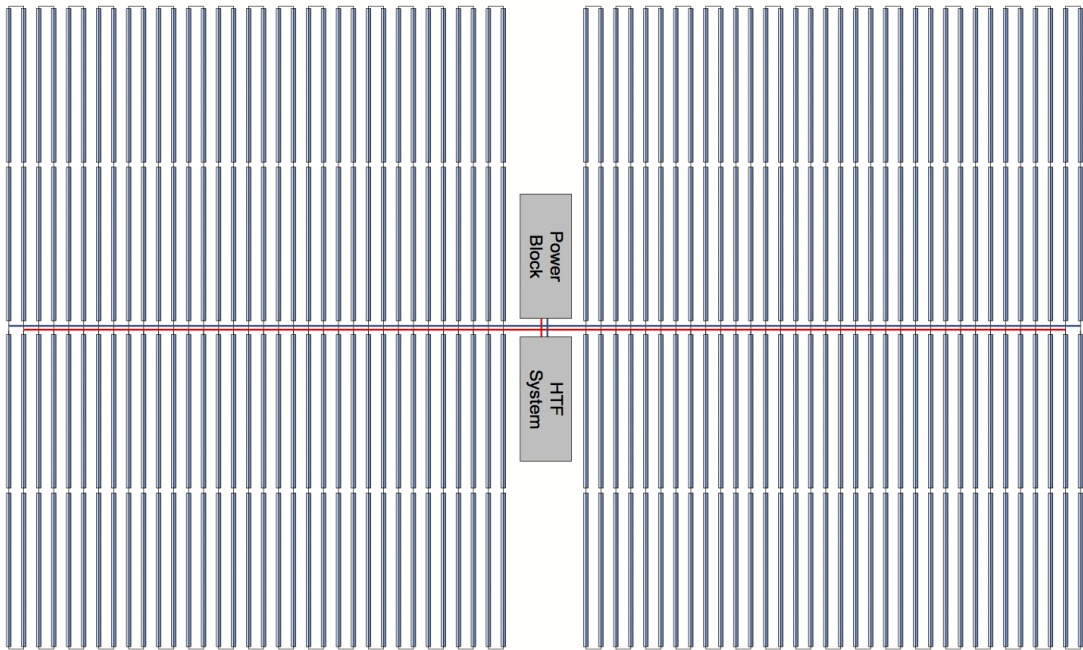


Figure 42.: Typical configuration of a solar field layout with two field subsections for a Ultimate Trough (Riffelmann et al., 2014).

As mentioned before synthetic oil is used as HTF for the simulation of the PTC system. The current standard for HTF in PTC systems is Terminol VP-1. The input parameter for the HTF are shown in Figure 43 and are limited by the performance characteristics of Terminol VP-1 of 12 to 400 °C (Therminol, 2015). The velocity range of Therminol VP-1 should be in the range of 0.36 and 4.97 m/s (Wagner, 2014) and is affected by the inner tube diameter of the HCE, the HTF density and the loop flow rate (NREL, 2015e). A freeze protection temperature for the HTF of 150 °C is typically and also assumed for the simulation (Kearney et al., 2002).

The size of the solar field is strongly effected by the solar multiple and the thermal demand of the steam Rankine cycle. At a solar multiple of 1 (design thermal power of the steam generator) the solar field requires 453003 m² (\approx 45.3 ha) reflective aperture area of SCA. 65.86 (\approx 66) loops are required at a SM of 1. The number of loops and so also the field size multiplies by the value of the SM.

Heat Transfer Fluid

Field HTF fluid	Therminol VP-1
User-defined HTF fluid	Edit...
Field HTF min operating temp	12 °C
Field HTF max operating temp	400 °C
Design loop inlet temp	293 °C
Design loop outlet temp	391 °C
Min single loop flow rate	1.4 kg/s
Max single loop flow rate	15.9 kg/s
Min field flow velocity	0.375986 m/s
Max field flow velocity	4.96185 m/s
Header design min flow velocity	2 m/s
Header design max flow velocity	3 m/s

Figure 43.: Screenshot of HTF input parameter for SAM.

Also the the solar field area and thereby the total land area depending by the SM. Equation 6 shows the influence on the solar field area of the ratio between the row spacing and the SCA width. The roe spacing is assumed by 18 m between the parallel SCAs. The total land area results by Equation 7 and is the solar field area multiplies by the factor of non-solar field area. The factor is assumed by 1.4 in the simulation (NREL, 2015e).

$$\text{solar field area } (m^2) = \text{aperture area } (m^2) \times \frac{\text{row spacing } (m)}{\text{SCA width } (m)} \quad (6)$$

$$\text{total land area } (m^2) = \text{solar field area } (m^2) \times \text{non-solar field multiplier} \quad (7)$$

Table 15 shows the solar field simulation parameter of the PTC system for the simulation configuration values of the solar multiple. The parameters of the Table comes from the above mentioned relations between the Items. The design power of the steam generator (SG) stays at 318.0 MW_{th} while the solar field thermal output rises proportional through the SM.

Item	Unit	Value						
SG Design power	MW _{th}	318.0						
Design-point DNI	W/m	950						
Solar multiple		2.0	2.5	3.0	3.5	4.0	4.5	5.0
Field th. output	MW _{th}	636	795	954	1 113	1 272	1 431	1 590
Number of loops	-	132	165	198	231	264	297	330
Aperture refl. area	ha	90.6	113.3	135.9	158.6	181.2	203.9	226.5
Total land area	ha	675	845	1013	1 182	1 351	1 540	1 689

Table 15.: PTC solar field parameter.

Thermal energy storage (TES)

The thermal energy storage (TES) of the simulated PTC system uses a indirect two-tank molten salt system with "Hitec Solar Salt" as storage fluid. This storage fluid is made from sodium nitrate (60 % NaNO₃) and potassium nitrate (40 % KNO₃). Solar Salt needs an minimum operating temperature of 238 °C and has a maximum operating temperature of 593 °C. (Suite, 2011; Kearney et al., 2003)

The storage design temperatures depends from the solar field design temperatures, so the designed temperature difference is 98 K. As it is shown in Table 16 the operating temperature limits fits with the storage tank design temperatures. The heater set point is 265 °C for both storage tanks. The TES full load hours goes from 6 to 16 in steps of 2. The thermal capacity and also the storage volume rises with the TES full load hours. The simulated stored thermal capacity reaches from 1 908 MWh_{th} at 6 full load hours up to 5 087 MWh_{th} at 6 full load hours.

Item	Unit	Value						
Storage type	-	indirect two-tank molten salt						
Storage fluid	-	Hitec Solar Salt						
Hot tank design temp.	°C	391						
Cold tank design temp.	°C	293						
TES full load hours	h	6	8	10	12	14	16	
Thermal capacity	MWh _{th}	1 908	2544	3 180	3 816	4 452	5 087	
Storage volume	m ³	25 805	34 407	43 008	51 610	60 212	68 813	

Table 16.: PTC system TES parameter.

It is obviously, that the storage volume of the PTC needs to be more than 3 times that much than the storage volume of the CR system. This is the result of lower temperature difference of the HTF and the turbine design capacity.

Also for the simulation of the PTC system the dispatch control of the turbine output fraction in the storage settings was used. Figure 44 shows the dispatch control matrix for the turbine output fraction.

	12am	1am	2am	3am	4am	5am	6am	7am	8am	9am	10am	11am	12pm	1pm	2pm	3pm	4pm	5pm	6pm	7pm	8pm	9pm	10pm	11pm
	Turb. out. fraction																							
Jan	9	9	9	9	9	9	9	7	7	7	7	6	6	6	6	5	4	3	7	7	7	9	9	
Feb	9	9	9	9	9	9	9	6	7	7	7	6	6	6	6	5	4	7	7	7	7	9	9	
Mar	9	9	9	9	9	9	9	4	6	7	7	6	6	6	6	5	5	3	7	7	6	6	9	9
Apr	8	8	8	8	8	8	8	3	3	6	7	7	7	7	5	4	4	6	5	5	3	3	8	8
May	8	8	8	8	8	8	8	5	6	6	5	5	5	5	5	4	3	4	4	4	3	2	8	8
Jun	8	8	8	8	8	8	8	2	2	4	4	4	4	4	4	3	3	2	2	2	2	8	8	
Jul	8	8	8	8	8	8	8	2	2	4	4	4	4	4	4	3	3	2	2	2	2	8	8	
Aug	8	8	8	8	8	8	8	2	2	6	6	6	6	6	6	5	4	7	4	3	2	2	8	8
Sep	8	8	8	8	8	8	8	2	7	7	7	7	7	5	5	4	4	3	5	5	5	2	8	8
Oct	9	9	9	9	9	9	9	4	6	7	7	7	6	6	5	5	4	3	5	5	5	5	9	9
Nov	9	9	9	9	9	9	9	7	7	7	7	6	6	6	6	5	4	7	7	7	7	7	9	9
Dec	9	9	9	9	9	9	9	7	7	7	7	7	7	7	7	5	4	5	7	7	7	7	9	9

Figure 44.: TES dispatch control matrix for turbine output fraction of PTC simulation in SAM.

Financial parameter

The financial parameter for calculating the LCOE of the simulated configuration are shown in Table 17. As before at the CR is the PTC power plant calculated over a lifetime of 25 years using a real interest rate of 7.5 % (Fraunhofer ISE, 2013). Also the total plant availability of 15 % once-off surcharge for EPC and contingencies on the total investment costs are equal to the CR (Platzer, 2014).

The specific costs for the collector field inclusive HTF-system is assumed with 275 \$/m² from (Morin et al., 2012). These specific cost could also be reduced by 25 % by using the assumed cost reduction from Flabeg (FLABEG FE GmbH, 2015). So the for the simulation assumed costs are highly conservative.

The specific costs for the power block are the same as at the CR but from other sources (Platzer, 2014).

The specific costs of 50 \$/kWh_{th} for the TES of the PTC are up to 50% higher than the CR costs (Platzer, 2014). This is reduce to the lower energy density using lower storage temperatures (Steinmann, 2015). Other expected specific costs between 35 and 50 \$/kWh_{th} (Steinmann, 2012).

As before Fichtner analyzed also the annual O&M costs for PTC power plants in SA and results costs of 1.96-1.97 % of the total investment costs (Fichtner, 2010). The value of 2 % can so also be assumed as conservative.

The costs for the land purchase comes from the "African Agriculture Review" report of the Nedbank Capital, which reported the prices for farmland in SA. For the LCOE calculation of the CSP and PV system was the land purchase costs of \$3,000/ha assumed which is based on these report (Cassell, 2012).

Item	Symbol	Value	Unit	Source
Collector field/HTF-system	c_{CF}	275	\$/m^2	(Morin et al., 2012)
Power block	$c_{PB,PTC}$	1000	\$/kW_{el}	(Platzer, 2014)
Thermal energy storage	$c_{TES,PTC}$	50	\$/kWh_{th}	(Platzer, 2014)
Land purchase	c_{LP}	3 000	\$/ha	(Cassell, 2012)
Annual O&M	$f_{O\&M,PTC}$	2	%	(Fichtner, 2010)
Lifetime	n	25	years	(Fraunhofer ISE, 2013)
Interest rate	i_{PTC}	7.5	%	(Fraunhofer ISE, 2013)
Surcharge for EPC, project management and risk	$f_{EPC,PTC}$	15	%	(Platzer, 2014)
Total plant availability	$f_{avail,plant,PTC}$	96	%	(Morin et al., 2012)

Table 17.: Financial input parameter for PTC-simulation in SAM.

5.4. PV power plant with electrical energy storage design and simulation

For this simulation a PV power plant was extended with an electrical energy storage (EES). This extended PV power plant was simulated in SAM's "Photovoltaic (detailed)" model with enabled battery storage option. Also for this simulation was the EPW weather file for Upington from Section 5.1.2 used. For the PV simulation SAM uses the following input data:

- Latitude (°)
- Longitude (°)
- Elevation above sea level (m)
- GHI, DNI and DHI (W/m²)
- Dry bulb temperature (°C)
- Wind velocity (m/s)

This section describes in detail the residual input data of the PV power plant with adapted battery storage. As before in the sections of simulated CSP technologies first the essential components of the system are defined. The financial parameters and the LCOE for this simulation was also here calculated separately and is documented in Appendix B on Page 98.

As mentioned at the beginning of these Chapter this must be seen as theoretical simulation. Actually there are not that large electrical energy storage systems in form of battery storage available.

For this simulation the load was connected to the PV and Battery system as shown on Figure 45. The load shape was defined as before specified before in Chapter 5.1.1 and simulates the demand of the power grid. As it is shown there is also the actual power grid connected as additional component, but for this simulation just the power flows between PV, battery and load is in focus. As it is shown in the Figure, SAM actually just supports the battery connection at the AC-bus via a power conversion system and is not able to simulate direct DC-connected batteries besides the PV-array before the PV-inverter. However in order to produce comparable results SAM was also used for the simulation of the PV power plant. As mentioned before this system contains out of the PV system with solar modules, solar and inverter and are described in the following section as well as the electrical energy storage.

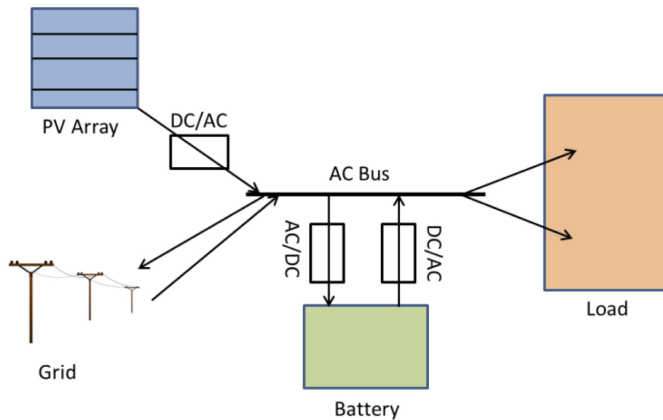


Figure 45.: Model of the configured PV plus battery scheme (Diorio et al., 2015).

Simulated configurations

The configurations of the PV system with adapted electrical energy storage has also the target to reach 90 % of the scheduled production curve from Section 5.1.1. To reach this target it is necessary to over scale the energy production of the PV system to produce enough power to cover the given load and load the storage during the day. This is quite similar to the solar multiple of the CSP system, but can not be put on a same level. Therefore this over scaling will be called "PV multiple" (PVM) and means the multiple of the PV inverter output. For example the system with a maximum inverter output of $100 \text{ MW}_{\text{el}}$ is a PVM of 1 than has the PV system with a PVM of 2 a maximum inverter output of $200 \text{ MW}_{\text{el}}$. The simulated system load is maximum $100 \text{ MW}_{\text{el}}$, so this is also the maximum supply of the system. The PV system was simulated one time without storage and a maximum inverter output of $100 \text{ MW}_{\text{el}}$ which is a PVM of 1. After that, the system was simulated in steps 0.2 of the PVM from 1.8 to 2.6. The adapted

energy storage capacity was simulated from 4 to 8 hours in hourly steps. This storage capacity range is also defined for large-scale off-grid application in (IEA, 2014). Table 18 summarizes the simulated configurations.

PV system

The simulated PV system is orientated at actual PV systems in SA. Therefore the currently under construction situated Mulilo Sonnedix Prieska PV Project in the Northern Cape will serve as a role model for the main components. In this 75 MW_{ac}-project are poly crystalline 305 W_{dc} modules of type BYD 305P6C-36 from BYD installed. The efficiency of the modules is about 15.72 %. The full module specification is in Table 19. The peak performance of the project is 86.23 MW_{dc}. (Morse, 2014)

These for the simulation selected module type was already deposited in the module library in SAM. This large library is based on the database of Go Solar California for photovoltaic modules and inverters from the California Energy Commission (NREL, 2015c).

Figure 46 shows the modules currentvoltage characteristic with a short circuit voltage of 8.9 A and an open circuit voltage of 45.5 V.

Item	Unit	Value							
Maximum load supply	MW _{el}	100							
PV multiple	-	1.0 1.8							
EES capacity	h	- 4 5 6 7 8							
PV multiple	-	2.0 2.2							
EES capacity	h	4	5	6	7	8	4	5	6 7 8
PV multiple	-	2.4 2.6							
EES capacity	h	4	5	6	7	8	4	5	6 7 8

Table 18.: Simulated configurations of the PV system with adapted EES.

Item	Value	Unit
Manufacturer	BYD COMPANY LIMITED	-
Model	BYD 305P6C-36	-
Cell type	poly-crystalline silicon	-
Maximum power	304.99	W _{dc}
Nominal efficiency	15.72	%
Maximum power voltage	36.2	V _{dc}
Maximum power current	8.4	A _{dc}
Open circuit voltage	45.5	V _{dc}
Short circuit current	8.9	A _{dc}
Temperature efficiency	-0.41	%/ °C
Module area	1.94	m ²
Number of cells	72	-

Table 19.: Module specification of BYD 305P6C-36 under STC: 1000 W/m², cell temperature 25 °C (NREL, 2015c).

The Mulilo Sonnedix Prieska PV Project install inverter from AEG. These specific AEG Protect PV.800 inverter is not available in the library of SAM, but a similar model with almost the same power rating was selected. Table 20 depicts the specifications of the for the simulation used Ingeteam inverter INGECON SUN 805TL U X420 Outdoor with 805 kW_{ac} power at an efficiency of 98.33 %. The efficiency curve of the inverter can be seen in Figure 47.

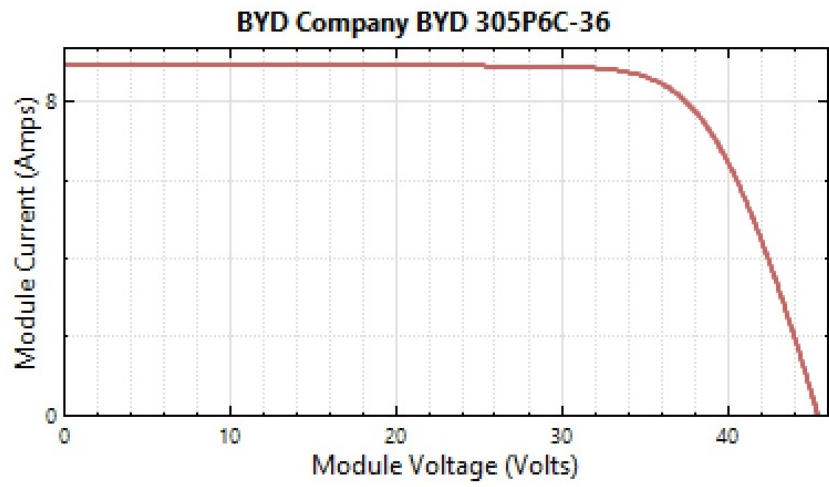


Figure 46.: Currentvoltage characteristic under STC of module BYD 305P6C-36 (NREL, 2015c).

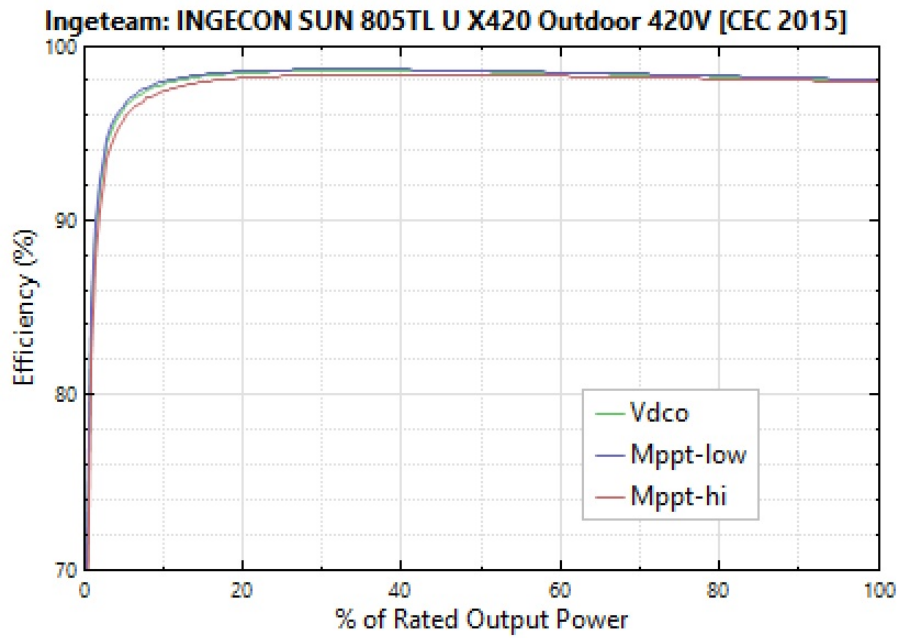


Figure 47.: Efficientcy characteristic of Ingecon Sun 805TL U X420 Outdoor (Ingeteam INC., 2015; NREL, 2015c).

Item	Value	Unit
Manufacturer	Ingeteam Power Technology	-
Model	Ingecon Sun 805TL U X420 Outdoor	-
Type	central inverter	-
Input (dc)		
Maximum power	821.39	kW _{dc}
Voltage range	611-820	V _{dc}
Maximum voltage	1 000	V _{dc}
Maximum current	1 350	A _{dc}
Nominal voltage	715.91	V _{dc}
Output (ac)		
Maximum power	805	kW _{ac}
Nominal voltage	420	V _{ac}
Maximum current	1.35	A _{ac}
Frequency	50-60	Hz
cos ϕ	1	-
Maximum efficiency	98.33	
European efficiency	98.29	
Power consumption in operation	1.25	kW _{dc}
Power consumption at night	0.12	kW _{ac}

Table 20.: Inverter specifications of Ingecon Sun 805TL U X420 Outdoor (Ingeteam INC., 2015; NREL, 2015c).

As mentioned before the PV system was design under similar condition that the Mulilo Sonnedix Prieska PV Project. There a dc/ac ratio of 1.15 is used (Morse, 2014). This power ratio compares the photovoltaic array power to the inverter capacity (Woodcock, 2013). For the simulated PV system the same ratio was assumed. So at 100 MW_{ac} inverter output, a total module capacity of 115 MW_{dc} is needed. From the discussed parameter and the PVM SAM calculates the resulting number of modules and inverters as well as other parameters on its own. These PV system parameter are summarized in Table 21.

For the orientation of the simulated PV-modules the latitude of Upington was used as tilt angle (28.4°) and the azimuth is 0° , so directly facing north. The self-shading model was selected, without external shading parameter. Therefore 2 modules along the side of row and 10 along the bottom of row was selected. Therefrom a shading loss of 0.545 % on the solar radiation incident on the subarray. Further assumed losses are soiling, mismatch, diodes and connections and wiring losses. The assumed soiling losses reduce the solar radiation incident on the subarray of about 5 %. The assumed mismatch loss of about 2 % is related to slight differences in

Item	Unit	Value					
Module azimuth	°	0 (north)					
Module tilt	°	28.4					
Modules per string	-	21					
String open circuit voltage	V _{oc}	955.3					
String max. power rated voltage	V _{mp}	759.8					
Maximum dc-voltage	V _{dc}	1 000					
Aspired dc/ac-ratio	-	1.15					
PV multiple	-	1.0	1.8	2.0	2.2	2.4	2.6
Total inverter capacity	MW _{ac}	99.8	180.3	199.6	219.8	239.9	260.0
Total module capacity	MW _{dc}	115.0	207.0	230.0	253.0	276.0	299.0
Strings in parallel	-	17 954	32 318	35 909	39 500	43 091	46 682
Number of modules	-	377 034	678 678	754 089	829 500	904 911	980 322
Number of inverter	-	124	224	248	273	298	323
Total module area	ha	73.1	131.7	146.3	160.9	175.6	190.1
Total land area	ha	244	439	488	536	585	634

Table 21.: PV system design parameter.

performance of individual modules in the array. Voltage drops across blocking diodes and electrical connections leads to a assumed diodes and connections loss of 0.5 %. There are also assumed resistive losses of 2 % in wiring on the dc-side and 1 % wiring loss between the inverter and the grid connection point on the ac-side of the system.

Electrical energy storage (EES)

The electrical energy storage is adapted though the system as it is shown in Figure 45 on Page 75. The EES basically consists out of two parts - the power conversions system (PCS) and the storage unit - as it is shown in Figure 34 on Page 50. For the simulation in SAM the PCS was simplified to the conversion efficiency. The AC to DC conversion efficiency was assumed with 99 % as well as the DC to AC efficiency. Nevertheless for the LCOE calculation it is still relevant to define the performance of the PCS. As it is shown in Table 21 the inverter capacity range is between 240 and 320 MW_{ac} for the simulation cases with adapted storage. The maximum scheduled load from Section 5.1.1 is 100 MW. So depending from the PV inverter capacity the PCS capacity needs to variate as well to collect the PV-overproduction. For the calculation of the LCOE it was assumed that the PCS needs to collects the inverter capacity minus the 100 MW daily base load.

As mentioned before the storage unit consists out of a Li-Ion battery, more precisely a using a Nickel Cobalt Aluminum ($LiNiCoAlO_2$ or NCA) cathode. This battery excels through a less expensive cathode material with improved safety characteristics and high specific energy (NREL, 2015e). The voltage characteristics of these battery for the simulation are shown in Figure 48. The NCA battery is inter alia installed in the Tesla Model S and X (Nykvist & Nilsson, 2015) which uses currently Panasonic cells and will also be installed in Teslas Power Wall system (Shahan, 2015). The performance and lifetime of the NCA batteries depending on how they are used. Tesla names the lifetime of 5 000 cycles without mentioning the assumed depth of discharge (DOD) (Shahan, 2015).

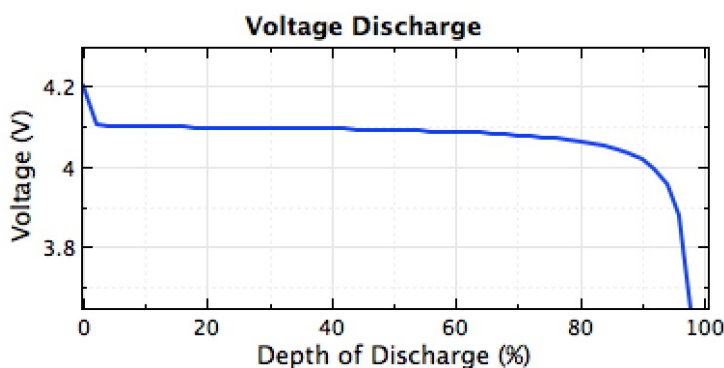


Figure 48.: Voltage properties of NCA Li-Ion battery..

The DOD is the amount of capacity in the battery that is usable by the system. For electric vehicles (EV) the DOD is set between 80-95 % at the "top" end of the battery and 10-20 % at the "bottom" end (Warner, 2014). The state of charge (SOC) is an expression of the present battery capacity as a percentage of maximum capacity and is the inverse of the DOD. It must be noted, that the nominal capacity of a battery is not the effective usable capacity of a battery and depends on the DOD. Also the DOD effects the cycle life of the batteries. The higher the DOD, the lower the cycle life. In other words, the lower the SOC, the longer the cycle life. (MIT Electric Vehilce Team, 2008)

SAM visualizes the decreasing capacity of the battery over the number of cycles with capacity fades as it is shown in Figure 49 for the NCA. The figure shows the characteristic for 20 % and 80 % DOD. As mentioned above the graph shows the higher decreasing of the effective capacity at higher DOD. The performance data behind this graph is coming from (Dahn & Ehrlich, 2011) and correspond with other tests (Read et al., 2009).

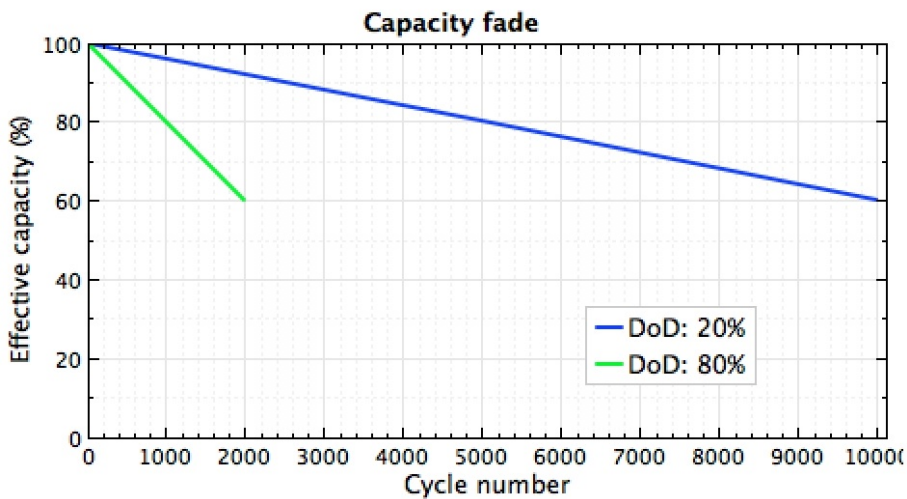


Figure 49.: Capacity fade of Nickel Cobalt Aluminum Lithium-Ion battery.

It must be noted, that the cycle lifetime is not only affected by the DOD but also by other conditions such as temperature and humidity (MIT Electric Vehilce Team, 2008). SAM designs the cycle lifetime for the batteries at a constant room temperature of 20 °C therefore the storage room needs to be conditioned. Also the charging and discharging of the battery results losses in form of heat which needs to get led away. The cooling demand of the EES system is not included in the simulation, but must be actually significant. (Diorio et al., 2015)

The system was designed for a lifetime of 25 years. Therefore also the EES is designed for this period. For the simulation a amount of 365 cycles per year was assumed. So the NCA was designed for 9 125 cycles whiteout using a battery bank replacement. SAM also can analyses the cycle lifetime of the batteries. This analyses showed that the NCA battery reaches this cycle lifetime with a DOD of 50 %. But under this conditions the effective capacity of the battery

is nearly 0 % after 25 years. As it is shown in Figure 49 the effective capacity of the NCA battery decreases almost lineal with the cycle number. There are two opportunities to reduce the loss to the effective capacity increasing over the lifetime of the system. First is a battery bank replacement after a specified schedule or loss of effective capacity to a specified amount and second is to use a lower DOD which leads also to a lower effective usable capacity of the battery, so a higher nominal capacity of the battery would be necessary.

Further is to note that Li-Ion batteries has a expiry period (Jossen & Weydanz, 2006). Tesla gives a warranty of 10 years of the batteries (Shahan, 2015) so it can be expected, that the expiry period is close to these warranty. So also for the simulation an battery bank replacement is indispensable.

The for a long lifetime an average SOC of 30-70 % is recommended for Li-Ion batteries (Jossen & Weydanz, 2006). Consequently the SOC was set to a maximum of 30 % and a minimum of 70 % for the simulation. So a total DOD of 40 % which signified 40 % of the nominal battery capacity was assumed as usable. In order to have high storage availability over the total system lifetime it was assumed that the battery bank will replaced at a effective capacity loss of 20 %. This is also advised for EES in electronic consumer devices (Spotnitz, 2003). Resulting from this assumptions the cycle lifetime of the cells in the battery bank is 2 500 cycles. Therefore the battery bank needs to be replaced after 6-7 years. So the battery bank needs to be replaced three times in the total lifetime of the system.

Table 22 summarizes results of the discussed parameter for the simulation. The adapted voltage level for this large-scale EES application from 820 V_{dc} per string is coming from (Leuthold, 2014). The remaining values results from the above discussed parameter or are adapted from the SAM library (Diorio et al., 2015).

Item	Unit	Value					
Chemistry	-	Lithium ion: nickel cobalt aluminum oxide					
Cell nominal voltage	V _{dc}	3.6					
Internal resistance	Ohm	0.1					
Fully charged cell voltage	V _{dc}	4.2					
Exponential zone cell voltage	V _{dc}	4.1					
Nominal zone cell voltage	V _{dc}	3.6					
Nominal bank voltage	V _{dc}	820					
Cells in series	-	228					
Cell capacity	Ah	55					
C-rate of discharge curve	-	0.2					
Maximum C-rate charge	per/h	1					
Maximum C-rate discharge	per/h	1					
Total DOD	%	20					
Storage capacity at 100 MW output		h	4	5	6	7	8
Effective capacity	MWh	400	500	600	700	800	
Nominal capacity	MWh	1 000	1 250	1 500	1 750	2 000	
Cells	×10 ⁶	5.1	6.3	7.6	8.8	10.1	

Table 22.: EES system design parameter.

Financial parameter

The financial parameter for the LCOE calculation are composed in Table 23. As mentioned before was the LCOE calculation for this simulation made separately in Microft Excel using a simplified method which is documented in Appendix B on Page 98. As for the other systems is the PV power plant designed for a lifetime of 25 years.

The specific large-scale PV system costs in South Africa amount to $1.285 \text{ \$/W}_{\text{DC,Peak}}$ ($14.5 \text{ ZAR/W}_{\text{DC,Peak}}$ using 11.286 USD/ZAR average in 2014 (IRS, 2015)) which leads from an in 2014 actually built PV system (Terblanche, 2015). These specific costs are close to utility-scale PV systems in Europe with specific investments of $1 \text{ \$/W}_{\text{DC,Peak}}$ (Fraunhofer ISE, 2013), corresponding to $1.33 \text{ \$/W}$ (using the average exchange rate in 2014 of $1.33 \text{ \$/W}$ (Statista GmbH, 2015)).

The LCOE was calculated with different interest rates and O&M costs for the PV power plant and the EES system. The real interest rate for the PV power plant was assumed with 2.8 % (Fraunhofer ISE, 2013) and the annual O&M costs are 1 % of the PV investment costs (International Energy Agency, 2014c). A degradation of 1 % per year of the annual energy output was assumed for the ageing phenomena of the PV cells (Tidball et al., 2010).

The storage costs are calculated from three parts. The costs for the PCS, the battery bank and the replacement costs of the battery bank during the lifetime of the system.

The costs of the PCS of $615 \text{ \$/kW}$ ($463 \text{ \$/kW}$ using the average exchange rate in 2014 of $1.33 \text{ \$/W}$ (Statista GmbH, 2015)) was taken over from a study toward comparative life cycle cost analysis of EES (Zakeri & Syri, 2015). This is the average value of a wide cost range (250-600/kW) of PCS for Li-Ion EES systems.

For the storage part of the EES a highly optimistic value of $300 \text{ \$/kWh}$ was assumed from (Nykvist & Nilsson, 2015). The average storage part cost for Li-Ion EES in other studies is $914 \text{ \$/kWh}$ (Zakeri & Syri, 2015).

For the replacement costs of the an other highly optimistic value of $150 \text{ \$/kWh}$ was assumed. The cost for the replacement of the storage in (Zakeri & Syri, 2015) are approximately the half of the storage costs. This costs was also assumed with a look to Figure 52 on Page 92.

The assumed EES battery bank replacements during the lifetime was described in this Chapter already.

The annual O&M costs of $9.18 \text{ \$/kW}$ was also a adaption from (Zakeri & Syri, 2015) as well as the real interest rate of 8.0 %

As before for the other solar power plants also for the PV system was land purchase costs of $\$3,000/\text{ha}$ (Cassell, 2012) assumed.

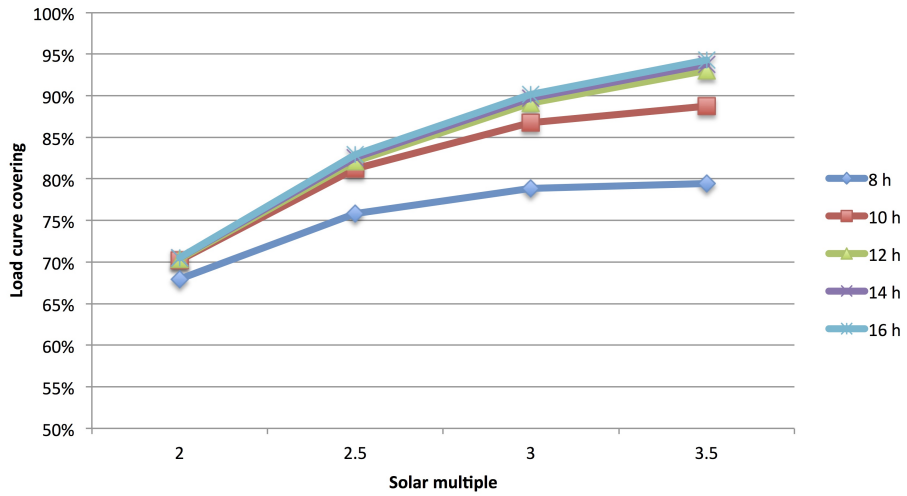
Item	Symbol	Value	Unit	Source
Lifetime	n	25	years	(Fraunhofer ISE, 2013)
Solar modules	c_{sm}	0.481	\$/W_{dc}	(Terblanche, 2015)
Structural	c_{st}	0.138	\$/W_{dc}	(Terblanche, 2015)
Electrical parts	c_{ep}	0.116	\$/W_{dc}	(Terblanche, 2015)
Inverters	c_{inv}	0.117	\$/W_{dc}	(Terblanche, 2015)
Engineering and labour costs	c_{elc}	0.242	\$/W_{dc}	(Terblanche, 2015)
Security and infrastructure	c_{si}	0.091	\$/W_{dc}	(Terblanche, 2015)
Transport and logistics	c_{tl}	0.067	\$/W_{dc}	(Terblanche, 2015)
Sub-Station	c_{ss}	0.071	\$/W_{dc}	(Terblanche, 2015)
Total PV system costs	c_{PV}	1.285	\$/W_{dc}	(Terblanche, 2015)
Annual degradation factor	f_{degrad}	1	%	(Tidball et al., 2010)
Annual PV O&M costs factor	$f_{O\&M,PV}$	1	%	(International Energy Agency, 2014c)
Interest rate of PV	i_{PV}	2.8	%	(Fraunhofer ISE, 2013)
EES PCS costs		615	\$/kW	(Zakeri & Syri, 2015)
EES battery bank costs		300	\$/kWh	(Nykvist & Nilsson, 2015)
EES battery bank replacement costs		150	\$/kWh	(Zakeri & Syri, 2015)
Assumed EES battery bank replacements during lifetime	-	3	-	-
Annual EES O&M costs		9.18	\$/kW	(Zakeri & Syri, 2015)
Interest rate of EES	i_{EES}	8.0	%	(Zakeri & Syri, 2015)
Land purchase	CLP	3 000.00	\$/ha	(Cassell, 2012)

Table 23.: Financial input parameter for PV-simulation in SAM.

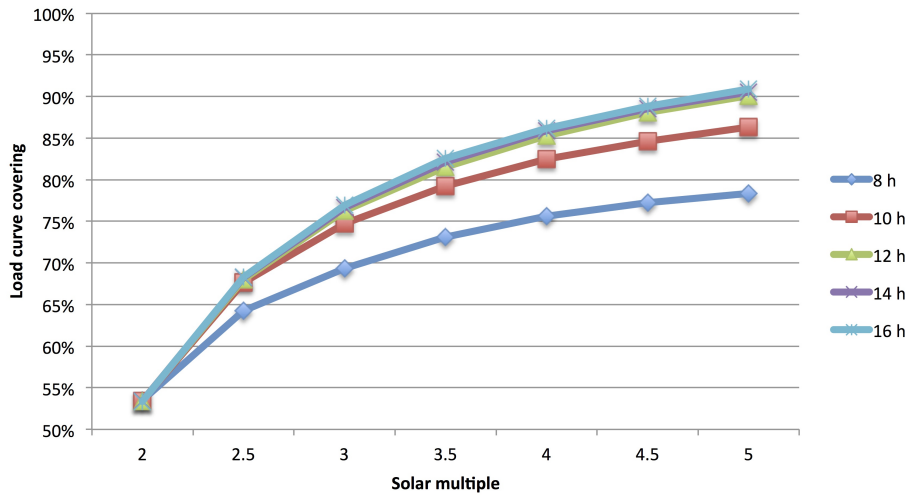
5.5. Simulation results

PV unity scale without storage 6-7.5 cent/kWh (GHI 2000kWh/m²) in 2013 (Fraunhofer ISE, 2013)

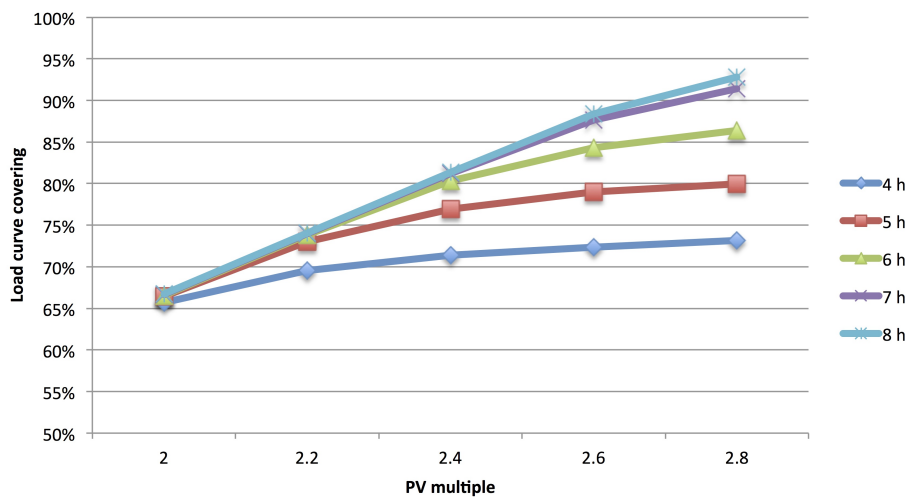
CSP



(a) CR power plant



(b) PTC power plant

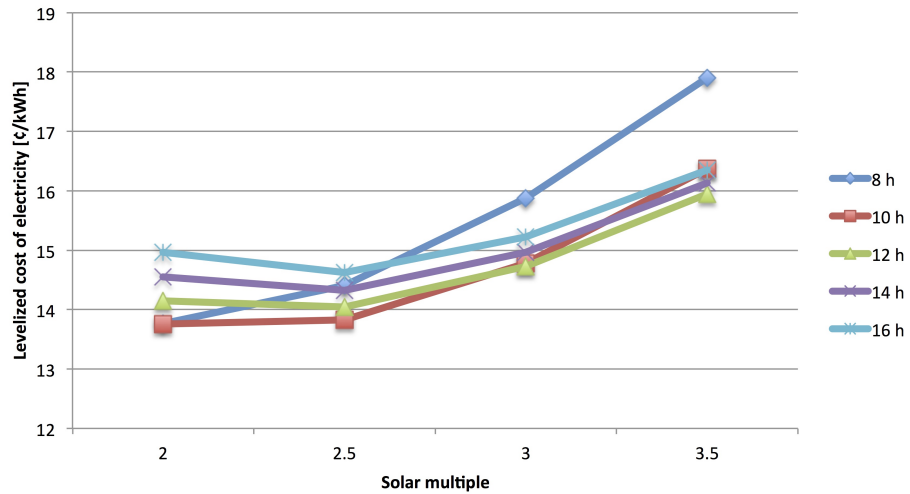


(c) PV power plant with addapted EES

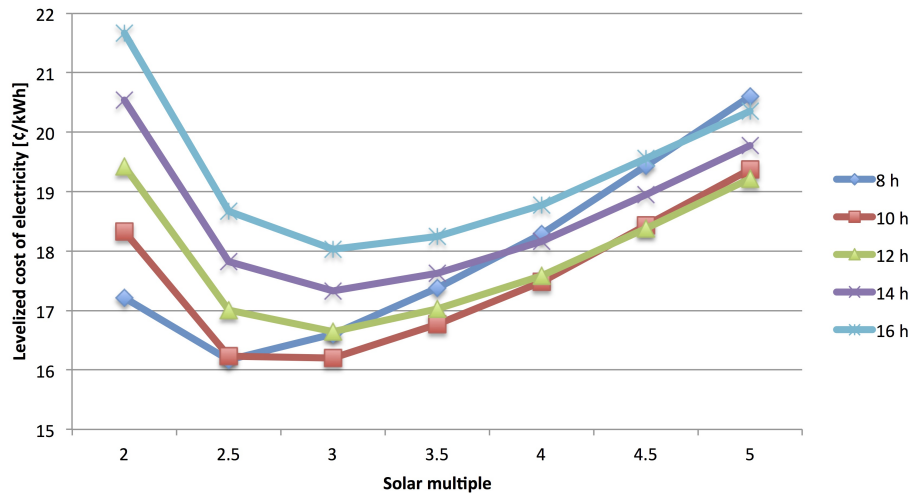
Figure 50.: Load curve covering results of simulated solar power plants.

5.6. Interpretation and comparison of results

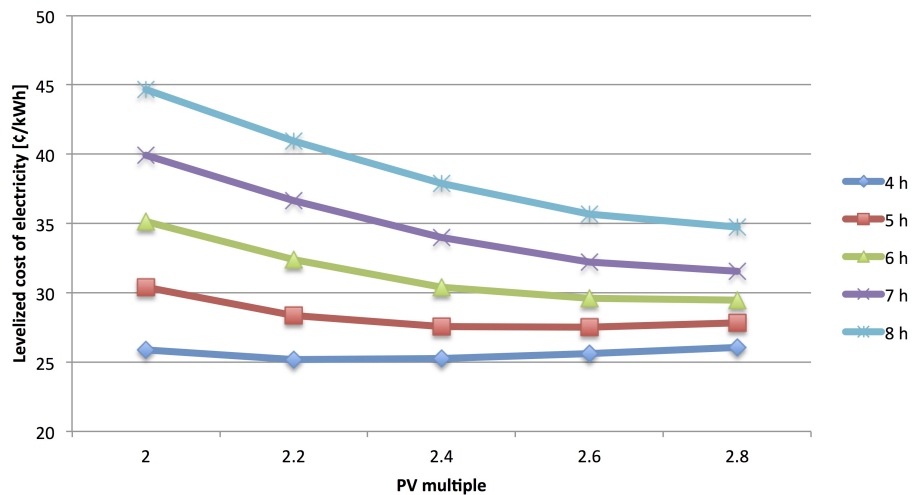
PV-Storage → Battery lifetime Spinnennetzdiagramm



(a) CR power plant



(b) PTC power plant



(c) PV power plant with addapted EES

Figure 51.: Levelized costs of electricity results of simulated solar power plants.

6. Current economical situation and digression potential of main technologies to a long therm marked potential

6.1. CSP

(Smith, 2012)

6.2. PV plant

6.2.1. Electrical storage

lead-acid

Li-ion(Nykqvist & Nilsson, 2015)

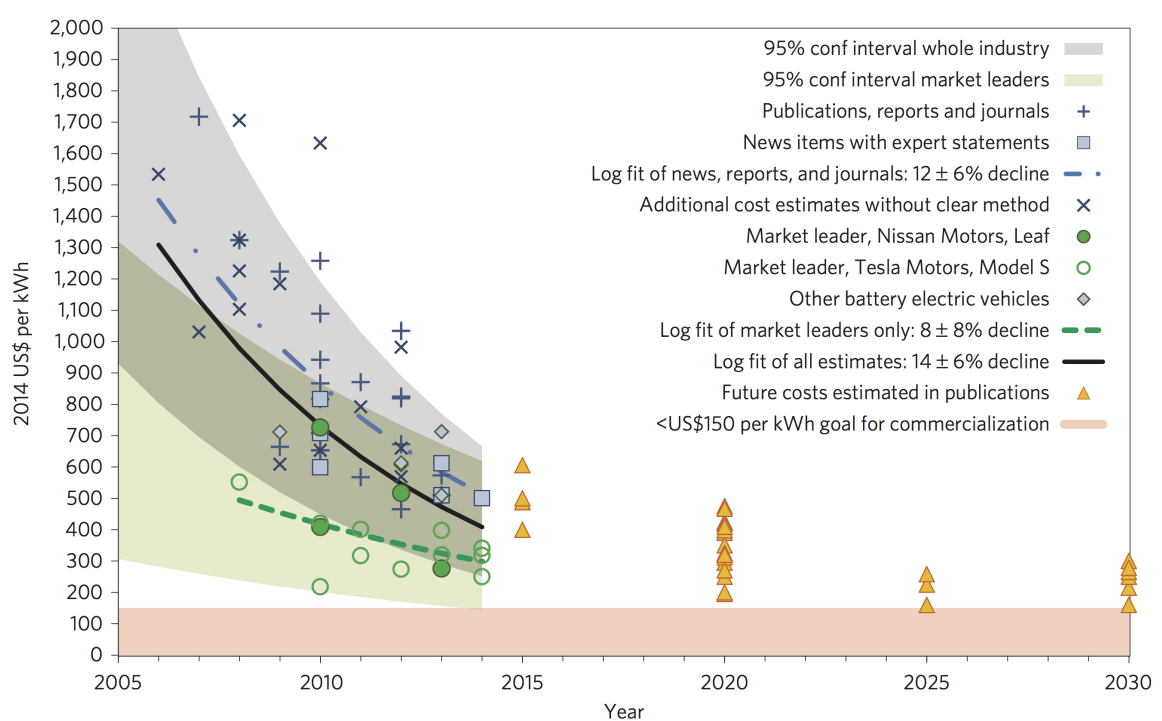


Figure 52.: Cost of Li-ion battery packs in battery electric vehicles (Nykvist & Nilsson, 2015).

7. Conclusion and outlook

Spinnennetzdiagramm (cost reduction potential, Current LCOE, market maturity, contribution to grid stability, capacity factor, load curve covering factor) Auf Christophs arbeit verweisen und auf hybridPV: <http://www.beselectric.com/de/hybrid/>

Sehr optemistischer LCOE bei PV ohne speicher. Keine kühlung verlust durch alterung nur bedingt betrachtet

A. Appendix I

A.1. Part A

Production from:	Electricity [GWh]:
- coal	239 344
- oil	194
- gas	0
- biofuels	293
- waste	0
- nuclear	13 073
- hydro (incl. PSP)	4 860
- geothermal	0
- solar PV	50
- solar thermal	0
- wind	103
- tide	0
- other sources	0
Total production:	257 919
Imports	10 006
Exports	-15 035
Domestic supply:	252 890
Statistical differences	-2 769
Energy industry own use	30 678
Losses	22 351
Final consumption:	197 092
Industry	117 272
Transport	3 826
Residential	38 779
Commercial and public services	28 183
Agriculture / forestry	5 709
Other non-specified	3 323

Table 24.: Electricity flow in South Africa 2012(International Energy Agency, 2015).

Technology	Units	Parabolic Trough	Fresnel Trough	Molten Salt Solar Tower	Water Steam Solar Tower	Parabolic Dish
Technical Parameters						
Plant Size, envisaged	[MWe]	50 - 300 *	30 - 200	10 - 200 *	10 - 200	0.01 - 850
Plant Size, already realized	[MWe]	50 (7.5 TES), 80 (no TES)	5	20	20	1.5 (60 units)
Collector / Concentration	[-]	Parabolic trough (70 - 80 suns)	Fresnel trough / > 60 suns, depends on secondary reflector	Heliostat field / > 1,000 suns	Heliostat field / > 1,000 suns	Single Dish / > 1,300 suns
Receiver / Absorber	[-]	Absorber fixed to tracked collector , complex design	Absorber fixed to frame, no evacuation, secondary reflector	External tube receiver	External or cavity tube receiver, multi receiver systems	Multi receiver system
Storage System	[-]	Indirect two-tank molten salt (380°C, dT = 100K)	Short-time pressurized steam storage (<10min)	Direct two-tank molten salt (550°C, dT = 300K)	Short-time pressurized steam storage for saturated steam (<10min)	No storage for dish Stirling, chemical storage under development
Hybridisation	[-]	Yes, indirect (HTF)	Yes, direct (steam boiler)	Yes	Yes, direct (steam boiler)	Not planned
Grid Stability	[-]	medium to high (TES or hybridisation)	medium (back-up firing possible)	high (large TES)	medium (back-up firing possible)	low
Cycle	[-]	Rankine steam cycle	Rankine steam cycle	Rankine steam cycle	Rankine steam cycle	Stirling cycle, Brayton cycle, Rankine cycle for distributed dish farms
Steam conditions	[°C/bar]	380°C / 100 bar	260°C / 50 bar	540°C / 100 - 160 bar	up to 540°C / 160 bar	up to 550°C / 150 bar
Land requirements **	[km²]	2.4 - 2.6 (no TES) 4 - 4.2 (7h TES)	1.5 - 2 (no TES)	5 - 6 (10 - 12 h TES)	2.5 - 3.5 (DPT on the lower site)	2.5 - 3
Required slope of solar field	[%]	< 1-2	< 4	< 2-4 (depends on field design)	< 2-4 (depends on field design)	>10%
Water requirements ***	[m³/MWh]	3 (wet cooling) 0.3 (dry cooling)	3 (wet cooling) 0.2 (dry cooling)	2.5-3 (wet cooling) 0.25 (dry cooling)	2.5-3 (wet cooling) 0.25 (dry cooling)	0.05 - 0.1 (mirror washing)
Annual Capacity Factor	[%]	25 - 28% (no TES) 40 - 43% (7h TES)	22 - 24%	55% (10h TES), larger TES possible	25 - 30% (solar only)	25 - 28 %
Annual Solar-to-Electricity Efficiency (net)	[%]	14 - 16%	9 - 10% (saturated)	15 - 17%	15 - 17%	20-22%

* maximum/optimum depends on storage size ** 100 MWe plant size ***Depends on water quality

Figure 53.: CSP Technologies Comparison I (Fichtner, 2010).

Technology	Units	Parabolic Trough	Fresnel Trough	Molten Salt Solar Tower	Water Steam Solar Tower	Parabolic Dish
Commercial Aspects						
Maturity	[-]	- Proven Technology on large scale; - Commercially viable today	- Demonstration projects, first commercial projects under construction - Commercially viable 2011 onwards	Demonstration projects, first commercial projects under construction Commercially viable 2011 onwards	- Saturated steam projects in operation - Superheated steam demonstration projects, first commercial projects under construction - Commercially viable 2012 onwards	- demonstration projects, first commercial projects (first units) in 2011; - Commercially viable 2012 onwards
Total Installed Capacity (in operation Q4 2010)	[MWe]	1,000	7	10	10 (superheated /demo) 30 (saturated steam)	1.7
Estimated total Installed Capacity (in operation 2013)	[MWe]	3,000 - 4,000	200 - 300	200 - 400	400 - 500	500 - 1,000
Number of Technology Provider	[-]	high (> 10), Abengoa Solar / Abener, Acciona, ASC Cobra / Sener, Albiasa Solar, Aries Ingeniera, Iberdrola, MAN SolarMillenium, Samca, Solel / Siemens, Torresol etc.	medium (3 - 4), Aeva, Novatec Biosol AG, Sky Fuels, Solar Power Group, etc.	medium (2 - 5) Solar Reserve and Torresol others like Abengoa Solar and eSolar, SolarMillenium are planning entry	medium (3 - 4), Abengoa Solar, BrightSource Energy, eSolar etc.	medium (4 - 5), Abengoa Solar, Infinia, SES / Tessera Solar, SB&P, Wizard Power
Technology Development Risk	[-]	low	medium	medium	medium	medium
Investment costs for 100MW	[\$/kW]	4,000-5,000 (no storage) 6,000-7,000 (7-8h storage)	3,500-4,500 (no storage)	8,000-10,000 (10h storage)	4,000-5,000 (no storage)	4,500-8,000 (depending on volume production)
O&M Costs	[m \$/a]	6 - 8 (no storage)	5.5 - 7.5	7 - 10 (molten salt with TES)	5 - 7 (water steam, no TES)	10 - 15 (water steam, no TES)

Figure 54.: CSP Technologies Comparison II (Fichtner, 2010).

B. Appendix B: Methodology for calculating the LCOE

The LCOE is a financial value to compare different power producing technologies with different financial parameters and generation structures over a hole economical lifetime of power plants. To calculate the LCOE a simplified method from (Morin et al., 2012), originally proposed by (Roy et al., 1997) was considered:

$$LCOE = \frac{C_{invest} \times (f_{annuity} + f_{ins.ann.}) + C_{O\&M}}{E_{el,net,ann.} \times f_{avail,plant}} \quad (8)$$

This equation is commonly used for CSP plants and don't contain a degradation factor as it is necessary for the lifetime consideration of PV power plants. So the equation was extended with the average degradation factor of full observation period $f_{Full,degrad}$:

For the calculation of the LCOE of all power plants the extended equation was used:

$$LCOE = \frac{C_{invest} \times (f_{annuity} + f_{ins.ann.}) + C_{O\&M}}{E_{el,net} \times f_{avail,plant} \times f_{Full,degrad}} \quad (9)$$

with:

$$f_{annuity} = \frac{(1+i)^n \times i}{(1+i)^n - 1} \quad (10)$$

$$f_{Full,degrad} = \frac{\sum_{t=0}^{n-1} \frac{1}{(1+f_{degrad})^t}}{n} \quad (11)$$

$LCOE$ leveled cost of electricity in \$/kWh

C_{invest} investment costs in \$

$C_{O\&M}$ annual operation and maintenance costs in \$

$E_{el,net}$ produced electricity in the first year in kWh

$f_{annuity}$ annuity factor in %

$f_{ins.ann.}$ annual insurance costs in %

$f_{avail,plant}$ total plant availability in %

$f_{Full,degrad}$ average degradation factor of full observation period in %

f_{degrad} annual degradation factor in %

n useful life and amortization period

i interest rate in %

t year of lifetime (1, 2, ...n)

B.1. CR power plant

The investment costs for the CR power plant are calculated with the parameters from Table 12 according to:

$$C_{invest,CR} = (C_{HF} + C_{LP,CR} + C_{PB,CR} + C_{T+R} + C_{TES,CR}) \times (1 + f_{EPC,CR}) \quad (12)$$

$C_{invest,CR}$ investment costs of CR in \$

C_{HF} heliostat field costs in \$

$C_{LP,CR}$ land purchase costs in \$

$C_{PB,CR}$ power block costs in \$

C_{T+R} tower and receiver costs in \$

$C_{TES,CR}$ thermal energy storage costs in \$

$f_{EPC,CR}$ surcharge for EPC, project management and risk in %

The individual investment costs segments of the CR system can be derived from:

$$C_{HF} = c_{HF} \times A_{reflective,CR} \quad (13)$$

$$C_{LP,CR} = c_{LP} \times A_{land,CR} \quad (14)$$

$$C_{PB,CR} = c_{PB,PTC} \times P_{gross,CR} \quad (15)$$

$$C_{T+R} = c_{T+R} \times P_{receiver,th} \quad (16)$$

$$C_{TES,CR} = c_{TES,CR} \times E_{storage,th,CR} \quad (17)$$

c_{HF} specific heliostat field costs in \$/m²

$A_{reflective}$ heliostat field reflective area in m²

c_{LP} specific land purchase costs in \$/ha

$A_{land,CR}$ total land area of CR power plant in ha

$c_{PB,CR}$ specific power block and balance of CR plant costs in \$/kW_e

$P_{gross,CR}$ turbine gross capacity of CR power plant in kW_e

c_{T+R} specific tower and receiver costs in \$/kW_{th}

$P_{receiver,th}$ receiver thermal power in kW_{th}

$c_{TES,CR}$ specific thermal energy storage costs for CR power plants in \$/kWh_{th}

$E_{storage,th,CR}$ thermal energy storage capacity of CR power plant in kWh_{th}

Also the annual operational and maintenance costs are calculated with parameters from Table 12 and the investment costs according to:

$$C_{O\&M,CR} = C_{invest,CR} \times f_{O\&M,CR} \quad (18)$$

$C_{O\&M,CR}$ annual O&M costs of CR power plant in \$

$C_{invest,CR}$ investment costs of CR power plant in \$m

$f_{O\&M,CR}$ annual O&M costs factor of CR power plant in %

The CR system assume an annual plant availability $f_{avail,plant,CR}$ of 96 % which is already included in $E_{el,net,ann}$. as a result from the simulation in SAM. For the CR is no annual degradation provided. The factor $f_{Full,degrad}$ can be neglected.

B.2. PTC power plant

The investment costs for the PTC power plant are calculated with the parameters from Table 17 according to:

$$C_{invest,PTC} = (C_{CF} + C_{LP,PTC} + C_{PB,PTC} + C_{TES,PTC}) \times (1 + f_{EPC,PTC}) \quad (19)$$

$C_{invest,PTC}$ investment costs of PTC in \$

C_{CF} collector field costs in \$

$C_{LP,PTC}$ land purchase costs in \$

$C_{PB,PTC}$ power block costs in \$

$C_{TES,PTC}$ thermal energy storage costs in \$

$f_{EPC,PTC}$ surcharge for EPC, project management and risk in %

The individual investment costs segments of the PTC system can be derived from:

$$C_{CF} = c_{CF} \times A_{reflective,PTC} \quad (20)$$

$$C_{LP,PTC} = c_{LP} \times A_{land,PTC} \quad (21)$$

$$C_{PB,PTC} = c_{PB,PTC} \times P_{gross,PTC} \quad (22)$$

$$C_{TES,PTC} = c_{TES,PTC} \times E_{storage,th,PTC} \quad (23)$$

c_{CF} specific parabolic trough collector field costs in \$/m²

$A_{reflective}$ parabolic trough collector field reflective area in m²

c_{LP} specific land purchase costs in \$/ha

$A_{land,PTC}$ total land area of PTC power plant in ha

$c_{PB,PTC}$ specific power block and balance of PTC plant costs in \$/kW_e

$P_{gross,PTC}$ turbine gross capacity of PTC power plant in kW_e

$c_{TES,PTC}$ specific thermal energy storage costs for PTC power plants in \$/kWh_{th}

$E_{storage,th,PTC}$ thermal energy storage capacity of PTC power plant in kWh_{th}

Also the annual operational and maintenance costs are calculated with parameters from Table 17 and the investment costs according to:

$$C_{O\&M,PTC} = C_{invest,PTC} \times f_{O\&M,PTC} \quad (24)$$

$C_{O\&M,PTC}$ annual O&M costs of PTC power plant in \$

$C_{invest,PTC}$ investment costs of PTC power plant in \$

$f_{O\&M,PTC}$ annual O&M costs factor of PTC power plant in %

The PTC system assume an annual plant availability $f_{avail,plant,PTC}$ of 96 % which is already included in $E_{el,net,ann.}$ as a result from the simulation in SAM. For the CR is no annual degradation provided. The factor $f_{Full,degrad}$ can be neglected.

B.3. PV power plant

The investment costs for the PV system with storage are calculated with the parameters from Table 23 according to:

$$C_{invest,PV} = C_{PV-field} + C_{EES} + C_{LP,PV} \quad (25)$$

$C_{invest,PV}$ investment costs of PV power plant in \$

$C_{PV-field}$ PV plant costs without storage in \$

C_{EES} electrical energy storage costs in \$

$C_{LP,PV}$ land purchase costs in \$

The individual investment cost segments of the PV power plant with electrical energy storage can be derived from:

$$C_{PV-field} = P_{peak} \times (c_{sm} + c_{st} + c_{ep} + c_{inv} + c_{elc} + c_{si} + c_{tl} + c_{ss}) \quad (26)$$

$$C_{EES} = c_{EES} \times E_{storage,el} \quad (27)$$

$$C_{LP,PV} = c_{LP} \times A_{land,PV} \quad (28)$$

P_{peak} total PV module peak power in W_p

c_{sm} solar module costs in \$/W_p

c_{st} structural costs in \$/W_p

c_{ep} electrical parts costs in \$/W_p

c_{inv} inverter costs in \$/W_p

c_{elc} engineering and labour costs in \$/W_p

c_{si} security and infrastructure costs in \$/W_p

c_{tl} transport and logistics costs in \$/W_p

c_{ss} sub-station costs in \$/W_p

c_{EES} specific electrical energy storage costs in \$/kWh_{el}

$E_{storage,el}$ electrical energy storage capacity in kWh_{el}

c_{LP} specific land purchase costs in \$/ha

$A_{land,PV}$ total land area of PV power plant in ha

Also the annual operational and maintenance costs are calculated with parameters from Table 23 and the investment costs according to:

$$C_{O\&M,PV} = C_{invest,PV} \times f_{O\&M,PV} \quad (29)$$

$C_{O\&M,PV}$ annual O&M costs of PV power plant in \$

$C_{invest,PV}$ investment costs of PV power plant in \$

$f_{O\&M,PV}$ annual O&M costs factor of PV power plant in %

The annual operational and maintenance costs of the EES is already in the c_{EES} included. The annual plant availability $f_{avail,plant}$ is assumed with 100%. The $f_{annuity}$ for the PV plant is constituted by $f_{annuity,PV}$ and $f_{annuity,EES}$ calculated with:

$$f_{annuity} = \frac{f_{annuity,PV} \times (C_{PV-field} + C_{LP,PV}) + f_{annuity,EES} \times C_{EES}}{C_{invest,PV}} \quad (30)$$

Bibliography

- Abbas, R., Martínez-Val, J. M., Muñoz-Antón, J., Valdés, M., Ramos, A., Rovira, A., Montes, M. J., Sait, H., Muñoz, R., Gamarra, Á. & Villén, M., 2015. A Quest to the Cheapest Method for Electricity Generation in Concentrating Solar Power Plants. *Energy Procedia*, 75, pp.514–520. Available at: <<http://linkinghub.elsevier.com/retrieve/pii/S1876610215012102>> [Accessed !no date!].
- Abengoa, 2014. Khi Solar One. , p.2. Available at: <http://www.abengoasolar.com/web/en/nuestras_{_}plantas/plantas_{_}en_{_}construccion/sudafrica/index.html> [Accessed !no date!].
- Abengoa Solar, S., 2013a. *A New Generation of Parabolic Trough Technology*. number April. Phoenix. Available at: <http://energy.gov/sites/prod/files/2014/01/f7/csp_{_}review_{_}meeting_{_}042513_{_}price.pdf> [Accessed !no date!].
- Abengoa Solar, S., 2013b. Solana Factsheet. , p.2.
- Abengoa Solar, S., 2013c. *SolanaStorage*. Available at: <<http://www.abengoasolar.com/web/es/multimedia/>> [Accessed 2015-10-02].
- Abengoa Solar, S., 2015a. *Atacama-1 dossier*. Available at: <http://www.abengoa.com/export/sites/abengoa_{_}corp/resources/pdf/noticias_{_}y_{_}publicaciones/destacado_{_}cerro_{_}dominador/Dossier_{_}Cerro_{_}Dominador_{_}en.pdf> [Accessed 2015-10-04].
- Abengoa Solar, S., 2015b. *Atacama-1 Factsheet*. Available at: <http://www.abengoa.com/export/sites/abengoa_{_}corp/resources/pdf/noticias_{_}y_{_}publicaciones/destacado_{_}cerro_{_}dominador/Factsheet_{_}Cerro_{_}Dominador_{_}en-1.pdf> [Accessed 2015-10-05].
- Alcauza, J., 2013. Abengoa 's subsidiary Rioglass has bought Siemens CSP assets. *CSP World*, . Available at: <<http://www.csp-world.com/news/20130918/001173/abengoas-subsidiary-rioglass-has-bought-siemens-csp-assets>> [Accessed !no date!].
- Alexopoulos, S. & Hoffschmidt, B., 2013. *Concentrating Receiver Systems*. New York, NY: Springer New York. Available at: <<http://energy.gov/articles/top-6-things-you-didnt-know-about-solar-energyhttp://link.springer.com/10.1007/978-1-4614-5806-7>> [Accessed !no date!].

- Alguacil, M., Prieto, C., Rodriguez, a. & Lohr, J., 2014. Direct Steam Generation in Parabolic Trough Collectors. *Energy Procedia*, 49, pp.21–29. Available at: <<http://linkinghub.elsevier.com/retrieve/pii/S1876610214004573>> [Accessed !no date!].
- Archimede Solar Energy, 2015. *HCEMS11 - Technical Data*. Available at: <<http://www.archimedesolarenergy.it/hcems11.pdf>> [Accessed 2015-10-16].
- Baum, V., Aparasi, R. & Garf, B., 1957. High-power solar installations. *Solar Energy*, 1(1), pp.6–12. Available at: <<http://linkinghub.elsevier.com/retrieve/pii/0038092X5790049X>> [Accessed !no date!].
- bergermann und partner, S., 2010. *Kollektoren*. Available at: <<http://www.renewables-made-in-germany.com/en/renewables-made-in-germany/corporate-news/detail/article/ultimate-troughR-the-next-generation-collector-for-parabolic-trough-power-plants-first-demo.html>> [Accessed 2015-08-30].
- Bisseker, C., 2015. *How load shedding hurts the economy*. South Africa: rdm.co.za. Available at: <<http://www.rdm.co.za/business/2015/02/11/how-load-shedding-hurts-the-economy>> [Accessed !no date!].
- Blackmon, J. B., 2012. Heliostat size optimization for central receiver solar power plants. *Concentrating solar power technology*, pp.536–576.
- BP, 2014. *BP Statistical Review of World Energy June 2014*. Available at: <http://www.bp.com/content/dam/bp/excel/Energy-Economics/statistical-review-2014/BP-StatisticalReview_of_world_energy_2014_workbook.xlsx> [Accessed 2015-03-18].
- BP, 2015. *BP Energy Outlook 2035 - February 2015*. number February. Available at: <bp.com/energyoutlook> [Accessed 2015-03-04].
- Bradshaw, R. W., Dawson, D. B., De la Rosa, W., Gilbert, R., Goods, S. H., Hale, M. J., Jacobs, P., Jones, S. a., Kolb, G. J., Pacheco, J. E., Prairie, M. R., Reilly, H. E., Showalter, S. K. & Vant-Hull, L. L., 2002. Final Test and Evaluation Results from the Solar Two Project. *Sandia National Laboratories*, (January), p.294.
- BrightSource Energy, 2014. Ivanpah fact sheet. , . Available at: <http://www.brightsourceenergy.com/stuff/contentmgr/files/0/8a69e55a233e0b7edfe14b9f77f5eb8d/folder/ivanpah_fact_sheet_3_26_14.pdf> [Accessed !no date!].
- Caldés, N. & Lechón, Y., 2012. Socio-economic and environmental assessment of concentrating solar power (CSP) systems. *Concentrating Solar Power Technology*, pp.120–150. Available at: <<http://linkinghub.elsevier.com/retrieve/pii/B9781845697693500054>> [Accessed !no date!].

- Cassell, M., 2012. *African Agriculture Review* 09/2012. Available at: <[http://www.capitalnedbank.co.za/nedbank/action/media/downloadFile?media\[_\]fileid=808](http://www.capitalnedbank.co.za/nedbank/action/media/downloadFile?media[_]fileid=808)> [Accessed !no date!].
- CMI Energy, 2015. *KhiSolarOneReceiver*. Available at: <<http://www.cmigroupe.com/en/p/thermal-solar-receivers>> [Accessed 2015-10-09].
- Cordaro, J. G., Kruizenga, A. M., Altmaier, R., Sampson, M. & Nissen, A., 2011. Thermodynamic properties of molten nitrate salts. *Water*, 1(925), p.2011.
- Dahn, J. & Ehrlich, G. M., 2011. *LITHIUM-ION BATTERIES*. 4. edition edition: McGraw Hill Professional. Available at: <[http://accessengineeringlibrary.com/browse/lindens-handbook-of-batteries-fourth-edition/p2001c2f299726\[_\]1001](http://accessengineeringlibrary.com/browse/lindens-handbook-of-batteries-fourth-edition/p2001c2f299726[_]1001)> [Accessed !no date!].
- Department of Energy, 2012. *2012-Commodity-Flow-and-Energy-Balance*. Available at: <[http://www.energy.gov.za/files/energyStats\[_\]frame.html](http://www.energy.gov.za/files/energyStats[_]frame.html)> [Accessed !no date!].
- Department of Energy, 2013. *Integrated Resource Plan for Electricity (IRP update)*. number November. Available at: <[www.doe-irp.co.za/content/IRP2010\[_\]updatea.pdf](http://www.doe-irp.co.za/content/IRP2010[_]updatea.pdf)> [Accessed 2015-03-10].
- Department of Environmental Affairs, 2015. *South African Governments position on Climate Change*. Available at: <<http://www.climateaction.org.za/cop17-cmp7/sa-government-position-on-climate-change>> [Accessed 2015-03-05].
- Diorio, N., Dobos, A., Janzou, S., Nelson, A., Lundstrom, B., Diorio, N., Dobos, A., Janzou, S., Nelson, A. & Lundstrom, B., 2015. Technoeconomic Modeling of Battery Energy Storage in SAM Technoeconomic Modeling of Battery Energy Storage in SAM. , (September). Available at: <<http://www.nrel.gov/docs/fy15osti/64641.pdf>> [Accessed !no date!].
- Duffie, J. A. & Beckman, W. A., 2013. *Solar Engineering of Thermal Processes*. Vol. 51. Hoboken, NJ, USA: John Wiley & Sons, Inc. Available at: <<http://doi.wiley.com/10.1002/9781118671603>> [Accessed !no date!].
- EASAC, 2011. *Concentrating solar power: its potential contribution to a sustainable energy future*. number November. Halle (Saale), Germany. Available at: <[http://www.easac.eu/fileadmin/Reports/Easac\[_\]CSP\[_\]Web-Final.pdf](http://www.easac.eu/fileadmin/Reports/Easac[_]CSP[_]Web-Final.pdf)> [Accessed 2015-02-26].
- Eberhard, A., Leigland, J. & Kolker, J., 2014. *South Africas Renewable Energy IPP Procurement Program: Success Factors and Lessons*. number May. Available at: <<http://www.ee.co.za/article/south-africas-reippp-programme-success-factors-lessons.html>> [Accessed 2015-03-10].
- Eskom, 2014a. *Integrated Report 2014*. Available at: <<http://integratedreport.eskom.co.za/pdf/full-integrated.pdf>> [Accessed 2015-03-23].

- Eskom, 2014b. *Transmission and distribution equipment in service at 31 March 2014*. Available at: <<http://integratedreport.eskom.co.za/supplementary/app-transmission.php>> [Accessed 2015-04-20].
- Eskom, 2015. *Surplus capacity*. Available at: <<http://www.eskom.co.za/Whatweredoing/ElectricityGeneration/LoadManagement/Pages/SurplusCapacity.aspx>> [Accessed 2015-03-11].
- Fernández-García, a., Zarza, E., Valenzuela, L. & Pérez, M., 2010. Parabolic-trough solar collectors and their applications. *Renewable and Sustainable Energy Reviews*, 14(7), pp.1695–1721.
- Fichtner, 2010. *Assessment of Technology Options for Development of Concentrating Solar Power in South Africa*. number December. Available at: <[https://www.climateinvestmentfunds.org/cif/sites/climateinvestmentfunds.org/files/Presentation-WB\(Eskom\)Project-20101207.pdf](https://www.climateinvestmentfunds.org/cif/sites/climateinvestmentfunds.org/files/Presentation-WB(Eskom)Project-20101207.pdf)> [Accessed 2015-09-16].
- FLABEG FE GmbH, 2015. *ULTIMATE TROUGH* . Available at: <<http://www.flabeg-fe.com/engineering/ultimate-trough.html>> [Accessed 2015-09-24].
- Forder, S., 2015. *The Energy Blog - Project Database*. Available at: <<http://energy.org.za/knowledge-tools/project-database>> [Accessed 2015-06-05].
- Fraunhofer ISE, F. I. f. S. E. S., 2013. Levelized Cost of Electricity Renewable Energy Technologies. , (November). Available at: <<https://www.ise.fraunhofer.de/en/publications/veroeffentlichungen-pdf-dateien-en/studien-und-konzeptpapiere/study-levelized-cost-of-electricity-renewable-energies.pdf>> [Accessed !no date!].
- Giglmayr, S., 2013. Development of a Renewable Energy Power Supply Outlook 2015 for the Republic of South Africa. , p.121.
- Gil, A., Medrano, M., Martorell, I., Lázaro, A., Dolado, P., Zalba, B. & Cabeza, L. F., 2010. State of the art on high temperature thermal energy storage for power generation. Part 1-Concepts, materials and modellization. *Renewable and Sustainable Energy Reviews*, 14(1), pp.31–55.
- Hermann, S., Miketa, A. & Fichaux, N., 2014. *Estimating the Renewable Energy Potential in Africa*. Abu Dhabi. Available at: <http://www.irena.org/DocumentDownloads/Publications/IRENA_Africa_Resource_Potential_Aug2014.pdf> [Accessed 2015-03-05].
- Hildebrandt, A. F., Haas, G. M., Jenkins, W. R. & Colaco, J. P., 1972. Large-scale concentration and conversion of solar energy. *Eos, Transactions American Geophysical Union*, 53(7), p.684. Available at: <<http://doi.wiley.com/10.1029/EO053i007p00684>> [Accessed !no date!].

- Hoffschmidt, B. P. D., 2014. *Receivers for Solar Tower Systems*. Font Romeu, France. Available at: <<http://sfera2.sollab.eu/uploads/images/networking/SFERASUMMERSCHOOL2014-PRESENTATIONS/SolarTowerReceivers-BernhardHoffschmidt.pdf>> [Accessed !no date!].
- IEA, 2014. *Energy Technology Perspectives 2014*. Energy Technology Perspectives: IEA.
- IEA, 2015. *Tracking Clean Energy Progress 2015*. Available at: <http://www.iea.org/publications/freepublications/publication/Tracking_clean_energy_progress_2015.pdf> [Accessed 2015-11-20].
- Ingeteam INC., 2015. *Specification of 805TL U X420 Outdoor / 1070TL U X420 Outdoor*. Available at: <http://www.ingeteam.com/Portals/0/Catalogo/Producto/Documento/PRD_1991_Archivo_ingecon-sun-powermax-tl-u-x420v.pdf> [Accessed 2015-11-16].
- International Energy Agency, 2014a. *Africa Energy Outlook - a focus on energy prospects in sub-saharan africa*. Paris, France. Available at: <http://www.iea.org/publications/freepublications/publication/WEO2014_AfricaEnergyOutlook.pdf> [Accessed 2015-02-26].
- International Energy Agency, 2014b. *Technology Roadmap - Energy storage*. Paris, France. Available at: <<http://www.iea.org/publications/freepublications/publication/TechnologyRoadmapEnergystorage.pdf>> [Accessed 2015-02-26].
- International Energy Agency, 2014c. *Technology Roadmap: Solar Photovoltaic Energy - 2014 edition*. Paris, France. Available at: <http://www.iea.org/publications/freepublications/publication/TechnologyRoadmapSolarPhotovoltaicEnergy_2014edition.pdf> [Accessed 2015-02-26].
- International Energy Agency, 2014d. *Technology Roadmap: Solar Thermal Electricity - 2014 edition*. Paris, France. Available at: <http://www.iea.org/publications/freepublications/publication/TechnologyRoadmapSolarThermalElectricity_2014edition.pdf> [Accessed 2015-02-26].
- International Energy Agency, 2015. *Energy Report: South Africa for 2012*. Available at: <<http://www.iea.org/statistics/statisticssearch/report/?year=2012&country=SOUTHAFRIC&product=ElectricityandHeat>> [Accessed 2015-03-26].
- IRS, U. I. R. S. I., 2015. *Yearly average currency exchange rates translating foreign currency into U.S. dollars*. Available at: <<http://www.irs.gov/Individuals/International-Taxpayers/Yearly-Average-Currency-Exchange-Rates>> [Accessed 19.11.2015].
- Jossen, A. & Weydanz, W., 2006. *Moderne Akkumulatoren richtig einsetzen*. Untermeitingen, Germany: Ubooks Verlag.

- Kalogirou, S. A., 2014. *Solar Thermal Power Systems*: Elsevier. Available at: <<http://linkinghub.elsevier.com/retrieve/pii/B9780123972705000108>> [Accessed !no date!].
- Kearney, D., Kelly, B., Cable, R., Potrovitz, N., Herrmann, U., Nava, P., Mahoney, R., Pacheco, J., Blake, D. & Price, H., 2003. Overview on use of a Molten Salt HTF in a Trough Solar Field. *NREL Parabolic Trough Thermal Energy Storage Workshop*, .
- Kearney, D., Kelly, B., Cable, R., Potrovitz, N., Nava, P., Herrmann, U., Mahoney J. Pacheco, R., Price, H. & Blake, D., 2002. Assessment of a Molten Salt Heat Transfer Fluid in a Parabolic Trough Solar Field. *Jsee*, (April 2002), pp.1–20. Available at: <<http://pointfocus.com/images/pdfs/saltw-troughs.pdf>> [Accessed !no date!].
- Kelly, B. & Kearney, D., 2006. Thermal storage commercial plant design study for a 2-tank indirect molten salt system. , (July), pp.1–32.
- Kolb, G., Ho, C., Mancini, T. & Gary, J., 2011. Power tower technology roadmap and cost reduction plan. *SAND2011-2419*, *Sandia* . . . , (April), p.38. Available at: <<http://prod.sandia.gov/techlib/access-control.cgi/2011/112419.pdf>> [Accessed !no date!].
- Kolb, G. J., 2011. An Evaluation of Possible Next-Generation High-Temperature Molten-Salt Power Towers. , (December).
- Kolb, G. J., Jones, S. a., Donnelly, M. W., Gorman, D., Thomas, R., Davenport, R. & Lumia, R., 2007. Heliostat Cost Reduction Study. *Sandia Report*, SAND2007-3(June), pp.1–158. Available at: <http://www.osti.gov/bridge/product.biblio.jsp?query_id=1&page=0&osti_id=912923> [Accessed !no date!].
- Kulichenko, N. & Wirth, J., 2012. *Concentrating Solar Power in Developing Countries*: The World Bank. Available at: <<http://elibrary.worldbank.org/doi/book/10.1596/978-0-8213-9607-0>> [Accessed !no date!].
- Kutscher, C., Burkholder, F. & Kathleen Stynes, J., 2012. Generation of a Parabolic Trough Collector Efficiency Curve From Separate Measurements of Outdoor Optical Efficiency and Indoor Receiver Heat Loss. *Journal of Solar Energy Engineering*, 134(1), p.011012.
- Leuthold, M., 2014. *Energy Storage Technologies Battery Storage for Grid Stabilization*. Available at: <<https://www.iea.org/media/workshops/2014/egrdenergystorage/Leuthold.pdf>> [Accessed 2015-11-18].
- Lovegrove, K. & Pye, J., 2012. Fundamental principles of concentrating solar power (CSP) systems. *Concentrating Solar Power Technology: Principles, Developments and Applications*, pp.16–67.

- Lüpfer, E., 2013. *Parabolic Trough Solar Technology*. New York, NY: Springer New York Dordrecht Heidelberg London. Available at: <<http://energy.gov/articles/top-6-things-you-didnt-know-about-solar-energy><http://link.springer.com/10.1007/978-1-4614-5806-7>> [Accessed !no date!].
- Maccari, a., Bissi, D., Casubolo, G., Guerrini, F., Lucatello, L., Luna, G., Rivaben, a., Savoldi, E., Tamano, S. & Zuanella, M., 2015. Archimede Solar Energy Molten Salt Parabolic Trough Demo Plant: A Step Ahead towards the New Frontiers of CSP. *Energy Procedia*, 69, pp.1643–1651. Available at: <<http://linkinghub.elsevier.com/retrieve/pii/S1876610215004282>> [Accessed !no date!].
- Mason, a. & Reitze, E., 2014. Establishing Bankability for High Performance, Cost Reducing SkyTrough Parabolic Trough Solar Collector. *Energy Procedia*, 49, pp.155–162. Available at: <<http://linkinghub.elsevier.com/retrieve/pii/S1876610214004718>> [Accessed !no date!].
- Medrano, M., Gil, A., Martorell, I., Potau, X. & Cabeza, L. F., 2010. State of the art on high-temperature thermal energy storage for power generation. Part 2Case studies. *Renewable and Sustainable Energy Reviews*, 14(1), pp.56–72. Available at: <<http://linkinghub.elsevier.com/retrieve/pii/S1364032109001786>> [Accessed !no date!].
- Microthermő, 2012. *Gemasolar_tower_heatshield*. Available at: <<http://www.microthermgroup.com/high/EXEN/site/fairs-archivedetail.aspx?vPK=493{&}vCat={&}page=0>> [Accessed 2015-10-13].
- MIT Electric Vehilce Team, 2008. *A Guide to Understanding Battery Specifications*. number December. Available at: <http://web.mit.edu/evt/summary_{_}battery_{_}specifications.pdf> [Accessed 2015-11-17].
- Morin, G., Dersch, J., Platzer, W., Eck, M. & Häberle, A., 2012. Comparison of Linear Fresnel and Parabolic Trough Collector power plants. *Solar Energy*, 86(1), pp.1–12.
- Morse, W., 2014. *Mulilo Sonnedix Prieska PV (PTY) LTD - 75MW Solar PV Power Plant*. Available at: <<http://www.nersa.org.za/Admin/Document/Editor/file/Consultations/Electricity/Presentations/MuliloSonnedixPrieskaPV.pdf>> [Accessed !no date!].
- Moya, E. Z., 2012. Parabolic-trough concentrating solar power (CSP) systems. *Concentrating Solar Power Technology*, pp.197–239. Available at: <<http://linkinghub.elsevier.com/retrieve/pii/B9781845697693500078>> [Accessed !no date!].
- Noone, C. J., Torrilhon, M. & Mitsos, A., 2012. Heliostat field optimization: A new computationally efficient model and biomimetic layout. *Solar Energy*, 86(2), pp.792–803. Available at: <<http://dx.doi.org/10.1016/j.solener.2011.12.007>> [Accessed !no date!].
- NREL, N. R. E. L., 2008. *Andasol-1*. Available at: <http://www.nrel.gov/csp/solarpaces/project_{_}detail.cfm/projectID=3> [Accessed 2015-10-06].

- NREL, N. R. E. L., 2011. *Gemasolar Thermosolar Plant*. Available at: <<http://www.nrel.gov/csp/solarpaces/project{ }detail.cfm/projectID=40>> [Accessed !no date!].
- NREL, N. R. E. L., 2012. *Archimede*. Available at: <<http://www.nrel.gov/csp/solarpaces/project{ }detail.cfm/projectID=19>> [Accessed 2015-10-16].
- NREL, N. R. E. L., 2013a. *Andasol-2*. Available at: <<http://www.nrel.gov/csp/solarpaces/project{ }detail.cfm/projectID=4>> [Accessed 2015-10-06].
- NREL, N. R. E. L., 2013b. *Andasol-3*. Available at: <<http://www.nrel.gov/csp/solarpaces/project{ }detail.cfm/projectID=117>> [Accessed 2015-10-06].
- NREL, N. R. E. L., 2014a. *Ivanpah Solar Electric Generating System*. Available at: <<http://www.nrel.gov/csp/solarpaces/project{ }detail.cfm/projectID=62>> [Accessed 2015-10-18].
- NREL, N. R. E. L., 2014b. *Khi Solar One*. Available at: <<http://www.nrel.gov/csp/solarpaces/project{ }detail.cfm/projectID=244>> [Accessed 2015-10-06].
- NREL, N. R. E. L., 2015a. *Atacama-1*. Available at: <<http://www.nrel.gov/csp/solarpaces/project{ }detail.cfm/projectID=3275>> [Accessed 2015-10-04].
- NREL, N. R. E. L., 2015b. *KaXu Solar One*.
- NREL, N. R. E. L., 2015c. *PV inverter and module library in SAM*. Available at: <<https://sam.nrel.gov/sites/sam.nrel.gov/files/sam-library-cec-inverters-2015-6-30.csv>
<https://sam.nrel.gov/sites/sam.nrel.gov/files/sam-library-cec-modules-2015-6-30.csv>> [Accessed 2015-11-15].
- NREL, N. R. E. L., 2015d. Solana Generating Station. . . Available at: <<http://www.nrel.gov/csp/solarpaces/project{ }detail.cfm/projectID=23>> [Accessed !no date!].
- NREL, N. R. E. L., 2015e. *System Advisor Model (SAM)*. Available at: <<https://sam.nrel.gov/sites/sam.nrel.gov/files/content/help/sam-help-2015-5-30.pdf>> [Accessed 2015-07-07].
- NREL, N. R. E. L., 2015f. *System Advisor Model (SAM)*. Available at: <<https://sam.nrel.gov/download>> [Accessed 2015-08-10].
- Nykqvist, B. & Nilsson, M., 2015. Rapidly falling costs of battery packs for electric vehicles. *Nature Climate Change*, 5(April), pp.329—332.
- Osuna, R., Schiel, W., Langenkamp, J., Zarza, E., Lüpfert, E., Kotsaki, E. & Brakmann, G., 2001. Development of a Low Cost European Parabolic Trough Collector - EU-ROTRough. *European Commission*, pp.1–20. Available at: <cordis.europa.eu/documents/documentlibrary/51762451EN6.pdf> [Accessed !no date!].

- Pitz-Paal., R., Buck., R., Heller, P., Hirsch, T. & Steinmann, W.-D., 2013. Solar thermal power production in transition to renewable energy systems. *Transition to Renewable Energy Systems*, p.1008.
- Platzer, W., 2014. PVEnhanced Solar Thermal Power. *Energy Procedia*, 57, pp.477–486. Available at: <<http://linkinghub.elsevier.com/retrieve/pii/S1876610214015689>> [Accessed !no date!].
- Platzer, W. & Hildebrandt, C., 2012. Absorber materials for solar thermal receivers in concentrating solar power (CSP) systems. *Concentrating Solar Power Technology*, pp.469–494. Available at: <<http://linkinghub.elsevier.com/retrieve/pii/B9781845697693500157>> [Accessed !no date!].
- Prof. Dinter, F., 2015. *Mail correspondence about the Receiver in Khi*. Stellenbosch.
- PVsyst SA, 2015. *PVsyst 6.3.9*. Available at: <<http://www.pvsyst.com/en/>> [Accessed !no date!].
- Read, J. S. E.-J., Jeeverajan, J. P. D. N.-J., Patel, P. E.-J. & Bytella, J. B., 2009. *Performance and Safety Testing of Panasonic 2.9 Ah Li-ion NCR 18650 Cells*: NASA.
- Reilly, H. E. & Kolb, G. J., 2001. An evaluation of molten-salt power towers including results of the solar two project. *Sandia National Laboratories*, pp.1–94.
- Relloso, S. & Delgado, E., 2009. Experience with molten salts thermal storage in a commercial parabolic trough plant. Andasol-1 commissioning and operation. *Proceedings of the SolarPaces 2009 Conference*, .
- Richert, T., Riffelmann, K. & Nava, P., 2015. The Influence of Solar Field Inlet and Outlet Temperature on the Cost of Electricity in a Molten Salt Parabolic Trough Power Plant. *Energy Procedia*, 69, pp.1143–1151. Available at: <<http://linkinghub.elsevier.com/retrieve/pii/S1876610215004907>> [Accessed !no date!].
- Riffelmann, K., Richert, T., Nava, P. & Schweitzer, A., 2014. Ultimate Troughó A Significant Step towards Cost-competitive CSP. *Energy Procedia*, 49, pp.1831–1839. Available at: <<http://www.sciencedirect.com/science/article/pii/S1876610214006481>> [Accessed !no date!].
- Rioglass Solar International, 2014. *SYSTEM DESCRIPTION UVAC 70-7G*. Available at: <[http://www.rioglass.com/?page\[\]id=1925](http://www.rioglass.com/?page[]id=1925)> [Accessed 2015-10-16].
- Roy, A., Meinecke, W. & Blanco, M. M., 1997. Introductory Guidelines for Preparing Reports on Solar Thermal Power Systems. *SolarPACES Report No. III-3/97.*, .
- Schott, 2015. SCHOTT PTR 79 Receivers The 4th generation. Available at: <[www.schott.com/csp/english/download/schott\[\]ptr70\[\]4th\[\]generation\[\]brochure.pdf](http://www.schott.com/csp/english/download/schott[]ptr70[]4th[]generation[]brochure.pdf)> [Accessed 2015-10-16].

- Shahan, Z., 2015. 38 , 000 Tesla Powerwall Reservations In Under A Week (Tesla / Elon Musk Transcript). Available at: <<http://cleantechnica.com/2015/05/07/38000-tesla-powerwall-reservations-in-under-a-week-tesla-elon-musk-transcript/>> [Accessed !no date!].
- Smith, S., 2012. The long-term market potential of concentrating solar power (CSP) systems. *Concentrating Solar Power Technology*, pp.437–e3. Available at: <<http://linkinghub.elsevier.com/retrieve/pii/B9781845697693500145>> [Accessed !no date!].
- Solar Millennium AG, 2008. *The Parabolic Trough Power Plants Andasol 1 to 3, The Largest Solar Power Plants in the WorldTechnology Premiere in Europe*. Available at: <<http://www.solarmillennium.de/english/downloads/index.html>> [Accessed !no date!].
- SolarGIS, 2013. *World Map of Direct Normal Irradiation*. Available at: <http://solargis.info/doc/_pics/freemaps/1000px/dni/SolarGIS-Solar-map-DNI-World-map-en.png> [Accessed 2015-03-10].
- SolarGIS, 2015a. *DHI-DIF*. Available at: <<http://solargis.info/doc/solar-and-pv-data\#GHI>> [Accessed 2015-08-19].
- SolarGIS, 2015b. *Map of Direct Normal Irradiation (DNI) in South Africa*. Available at: <http://solargis.info/doc/_pics/freemaps/1000px/dni/SolarGIS-Solar-map-DNI-South-Africa-en.png> [Accessed 2015-03-10].
- SolarGIS, 2015c. *Map of Global Horizontal Irradiation (GHI) in South Africa*. Available at: <http://solargis.info/doc/_pics/freemaps/1000px/ghi/SolarGIS-Solar-map-South-Africa-en.png> [Accessed 2015-03-10].
- Solarlite CSP Technology GmbH, 2014. *CSP technology description*. Available at: <<http://solarlite-csp.com/wp-content/uploads/2014/03/CSP-technology-description1.pdf>> [Accessed 2015-10-15].
- Spotnitz, R., 2003. Simulation of capacity fade in lithium-ion batteries. *Journal of Power Sources*, 113(August 2002), pp.72–80.
- Statista GmbH, 2015. *Jährliche Entwicklung des Wechselkurses des Euro gegenüber dem US-Dollar von 1999 bis 2014 (in US-Dollar)*. Vol. 2014. Available at: <<http://de.statista.com/statistik/daten/studie/200194/umfrage/wechselkurs-des-euro-gegenueber-dem-us-dollar-seit-2001/>> [Accessed 2015-11-16].
- Steinmann, W.-D., 2012. Thermal energy storage systems for concentrating solar power (CSP) plants. *Concentrating Solar Power Technology*, pp.362–394. Available at: <<http://linkinghub.elsevier.com/retrieve/pii/B978184569769350011X>> [Accessed !no date!].

- Steinmann, W.-D., 2015. *Thermal energy storage systems for concentrating solar power (CSP) technology*: Elsevier. Available at: <<http://linkinghub.elsevier.com/retrieve/pii/B9781782420880500213>> [Accessed !no date!].
- Steinmann, W.-D. & Eck, M., 2006. Buffer storage for direct steam generation. *Solar Energy*, 80(10), pp.1277–1282. Available at: <<http://linkinghub.elsevier.com/retrieve/pii/S0038092X05002203>> [Accessed !no date!].
- Suite, S., 2011. Low Melting Point Molten Salt Heat Transfer Fluid With Reduced Cost. *SolarPACES*, 1(2), pp.2–3.
- Tamme, R., Laing, D., Steinmann, W.-D. & Bauer, T., 2013. *Thermal Energy Storage*. New York, NY: Springer New York Dordrecht Heidelberg London. Available at: <<http://energy.gov/articles/top-6-things-you-didnt-know-about-solar-energyhttp://link.springer.com/10.1007/978-1-4614-5806-7>> [Accessed !no date!].
- Terblanche, U., 2015. *Large scale solar PV costs in South Africa, Research Engineer at CRSES (Center for Renewable and Sustainable Energy Studies), e-mail correspondence, Stellenbosch, South Africa..* Stellenbosch, South Africa..
- Therminol, 2015. *THERMINOL® VP-1 HEAT TRANSFER FLUID*. Available at: <<http://www.therminol.com/products/Terminol-VP1>> [Accessed 2015-10-27].
- Tidball, R., Bluestein, J., Rodriguez, N. & Knoke, S., 2010. *Cost and performance assumptions for modeling electricity generation technologies*. number November. Available at: <<http://www.nrel.gov/docs/fy11osti/48595.pdf>> [Accessed 2015-11-11].
- Trollip, H., Butler, A., Burton, J., Caetano, T., Godinho, C. & I, 2014. *Energy security in South Africa Final report*. Cape Town, South Africa: MAPS. Available at: <http://www.mapsprogramme.org/wp-content/uploads/Energy-Security_{ }in-South-Africa.pdf> [Accessed 2015-03-11].
- Trombe, F., 1957. Solar furnaces and their applications. *Solar Energy*, 1(2-3), pp.9–15. Available at: <<http://linkinghub.elsevier.com/retrieve/pii/0038092X57901159>> [Accessed !no date!].
- Tyner, C. & Wasyluk, D., 2014. eSolar's Modular, Scalable Molten Salt Power Tower Reference Plant Design. *Energy Procedia*, 49, pp.1563–1572. Available at: <<http://linkinghub.elsevier.com/retrieve/pii/S1876610214006195>> [Accessed !no date!].
- U.S. Department of Energy, 2013. *Concentrating Solar Power Basics*. Available at: <<http://energy.gov/eere/energybasics/articles/concentrating-solar-power-basics>> [Accessed 2015-10-14].

- U.S. Energy Information Adminisstration, 2014. *Levelized Cost and Levelized Avoided Cost of New Generation Resources in the Annual Energy Outlook 2014*. number April. Available at: <http://www.eia.gov/forecasts/aeo/pdf/electricity_generation.pdf> [Accessed 2015-03-10].
- US Energy Information Administration, 2015. *International Energy Statistics - Total Primary Energy Consumption per Capita*. Available at: <<http://www.eia.gov/cfapps/ipdbproject/iedindex3.cfm?tid=44&pid=45&aid=2&cid=ww,r6,SF,&syid=1980&eyid=2011&unit=MBTUPP>> [Accessed 2015-03-25].
- Ushak, S., Fernández, A. & Grageda, M., 2015. *Using molten salts and other liquid sensible storage media in thermal energy storage (TES) systems*: Elsevier. Available at: <<http://linkinghub.elsevier.com/retrieve/pii/B9781782420880500031>> [Accessed !no date!].
- Vant-Hull, L., 2012. *Central tower concentrating solar power (CSP) systems*: Woodhead Publishing Limited. Available at: <<http://linkinghub.elsevier.com/retrieve/pii/B978184569769350008X>> [Accessed !no date!].
- Von Reeken, F., Arbes, S., Weinrebe, G., Wöhrbach, M. & Finkbeiner, J., 2014. *A comprehensive documentation on the current state of the art of parabolic trough collector technology*. Available at: <http://www.ahkbrasilien.com.br/fileadmin/ahk_brasilien/download_dateien/meio_ambiente_eventos/Dia_Engenharia_Heliotermica/Palestras/19_03/Estado_da_arte_da_tecnologia_heliotermica_em_calhas_parabolicas_-Marcus_Balz.pdf> [Accessed 2012-09-10].
- Wagner, M., 2014. *Modeling Parabolic Trough Systems SAM Webinar Schedule for 2014*. Available at: <<https://sam.nrel.gov/sites/sam.nrel.gov/files/sam-webinars-2014-parabolic-trough-systems.pdf>> [Accessed 2015-10-27].
- Wagner, M. J. & Gilman, P., 2011. *Technical manual for the SAM physical trough model*. Vol. 303. Available at: <<http://www.nrel.gov/docs/fy11osti/51825.pdf>> [Accessed !no date!].
- Warner, J., 2014. *Lithium-Ion Battery Packs for EVs*: Elsevier. Available at: <<http://linkinghub.elsevier.com/retrieve/pii/B9780444595133000078>> [Accessed !no date!].
- White Box Technologies, I., 2015. *TMY3 data sets*. Available at: <<http://weather.whiteboxtechnologies.com/home>> [Accessed 2015-05-31].
- Woodcock, G., 2013. DC / AC Ratio Optimization. , pp.1–16. Available at: <https://sam.nrel.gov/sites/sam.nrel.gov/files/content/virtual_conf_july_2013/07-sam-virtual-conference-2013-woodcock.pdf> [Accessed !no date!].

Zakeri, B. & Syri, S., 2015. Electrical energy storage systems : A comparative life cycle cost analysis. *Renewable and Sustainable Energy Reviews*, 42, pp.569–596. Available at: <<http://www.sciencedirect.com/science/article/pii/S1364032114008284>> [Accessed !no date!].

List of Figures

Figure 1. Primary energy consumption by fuel excluding solid biomass and waste in South Africa 2013.	4
Figure 2. Total primary energy consumption and total primary energy consumption per capita 1980 to 2011 in South Africa.	5
Figure 3. Summer and winter load profiles.	6
Figure 4. Average monthly % operating reserves.	7
Figure 5. Electricity demand growth by sector in South Africa in the New Policies Scenario.	7
Figure 6. Eskom's transmission projects as at 31 March 2014.	8
Figure 7. Long-term monthly variability of direct (DNI) and diffuse (DHI) irradiation throughout the year for Aberdeen in the United Kingdom and Upington in South Africa.	10
Figure 8. Solar radiation maps of South Africa.	12
Figure 9. Allocation of all REIPPPP solar power plants in SA.	13
Figure 10. KaXu Solar One, a 100 MW parabolic trough plant with 2.5 hours of thermal storage in molten salts.	14
Figure 11. Overview of Solar Power Technologies.	15
Figure 12. Main components of a CSP plant.	16
Figure 13. Historical development of CSP technologies.	19
Figure 14. Schematic parabolic trough power plant concept.	21
Figure 15. PTC section dimensions of EuroTrough, LS-3, and other designs, in meters.	23
Figure 16. Solar Collector Assembly (SCA) composed of 12 EuroTrough collector elements (SCE).	24
Figure 17. Evolution of parabolic trough collector sizes over 3 development cycles (EuroTrough, HelioTrough, Ultimate Trough).	25
Figure 18. A typical evacuated receiver for parabolic-trough collectors.	26
Figure 19. Example of a EuroTrough collector field layout with 152 loops.	29
Figure 20. 280-MW Solana PTC power plant near Phoenix, Arizona.	30
Figure 21. Schematic CR power plant concept.	31
Figure 22. Schematic diagram of the PS10 solar tower using water/steam as HTF.	32
Figure 23. Heliostats used in solar power plants and their costs.	34
Figure 24. Basically distinguishable field design types.	35
Figure 25. External tube receiver concept and example of application.	36
Figure 26. Cavity receiver concept and example of application.	37

Figure 27. Scheme for CSP plant with integrated storage unit.	40
Figure 28. Basic storage concepts for CSP systems.	41
Figure 29. Simplified scheme of PTC power plants and storage concepts.	43
Figure 30. Overall view of Solana PTC facility with 12 storage tanks for molten salt.	44
Figure 31. Scheme of a steam accumulator.	45
Figure 32. Simplified scheme of Solar Two CRS power plant with direct storage of molten salt used as heat transfer fluid.	46
Figure 33. Schema of an electrical energy storage (EES) system and there energy losses. .	49
Figure 34. Total capital cost in Euro () of large-scale EES systems per unit of nominal power rating including costs of power electronics, storage part, fixed obtain and maintainence and maybe incidental replacement costs.	50
Figure 35. South Africa daily average system load/demand for summer and winter days, with scheduled power production curve.	53
Figure 36. Hourly values of irradiance over a full year from Upington used in the simulation.	55
Figure 37. Solar path diagram for Upington.	56
Figure 38. Simulated heliostat field layout at difrent solar multiples (SM).	60
Figure 39. TES dispatch control matrix for turbine output fraction of CR simulation in SAM.	63
Figure 40. Screenshot of Ultimate Trough input parameter for SAM.	67
Figure 41. Screenshot of Schott PTR80 input parameter for SAM.	68
Figure 42. Typical configuration of a solar field layout with two field subsections for a Ultimate Trough.	69
Figure 43. Screenshot of HTF input parameter for SAM.	70
Figure 44. TES dispatch control matrix for turbine output fraction of PTC simulation in SAM.	72
Figure 45. Model of the configurated PV plus batterie scheme.	75
Figure 46. Currentvoltage characteristic under STC of module BYD 305P6C-36.	78
Figure 47. Efficientcy characteristic of Ingecon Sun 805TL U X420 Outdoor.	78
Figure 48. Voltage proparties of NCA Li-Ion battery.	81
Figure 49. Capacity fade of Nickel Cobalt Aluminum Lithium-Ion battery.	82
Figure 50. Load curve covering results of simulated solar power plants.	88
Figure 51. Levelized costs of electricity results of simulated solar power plants.	90
Figure 52. Cost of Li-ion battery packs in battery electric vehicles.	92
Figure 53. CSP Technologies Comparison I	96
Figure 54. CSP Technologies Comparison I	97

List of Tables

Table 1. The main CSP technologies families.	17
Table 2. Performance Characteristics of main CSP technologies families.	18
Table 3. Characteristics of different parabolic trough collectors.	24
Table 4. Technical parameters of the receivers commercialized by Schott, Siemens and ASE.	27
Table 5. Main characteristics of sensible heat storage liquid materials.	42
Table 6. Location and characteristics for the simulation in SAM.	54
Table 7. Simulated CR solar multiple and thermal energy storage configurations.	58
Table 8. CR power block and condenser input parameter in SAM.	58
Table 9. CR heliostat parameter.	59
Table 10. CR heliostat field parameter.	61
Table 11. CR system TES parameter.	62
Table 12. Financial input parameter for CR-simulation in SAM.	64
Table 13. Simulated PTC solar multiple and thermal energy storage configurations.	65
Table 14. PTC power block and condenser input parameter in SAM.	66
Table 15. PTC solar field parameter.	71
Table 16. PTC system TES parameter.	71
Table 17. Financial input parameter for PTC-simulation in SAM.	74
Table 18. Simulated configurations of the PV system with adapted EES.	76
Table 19. Module specification of BYD 305P6C-36.	77
Table 20. Inverter specifications of Ingecon Sun 805TL U X420 Outdoor.	79
Table 21. PV system design parameter.	80
Table 22. EES system design parameter.	84
Table 23. Financial input parameter for PV-simulation in SAM.	86
Table 24. Electricity flow in South Africa 2012.	95

List of Code

List of Abbreviations

AC	alternative current
CF	capacity factor
CO₂	carbon dioxide
CPV	concentrating photovoltaic
CSP	concentrating solar power
CST	concentrating solar thermal
DC	direct current
DHI	diffuse horizontal irradiance
DNI	direct normal irradiance
DOD	depth of discharge
DSG	direct steam generation
EV	electric vehicles
FITs	feed-in tariffs
GDP	gross domestic product
GHI	global horizontal irradiance
GNI	global normal irradiance
GW	gigawatt
GWh	gigawatt hour
ha	hectare (1 ha = 10 000 m ²)
HTF	heat-transfer fluid
IEA	International Energy Agency
IRP	Integrated Resource Plan

kW	kilowatt
kWh	kilowatt hour
LCCF	load curve covering factor
LCOE	levelised cost of electricity
LFR	linear Fresnel reflector
Mtoe	million tonnes of oil equivalent
MW	megawatt
MWh	megawatt hour
NCA	Nickel Cobalt Aluminum
PCS	power conversions system
PSP	pumped storage plants
PT	parabolic trough
PTC	parabolic trough collector
PV	photovoltaic

REIPPPP Renewable Energy Independent Power Producer Procurement Program

SA	South Africa
SAPP	Southern African Power Pool
SCA	solar collector assembly
SCE	solar collector element
SM	Solar multiple
SOC	state of charge
STE	solar thermal electricity
TES	thermal energy storage
TWh	terawatt hour
W	watt
Wh	watt hour